KINETICS OF THIOMOLYBDATE AND COPPER-THIOMOLYBDATE INTERCONVERSION PROCESSES

A Thesis Submitted to the College of
Graduate Studies and Research
In Partial Fulfillment of the Requirements
For the Degree of Doctor of Philosophy
In the Department of Chemistry
University of Saskatchewan
Saskatoon

By

Rhett Clark

PERMISSION TO USE

In presenting this thesis in partial fulfillment of the requirements for a Postgraduate degree from the University of Saskatchewan, I agree that the Libraries of this University may make it freely available for inspection. I further agree that permission for copying of this thesis in any manner, in whole or in part for scholarly purposes may be granted by the professor who supervised my thesis work or, in his absence, by the Head of the Department or the Dean of the College in which my thesis work was done. It is understood that any copying or publication or use of this thesis or parts thereof for financial gain shall not be allowed without my written permission. It is also understood that due recognition shall be given to me and to the University of Saskatchewan in any scholarly use which may be made of any material in my thesis.

Request for permission to copy or to make other use of material in this thesis in whole or in part should be addressed to:

Head of the Department of Chemistry
University of Saskatchewan
110 Science Place
Saskatoon, Saskatchewan
S7N 5C9
CANADA

ABSTRACT

Copper (Cu) is an essential trace element in ruminants such as the cow. Its deficiency leads to a number of debilitating symptoms and can eventually cause death. Secondary Cu deficiency is caused by the presence of chemical antagonists such as the thiomolybdates (TMs) ($MoO_xS_{4-x}^{2-}$; x = 0 – 3). TMs form in the rumen and then form tightly bound insoluble complexes with Cu. These complexes are then excreted and the Cu is unavailable to the animal. The TMs and their effects on ruminant Cu are the focus of this thesis.

This study includes three main bodies of work. First, a method for quantifying the composition of TM mixtures in solution was developed. Second, the rate constants of TM interconversions were determined. Third, reactions between Cu and the TMs were studied. This work is part of an ongoing study in the Reid group to model Cu-ligand speciation in the rumen.

Thiomolybdates form by successive replacement of molybdate (MoO_4^{2-}) O ligands with S. This makes synthesis of the uncontaminated compounds difficult. Mixtures of TMs are best analyzed by UV-visible spectroscopy despite the considerable spectral overlap. The combination of these two issues makes the characterization of the spectra difficult. In this study, a method was developed to establish the spectra of the pure TMs despite cross-contamination. Multivariate curve fitting methods were used to establish the composition of synthesized samples simultaneously with the molar absorptivities of the pure TMs. This was done using a Beer's Law model. The composition was determined from a fit using assumed molar absorptivities. The absorptivities were then refined using the composition results. These processes were successively reiterated until both were optimized. The optimized absorptivities could then be used to determine the composition of any TM solution mixture.

The kinetics of TM formation under biologically relevant conditions were followed by UV-visible spectroscopy. The spectra were then analyzed, using the

method developed above, to determine all TM concentrations. Curve fitting methods were used to simultaneously determine the rate constants of all processes that occurred. Integrated rate equations used in the fitting process were developed using the Laplace Transform method. Rate constants were determined at varying pH, ionic strengths and temperatures. From this information it was shown that TM formation and hydrolysis occurs via an associative mechanism. It was also determined that H_2S and not HS^- was the sulfide nucleophile in TM formation reactions.

This study was then extended to include reactions involving Cu and the TMs. First, the UV-visible spectra of the reaction products of Cu with each TM were characterized. This allowed the kinetics of reactions between Cu and the TMs to be followed. This reaction has been found to proceed via an intermediate. Molar absorptivities for this intermediate were optimized along with the appropriate rate constants. This was done using a combination of mathematical simulations and the curve fitting methods used for the TM kinetics. The resulting rate constants can be compared with those obtained previously in the group using a Cu ion selective electrode.

These rate constants were used in conjunction with the TM formation rate constants to perform simulations. The results of these simulations provide a picture of what is expected to occur in the rumen. Reactions were also performed in which TM formation occurred in the presence of Cu. This was then extended to mimic bovine feeding habits. Here, portions of the reactions mixture was removed at various time intervals and replaced with fresh reagents. These experiments were used to gain a qualitative picture of Cu speciation in the presence of the TMs over time. The work presented in this thesis provides a crucial step toward understanding the problem of bovine copper deficiency.

ACKNOWLEDGEMENTS

I would like to sincerely thank my supervisor, Dr. Steve Reid, for his constant guidance, support and mentorship throughout this project. Thanks for your unwavering commitment and patience, especially during the struggles.

I would also like to thank my committee members, Dr. Bernie Kraatz, Dr. Stephen Urquhart, Dr. Stephen Foley and Dr. Ajay Dalai. Your suggestions and criticisms were both welcomed and appreciated. Thanks also to Dr. Dave Palmer and his research group for graciously allowing me to use their spectrometer.

The support of my various lab-mates, both past and present is greatly appreciated. Thanks to Darina Slamova, Dr. Joseph Essilfie-Dughan, Dr. Emmanuel Quagraine and Mildred Budu for the many discussions, both scientific and otherwise and for creating a friendly atmosphere in which to work.

I could not have reached this point without the everlasting love and support of my family and friends. Thanks for everything Mom and Dad, I did it! Thanks to my brothers, Ryan and Greg, for the encouragement from you and your families. Thanks, G-ma, for all that you've done. I would also like to thank Dale Fuhr and Ignace Moya, my friends that were always there for me. Thanks to Dr. Chris Phenix, my closest friend and confidant through this all.

Finally, I would like to acknowledge the funding for this project from the Agricultural Development Fund of Saskatchewan and the University of Saskatchewan.

To
My Parents

TABLE OF CONTENTS

LIST OF TABLES

LIST OF FIGURES

LIST OF ABBREVIATIONS

A	Absorbance
Å	Angstrom
α	Molar fraction
c	Concentration
°C	Degrees Celsius
χ^2	Reduced Chi squared
D	Determinant
DM	Dry matter
ε	Molar absorptivity
Fm	Formula mass
g	Grams
HMM	High molecular mass
I	Ionic strength
ISE	Ion selective electrode
k	Rate constant
k’	Pseudo rate-constant
K	degrees Kelvin
L	Liters
LEC	Long-Evans Cinnamon
log	Base 10 logarithm
λ	Wavelength
M	Molarity = moles of solute/Volume of solution in L
min	Minutes
mV	Millivolts
μ	Micro
^{95}Mo NMR	Molybdenum-95 nuclear magnetic resonance
NMR	Nuclear magnetic resonance
ν	frequency
pH	Negative log of the hydrogen ion activity

pKa	Negative log of the acid dissociation constant
PPh_3	Triphenylphosphine
py	Pyridine
Σ	Sum
T	Temperature
TM	Thiomolybdate
TM0	Molybdate (MoO_4^{2-})
TM1	Monothiomolybdate (MoO_3S^{2-})
TM2	Dithiomolybdate ($MoO_2S_2^{2-}$)
TM3	Trithiomolybdate ($MoOS_3^{2-}$)
TM4	Tetrathiomolybdate (MoS_4^{2-})
UV-vis	Ultraviolet – visible
VFA	Volatile fatty acid
z_x	Charge of ion x
[X]	Molar concentration of species X

1. INTRODUCTION

1.1 THE PROBLEM

Copper deficiency is a common problem for ruminants in Canada and other parts of the world. This can result from insufficient Cu intake (primary deficiency) or the presence of an antagonist that renders Cu unavailable for absorption (secondary deficiency). Unlike humans, ruminants are particularly susceptible to secondary copper deficiency because of the conditions present in the rumen (see section 1.6.2). When Mo intake is sufficient, thiomolybdates (MoS_xO_{4-x}, x = 0-4), herein referred to as TMx where x refers to the number of S ligands, form in sufficient quantities in the rumen to significantly antagonize Cu. Section 1.4 discusses thiomolybdate chemistry of Cu and Mo and section 1.5.3 looks at the chemistry of Cu-TM interactions

Cu deficiency is not always obvious as minor deficiencies may not produce clinical signs. See section 1.5.4 for a discussion of the history of Mo induced Cu deficiency. However, more severe deficiencies may produce symptoms like diarrhea, stunted growth, dull coat, swayback, and infertility (see section 1.6.4). If deficiency persists, death may occur. Fortunately, the effects of copper deficiency are largely reversible with proper treatment. However, this can be expensive and inefficient. Also, due to the risk of Cu poisoning, indiscriminate supplementation can be dangerous as well.

Reliable, efficient treatment is therefore important to be able to maximize the health of the herd and to minimize the cost and labor associated with treatment. Much of the previous work in this area has involved *in vivo* studies (section 1.5.5). In these cases, Cu levels are monitored under various conditions using various bio-markers.

These studies are expensive and time consuming and the results are very animal specific. Also, very little knowledge is gained about the specific chemical interactions taking place. An alternative method is to develop a means of accurately predicting Cu speciation given a set of conditions. An effective model can then be used to predict regions where Cu deficiency may develop and to improve the efficiency of treatments.

The development of a mathematical computer model of Cu speciation in the rumen is an overall goal in the Reid laboratory. Previous work in the Reid group has focused on Cu interactions with many of the major ligands present in the rumen. Stability constants of these interactions have been incorporated into a thermodynamic speciation model (see section 1.7). However, thiomolybdates are known Cu antagonists and are not as yet included in this model.

Thiomolybdates form in the rumen from molybdate (ingested in the feed) and sulfide (formed in the rumen by reduction of various forms of sulfur). Once formed, TMs form non-labile complexes with Cu that prevent Cu from being absorbed in the body. Thiomolybdate formation is a rather slow, kinetically controlled process. Therefore, before these species can be included into the model, an accurate kinetic analysis must be performed.

The TMs are most commonly analyzed by UV-visible spectroscopy. However, extensive spectral overlap has limited the efficiency of this method in the past (section 1.5). Curve fitting methods offer an improved means of reliably characterizing the UV-visible spectra of the TMs. See section A1 for more on curve fitting theory.

The kinetics of TM interconversions are difficult to ascertain due to the complexity of the reaction scheme. This has led previous researchers to make limiting assumptions when analyzing TM kinetics (section 1.5.2). Curve fitting methods allow complex reaction kinetics to be considered without these limiting assumptions. Section A2 outlines the requisite kinetic theories and discusses how rate constants can be determined by curve fitting.

Previous work involving reactions between Cu and the TMs has consisted primarily of structural analysis (section 1.5.3). Very little research into the nature of these reactions has been performed. A better understanding of these interactions will be gained from quantitative analysis.

1.2 GOALS OF THE STUDY

The work in this thesis focuses on three primary goals:

1. The first goal is to develop a reliable method of determining the composition of thiomolybdate mixtures in solution. The UV-visible spectra of the pure thiomolybdates will be characterized by curve fitting of the spectra of impure samples. This work will be described in section 3.1.

2. The second goal of this work is to perform accurate kinetic analyses of TM interconversion processes under bovine rumen-like conditions. The reaction scheme and existing rate constants will be determined simultaneously by curve fitting. TM kinetics will be discussed in section 3.2.

3. The third goal of this work is to quantitatively study Cu-TM interactions. First, the kinetics of the reactions of Cu with either tri- or tetrathiomolybdate will be studied. This will be followed up by looking at the effects of Cu on thiomolybdate formation from a molybdate starting point. These experiments will then be extended to mimic bovine feeding habits. Finally, thiomolybdate formation in the presence of Cu will be simulated using Microsoft Excel®. Cu related studies will be discussed in section 3.3.

1.3 GENERAL CHEMISTRY OF COPPER AND MOLYBDENUM

1.3.1 Copper

Copper (Cu) is a fourth row transition metal (d-block element) with an atomic number of 29. It is located in group 11 above silver and gold. ^{63}Cu and ^{65}Cu are the two significant isotopes of Cu and have natural abundances of 69.15 and 30.85, respectively, giving a molar mass of 63.54 [1]. The ground state electronic configuration is $1s^2 2s^2 2p^6 3s^2 3d^{10} 4s^1$ or $[Ar]3d^{10}4s^1$. Oxidation states of +1 to +4 are known to exist but the +1 and +2 oxidation states are by far the most common [2].

Cu(II) is a d^9 ion with an electron configuration of $[Ar]3d^9$. The open electron hole allows d-d transitions to occur when subject to visible light of about 600 – 900 nm. As a result, virtually all aqueous Cu(II) compounds are blue or green. Cu(II) has a single unpaired electron making it paramagnetic and EPR active. Consequently, ligand NMR resonances are subject to paramagnetic line broadening upon complexation with Cu(II).

Cu(I), on the other hand, has a d^{10} configuration and does not undergo d-d transitions. Therefore, most of its compounds are colorless. The exceptional compounds that exhibit color undergo charge transfer transitions, that is, ligand to metal or metal to ligand charge transfers. Cu(I) is diamagnetic and is therefore EPR inactive.

Cu(II) is generally more stable than Cu(I) and typically oxidizes to form Cu(II) in air and aqueous solution. The Cu(I)/Cu(II) redox processes can be defined as electrolytic oxidation and reduction (equation 1.1), disproportionation (equation 1.2) and the oxidation of Cu(I) by O_2 to yield H_2O (equation 1.3) [2]. The relative stability of a particular oxidation state, however, is dependent on the ligand, the disposition in space and the solvent [3]. For example, the stability of Cu(I) is increased when complexed with soft (large, polarizable) ligands or in a highly reducing environment such as the bovine rumen.

$$Cu^0 \overset{-e^-}{\rightleftharpoons} Cu^+ \overset{-e^-}{\rightleftharpoons} Cu^{2+} + 2e^- \quad \textbf{(1.1)}$$

$$2Cu^+ \rightleftharpoons Cu^{2+} + Cu^0 \quad \textbf{(1.2)}$$

$$4Cu^+ + O_2 + 4H^+ \longrightarrow 2H_2O + 4Cu^{2+} \quad \textbf{(1.3)}$$

In accordance with the hard and soft acid base theory, Cu(I) is a soft acid. It therefore creates its strongest complexes with soft ligands. These include heavy halogens, sulfur ligands and unsaturated ligands [3]. Coordination numbers of 2 – 5 have all been observed, but 4-coordinate compounds are most common. Tetrahedral geometry around the metal center is by far the most common. However, this gives little indication as to overall structure as mononuclear, binuclear, polynuclear and halide bridge formations are all known [4].

Cu(II) is considered a borderline hard acid. N-type and O-type ligands are the most common. Complexes with sulfur ligands and smaller halogens are also well known. Coordination numbers of 4 – 6 are dominant with 6-coordinate compounds being the most common. The geometry of Cu(II) complexes is complicated by the d^9 configuration. When in a cubic (octahedral or tetrahedral) environment, Jahn-Teller distortions are incurred [4].

The Jahn-Teller Effect occurs in non-linear molecules where an electronic degeneracy exists in the ground state. In order to remove this degeneracy, thus reducing the overall energy of the molecule, ligands are distorted from their typical geometric positions [5]. Jahn-Teller distortion only occurs when there is degeneracy in the valence d-shell. As such, it is relevant only to complexes of certain transition metals.

An example of this would be an octahedrally coordinated Cu^{2+} ion (Figure 1.1). In the ground state, the t_{2g} orbitals are filled while there is a single vacancy in the e_g

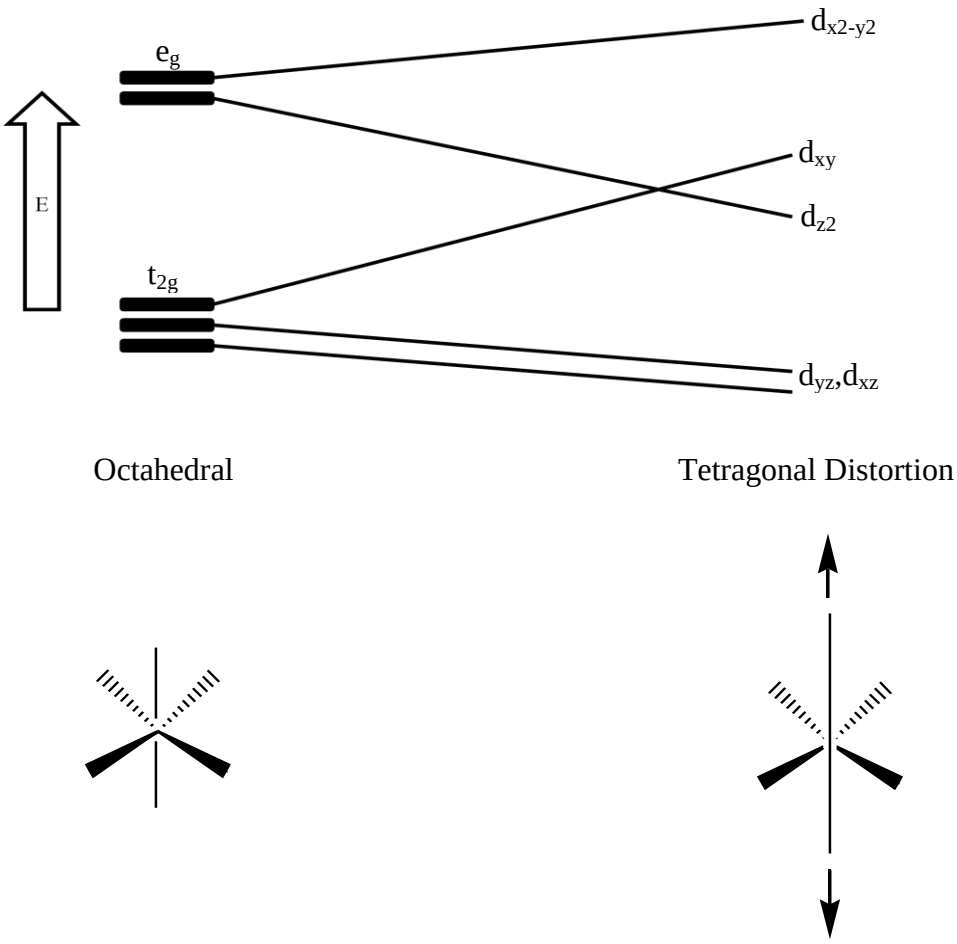

Figure 1.1. Energy level diagram depicting the Jahn-Teller effect. The change in energy of d orbitals in octahedral configuration being tetragonally distorted along the z-axis.

orbitals. This means that there are two possible configurations of equal energy; $d^2_{x^2-y^2}d^1_{z^2}$and $d^1_{x^2-y^2}d^2_{z^2}$. Let's assume that the $d^2_{x^2-y^2}d^1_{z^2}$case exists. In this case, the ligands along the z-axis are more screened from the charge of Cu^{2+} than are the ligands on the x and y axes. The z-axis ligands will therefore move further away from the metal center. The d_{z^2}orbital will decrease in energy becoming more stable than the $d_{x^2-y^2}$orbital. The destabilizing degeneracy is now removed. In extreme cases, tetragonal distortion may result in the removal of the axial ligands leaving a 4-coordinate square planar geometry.

For Cu^{2+} complexes, the type of distortion described here is typically observed. In other cases, elongation may occur along other axes. Compression may also be observed. For 4-coordinate, nominally tetrahedral, complexes, distortion will cause a flattening of the molecule toward square planar although accurately square planar configurations are not common. Regular tetrahedral complexes of Cu^{2+} are also not known. The overall extent of distortion, however, is affected by the nature of the ligands.

The aqueous chemistry of Cu^{2+} is dominated by the $[Cu(H_2O)_6]^{2+}$ ion. Jahn-Teller distortion results in a distorted octahedron with the axial ligands being weakly bound. All water ligands are very labile and can undergo rapid exchange with other ligands. In biological systems, there is a large variety of possible complexes that can form. This, in conjunction with the mobility of Cu^{2+} at physiological pH, makes free Cu toxic in the body.

1.3.2 Molybdenum

Molybdenum (Mo) is a fifth row transition metal (d-block element) with an atomic number of 42. It is in group 6 along with chromium (3d) and tungsten (5d). Mo is chemically similar to tungsten but much less so to chromium [4]. There are seven naturally occurring isotopes of Mo each with a natural abundance between 9 and 25 % giving a molar mass of 95.94 [1]. The ground state configuration is $[Kr]4d^5 5s^1$. Oxidation states of +1 to +6 are known with +4 and +6 being the most common. Although Mo(VI) is not as strong an oxidizing agent as chromates, reduction of molybdates from +6 to +5 in solution is easily incurred.

In nature, Mo is found mostly in the +4 oxidation state as molybdenite (MoS_2). It is also found in the +6 oxidation state as molybdates such as wulfenite ($PbMoO_4$) [4]. It is the molybdate ion that is of interest regarding Cu antagonism in ruminants. Alkali metal or NH_4^+ salts of MoO_4^{2-} are soluble while most other cations form insoluble salts. In weakly acidic solutions, molybdate can undergo condensation to form various

polyanions [5]. MoO_4^{2-} can be obtained from MoO_3 in aqueous alkali solution. In strong acidic solutions, however, molybdic acid ($MoO_3 \cdot 2H_2O$) is obtained. The dichromate analogue, $[Mo_2O_7]^{2-}$ can be converted to $[Mo_7O_{24}]^{6-}$ by the addition of a small cation. $[Mo_7O_{24}]^{6-}$ has been used as a precursor in thiomolybdate synthesis [6, 7].

Insoluble MoS_2 and MoS_3 are the most common sulfides of Mo. MoS_2 is the most stable at high temperatures and many sulfides revert to this form upon heating. MoS_4^{2-} can be formed by the addition of H_2S gas to $[Mo_7O_{24}]^{6-}$ in basic solution or by aqueous HS^- to MoO_4^{2-}. The chemistry of thiomolybdates is the subject of section 1.4.

^{95}Mo and ^{97}Mo are both NMR active. ^{95}Mo has a natural abundance of 15.92 % while ^{97}Mo is 9.55 % abundant and so ^{95}Mo is the most commonly studied isotope by NMR. ^{95}Mo, and ^{97}Mo, have a nuclear spin of 5/2. Any nucleus with a spin greater than 1/2 will have a quadrupole moment, including ^{95}Mo. This is because the charge in the nucleus is not distributed spherically (as with spin 1/2 nuclei) but ellipsoidally. The quadrupole effectively and rapidly causes relaxation of the nucleus. This rapid relaxation causes line broadening [8] which might then be expected in the ^{95}Mo NMR spectrum.

Line widths are also dependent on the symmetry of the molecule, with greater symmetry leading to narrower lines. TM0 and TM4, having regular tetrahedral symmetry have half bandwidths ($W_{1/2}$) of 0.5 and 0.3 Hz, respectively. TM2, with C_{2v} symmetry, has a $W_{1/2}$ of 2.8 Hz while the TM1 and TM3 (C_{3V} symmetry) have $W_{1/2}$ of 10 and 0.7 Hz, respectively. These are still wider than the 0.02 Hz that is achievable from a ^{1}H resonance. However, resolution in the ^{95}Mo spectrum is further enhanced because with each added S ligand, a downfield shift of ~500 ppm is observed (see section 1.5.1.2). ^{95}Mo is limited by its sensitivity, though, giving rise to long acquisition times (about 10 minutes). This will be discussed further in section 1.5.1.2.

Mo(VI) is a d^0 metal with an empty valence shell and so it is EPR inactive. However, Mo(V) and Mo(IV) can be measured by EPR, making it useful for structural studies containing these oxidation states.

1.4 THIOMOLYBDATE CHEMISTRY

1.4.1 General chemistry

The Lewis structures of the thiomolybdates are shown in Figure 1.2. Lone pairs

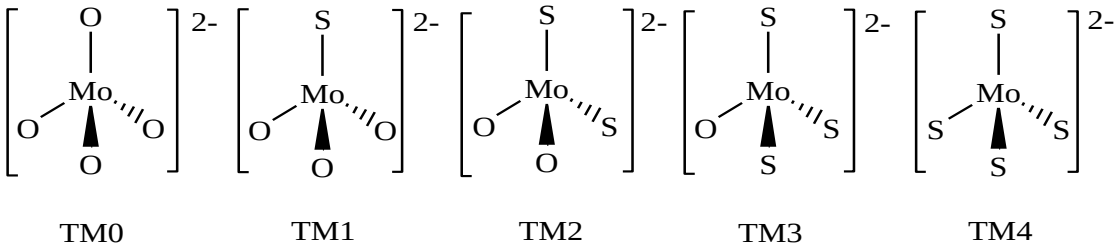

Figure 1.2. Thiomolybdate ion Lewis structures.

have been omitted for clarity. The thiomolybdates will herein be referred to as TMx, where TM stands for thiomolybdate and x is the number of S ligands. For consistency, TM0 is reserved for the molybdate ion. They are all divalent negatively charged tetrahedral ions. They differ only in the number of S and O ligands around the Mo center. Mo is in its highest formal oxidation state, +6, while S and O ligands are in the -2 state. Further donation of electron density from the ligands to the metal, though, would reduce the formal charge. All Mo-S bond lengths of TM4 are a similar 2.15 – 2.18 Å [9]. This is in agreement with crystallographic studies performed by Thome [10]. The Mo-S bond distance was also very similar in the other TMs while the Mo-O bond was consistently 1.74 – 1.78 Å. This suggests that the bond character is consistent amongst the TMs.

Thiomolybdates act as ligands in a wide array of complexes. Typically they keep their original form and act as bridging ligands with other metal centers. The resulting structures vary from simple linear and cubane structures to much more complex clusters. These compounds are of interest as nonlinear optical materials, industrial catalysts and as models to Fe-Mo-S cluster in nitrogenase [11]. Another major area of interest for thiomolybdate studies regards the Cu-Mo antagonism in biological systems. This forms the basis for the work presented in this thesis. The chemistry of Cu-TM interactions will be discussed in section 1.5.3.

The thiomolybdates are brilliantly colored. TM4 typically has a deep red color even though its pure crystalline form is an iridescent green, TM3 is a dark orange color, TM2 is a paler orange and TM1 has a pale yellow hue. These colors are due to low energy ligand to metal transitions [11]. The small energy difference between the transfer bands results from the extreme oxidation states of the metal and the ligands. A simplified molecular orbital diagram for TM4 is shown in Figure 1.3. The longest wavelength transitions in the UV-visible spectrum are due to the $t_1 \rightarrow 2e^*$ transition for all TMs. The higher energy transitions ($3t_2 \rightarrow 2e^*$ and $1t_1 \rightarrow 4t_2^*$) could not be unequivocally assigned but are qualitatively described as ligand to metal charge transfers [9, 12].

Upon addition of sulfide to TM0 in solution, successive replacement of O with S ligands occurs. With each successive step, the formation slows. If enough sulfide is added, the most thermodynamically stable of the TMs, TM4, is formed. Conversely, in aqueous solution void of sulfide, the reverse ("hydrolysis") reactions occur at an increasing rate until TM0 is formed. Overall the stability of the TMs in solution increases with each additional S ligand. TM stability is greater in basic solution. As the pH is lowered, hydrolysis occurs more rapidly. However, TM0 is, in general, more stable in aqueous solution than TM4.

It has also been postulated that polyanionic species such as $(Mo_2S_7)^{2-}$, $(Mo_4S_{13})^{2-}$ and $(Mo_4S_{15})^{6-}$ form during acidification of TM4 [13]. However, later studies showed only

the formation of MoS_3 under these conditions [14]. It has been shown that the addition of disulfides to an acidic TM4 solution do promote an internal redox reaction and cause the formation of polymeric species [15-17]. Other external oxidants such as S_8 [17, 18] and organic diselenides [15] have also been used. A review of a binary and tertiary thiomolybdate complexes has been written by Coucouvanis [19].

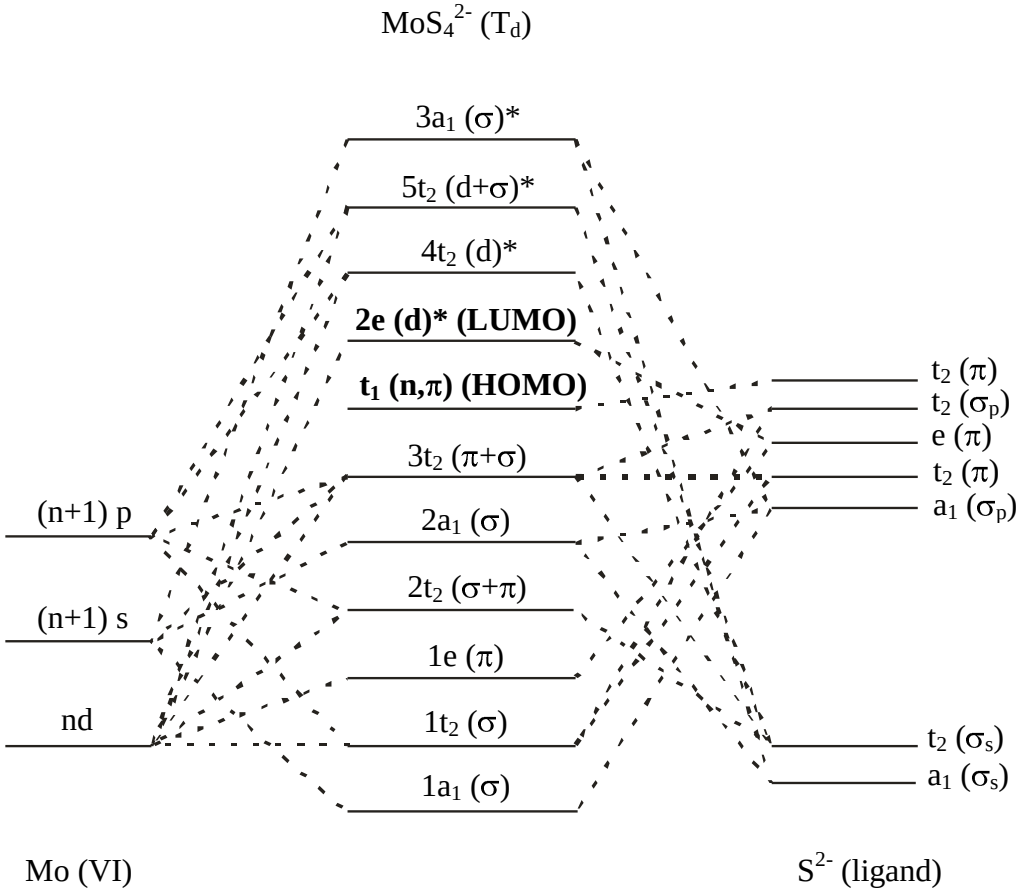

Figure 1.3. Simplified molecular orbital diagram for TM4 with T_d symmetry [12].

Since condensation of the thiomolybdates to form polymeric species happens at acidic pH, pre-protonation of S must occur. Based on the pKa's of H_2S ($pKa_1 = 7$) and H_2O ($pKa_1 = 15$), this pre-protonation is likely to occur more favorably with the oxothiomolybdates. Intramolecular condensation redox processes can therefore occur without the addition of sulfur [9].

In solid form the TMs are sensitive to oxygen and must be stored under anaerobic atmosphere. This is especially apparent with TM2. In air, the pale orange powder quickly turns brown, presumably because of disulfide formation. However, if the solid is stored properly, the pale orange colour is maintained.

TM0 is commercially available, most commonly as the ammonium and sodium salts. TM4 is also commercially available but is typically synthesized as needed since it is easily and cheaply obtained in high purity. The most common form of TM4 is the ammonium salt but other salts such as the sodium, potassium and PPh_4^+ salts are also known [11]. TM2 is also typically produced as the ammonium salt but the Et_4N^+ [20] as well as the Bu_4N^+ [21] and PPh_4^+ [22] salts are also known. TM3, on the other hand is most commonly produced as the cesium salt but has also been produced as the sodium salt [23] as well as the Bu_4N^+ and PPh_4^+ salts [21]. TM1 has only been isolated as the ammonium salt [24].

1.4.2 Factors Affecting Extent of TM Formation

The ability to study the TMs is greatly enhanced by the synthesis and isolation of each species. However, the TMs are formed by successive substitution of O ligands with S ligands. This complicates the synthesis of the pure compounds. As a particular TM is forming, further substitution may already be occurring. As such, there is likely a mixture of TMs at any given time. However, careful control of reaction conditions can maximize the proportion of a given product TM during synthesis. This was done by Quagraine [24]. The synthetic procedures for the TMs are detailed in section 2.2.

Before these factors can be discussed, a careful distinction must be made between rate of reaction and extent of reaction (the level of substitution achieved), since it is possible to change one without the other. If under a broad range of conditions, TM4 is the exclusive product, the extent of the reaction is unchanged. However, within this range of conditions, TM4 may form at a faster or slower rate. In this discussion, our

concern is with the extent of the reaction only, since it is the specific product(s) formed that matter, not how fast they are formed.

There are four major factors that affect the extent of TM formation and can be customized to favor the formation of a specific TM: temperature, S:Mo reagent ratio, pH and reaction time. In general, the formation of TM4 is favored by higher temperature, an increased S:Mo ratio, lower pH and a longer reaction time.

As with most reactions, raising the temperature positively affects the rate of TM formation. In this case, this leads to the reaction occurring to a greater extent. The decreasing rate of formation with each step is at least partially due to probability. With each addition of an S ligand, there is one less reaction site for further substitution. By increasing the temperature, there are an increased number of collisions of greater energy and so the reaction efficiency increases. This is important for the complete formation of TM4. TM1 and TM2 synthesis, therefore, are typically carried out in an ice bath as opposed to TM3 at room temperature and TM4 at 35 ºC.

An increase in S:Mo ratio also encourages greater TM formation. A higher concentration of sulfide kinetically favors the higher substituted TMs. As TMs form, a high concentration of free sulfide is maintained. This allows further reaction to proceed. Conversely, with a low S:Mo ratio, the free sulfide may be nullified before complete TM formation can occur. In practice, a S:Mo ratio of about 1:1 is used for TM1 synthesis while a ratio of 10:1 or greater is used for TM4.

The TMs are synthesized at basic pH (about 10 for TM1 to 13 for TM4). In this pH range sulfide is almost exclusively in the HS^- form. Decreasing the pH further would increase the extent of the reaction but would also increase the rate. This would make it more difficult to control the extent of the reaction. Furthermore, the lower pH would encourage the formation of insoluble MoS_3 [14]. The effect of pH on the kinetics of TM formation will be discussed in more detail in section 3.2.

The final factor that influences the extent of the TM formation reaction is reaction time. Even though reaction conditions may favor the formation of TM3 or TM4, they must still be allowed time to form. Conversely, even if TM1 is the favored product, TM2 will inevitably form given enough time. Therefore, the reaction time must be carefully adjusted to coincide with the desired product and reaction conditions used.

1.5 PREVIOUS THIOMOLYBDATE STUDIES

1.5.1 Thiomolybdate Characterization Techniques

Although the TMs have all been successfully synthesized, quantification and characterization have been ongoing challenges. The sequential nature of TM formation during synthesis leads to the inevitability of cross-contamination. Therefore, a reliable means of confirming the purity of TM samples, or at least, quantifying the composition of impure samples is required. Several methods have been used toward this goal with varying degrees of success.

1.5.1.1 Elemental Analysis

Elemental analysis has traditionally been the front line analytical technique used for establishing purity [7, 20, 25, 26]. However, elemental analysis only gives the overall percentage mass of individual elements; there is no provision for speciation. It is easily shown, to take an extreme example, that an equimolar sample of the sodium salts of TM2 and TM4 would give rise to exactly the same elemental analysis as an absolutely pure sample of the sodium salt of TM3. Given the sequential nature of TM formation, this is exactly the type of contamination which might be expected. It is obvious, therefore, that contamination of a TM3 sample by equimolar amounts of TM2 and TM4 - to any degree - would go undetected by elemental analysis. If different amounts of TM2 and TM4 were present in an impure TM3 sample, elemental analysis would suggest that only one contaminant (the more abundant one) existed, and to a smaller extent than the actual. We conclude that elemental analysis is of severely

limited use in determining the purity of these closely related, potentially cross-contaminated species.

1.5.1.2 ^{95}Mo NMR

^{95}Mo NMR is a potentially useful means of measuring TMs. Spectra were first acquired by Kroneck et al. [27] and predicted theoretically by Yu-ming et al. [28]. For a detailed discussion on the NMR properties of group 6 metals, see the review by Minelli et al. [29]. Some aspects of ^{95}Mo NMR were also discussed in section 1.3.

The distinct advantage of ^{95}Mo NMR is the excellent resolution. TM0 serves as the reference compound with a single peak at 0 ppm. With each substitution of a sulfur ligand there is a shift of approximately 500 ppm downfield as shown in Figure 1.4 [24]. The TM peaks are very sharp which is perhaps surprising. With a nuclear spin of 5/2, ^{95}Mo has a quadrupole moment. As discussed in section 1.3, this contributes to line broadening. Counter to this, though, the regular tetrahedral geometry and high level of symmetry, especially with TM0 and TM4, reduces the broadening effect. At first glance, this appears to be a very attractive technique for studying thiomolybdate mixtures. Upon closer inspection, however, there are some crucial disadvantages that prevent this from being a powerful quantitative tool.

The receptivity of a nucleus (how easy it is to acquire an NMR spectrum) is related to magnetogyric ratio (γ), the natural abundance (N) and the nuclear spin (I) and is proportional to $\gamma^3 NI(I + 1)$. ^{95}Mo has a natural abundance of 15.92 %. This falls well short of the near 100 % abundance of ^{1}H but is significantly greater than the 1.1 % abundance of ^{13}C. The nuclear spin of ^{95}Mo NMR is 5/2, compared with a spin of 1/2 for both ^{1}H and ^{13}C. The magnetogyric ratio for ^{95}Mo is -1.75 versus 26.75 and 6.73 for ^{1}H and ^{13}C, respectively [8]. Overall, the receptivity of ^{95}Mo is about three times greater than ^{13}C but more than 1000 times less than ^{1}H. A typical ^{13}C spectrum might take an hour or more to acquire. This may be lowered to several minutes at high concentrations. This suggests that it would also take several minutes and high concentrations to acquire

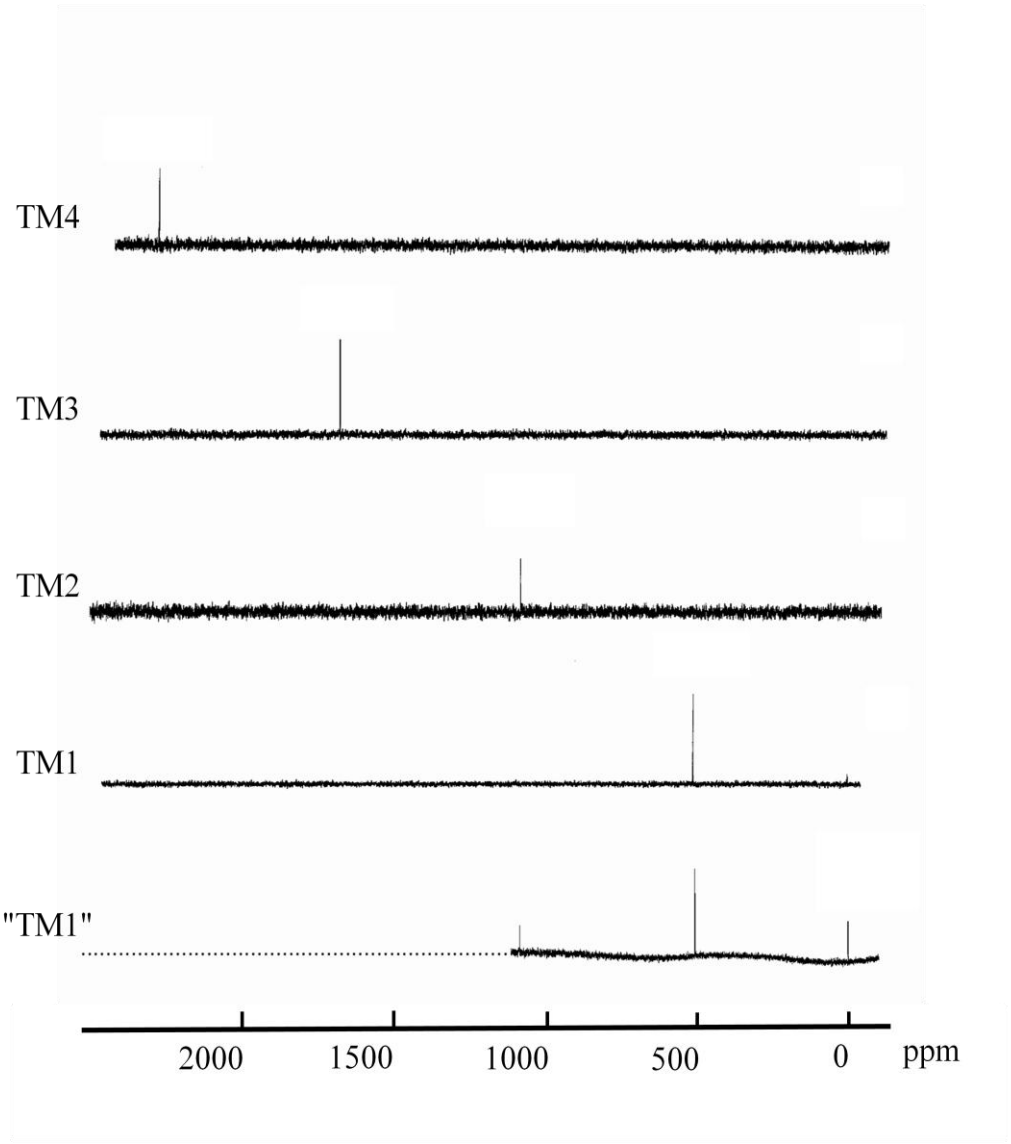

Figure 1.4. ^{95}Mo NMR spectra of the TMs. The "TM1" spectrum is for an impure TM1 sample.

a ^{95}Mo NMR spectrum. In practice the total acquisition time is typically between 5 and 20 minutes [24]. This would be sufficient time for hydrolysis to occur, especially in the case of TM1 and TM2 [26].

The sensitivity, which depends on the magnetogyric ratio, of a particular nucleus refers to the expected signal to noise ratio that would be expected in the NMR spectrum. Compared to ^{1}H, which is given a sensitivity of 1, ^{13}C has a sensitivity of 1.6 x 10^{-2}

while ^{95}Mo has a sensitivity of 3.2 x 10^{-3}. So even though the receptivity of ^{95}Mo NMR is greater than ^{13}C, its sensitivity is somewhat less. The low sensitivity means that a greater time is required to get a baseline resolved signal. This is particularly a problem for the contaminant species which may only comprise a couple of percent or less of total TM in the sample. In other words, the abundant species may give an adequate signal in a couple of minutes but it will take significantly longer to identify the contaminant(s).

If the TMs were stable in water, the ^{95}Mo NMR solvent, quality spectra could be obtained simply by longer acquisition times. However, the TMs hydrolyze in aqueous solution and so time is of the essence. Normally, one way to acquire quality spectra faster is to increase the TM concentration (~ 0.1 M). Increasing the concentration, though, increases the rate of hydrolysis. Once hydrolysis occurs, the resulting spectrum is no longer representative of the original sample. The combination of low sensitivity and the instability of the TMs in aqueous solution makes ^{95}Mo NMR inadequate for quantitative TM analysis.

1.5.1.3 UV-Visible Spectroscopy

UV-visible spectroscopy is advantageous because it is a simple, rapid technique that can measure relatively low concentrations with a high degree of precision. Absorbance measurements can then be readily related to concentrations making quantitative analysis easy. Also, absorbance measurements are additive. If two species with overlapping spectra were present in solution, the fraction of each can be determined if the individual pure spectra are known.

UV-visible spectroscopy has been the most common technique used to date for analyzing the TMs in solution. The region between 250 and 500 nm is most commonly studied and each TM has a characteristic UV-visible spectrum. Figure 1.5 shows the UV-visible spectra of the TMs as determined by Erickson and Helz [30]. This clearly

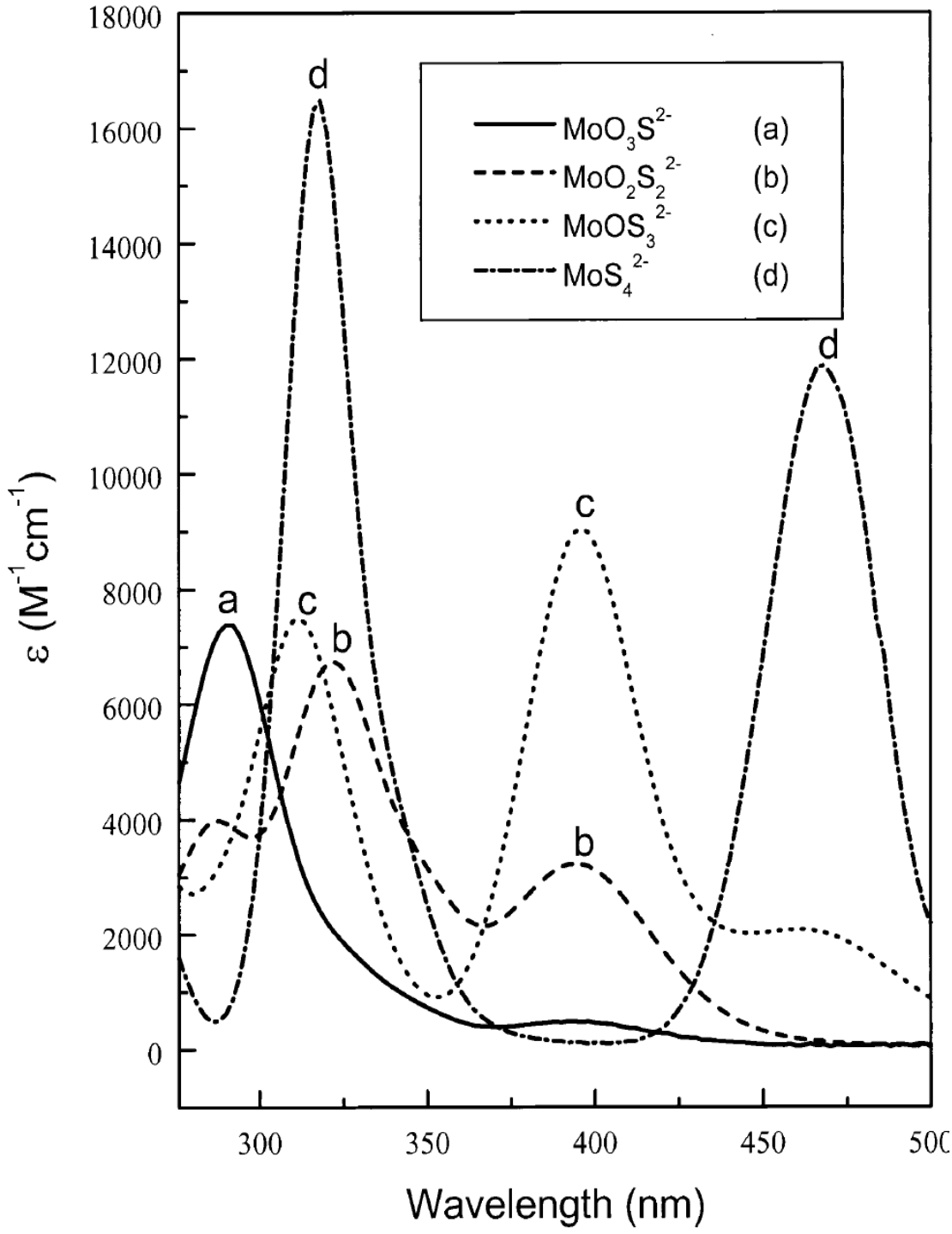

Figure 1.5. UV-visible spectra of the TMs From Erickson and Helz, 2000 [30].

shows the ubiquitous overlap throughout the region of interest. In order to utilize this technique, then, the pure spectra of the TMs must be known with certainty. As discussed in section 1.4.2, the nature of TM synthesis makes the synthesis of pure TMs difficult, if not unlikely. Therefore, simple measurement of the UV-visible spectrum of a synthesized TM is insufficient for establishing the identity of the pure TM's spectrum. In an attempt to circumvent this, elemental analysis was typically performed first in order to establish the purity of the sample. The UV-visible spectrum was then characterized by direct measurements. The limitations of using elemental analysis to establish TM purity were discussed in section 1.5.1.1.

Bernard and Tridot identified TM2, TM3 and TM4 in solution by UV-visible spectroscopy from the reaction of TM0 and H_2S in 1961 [31, 32]. Muller et al., in 1968, were able to synthesize and isolate these salts [33]. Aymonino et al. established the existence of TM1 in 1969 by observing absorption bands in solution as it formed from TM0 and H_2S [34]. TM1, however, was not isolated in solid form until 2002 by Quagraine [24].

Until then, the molar absorptivity had only been inferred during its formation in solution. Muller et. al. were the first to determine molar absorptivities for the TMs [35]. From then on, various workers have attempted to refine these values as shown in Table 1.1. Note that this is a representative sample including the key players and not an exhaustive list.

It is readily apparent looking at Table 1.1 that there is uncertainty amongst not only the published molar absorptivities but also in the λ_{max} values. The variable absorptivities alone suggest that samples of dubious purity were used for their determination. Where there is some agreement, for example between Erickson et al. and Quagraine, it is typically to not more than two significant figures. Because of the magnitude of the molar absorptivities, small differences in absorbance are likely to have significant effects on the TM concentration that would be calculated. This limits the level of quantitative analysis that can be performed using these values.

Perhaps more telling of impure TM samples is the λ_{max} values. Inspection of Figure 1.5, especially around 300 nm, shows that there are many peak maxima in a very narrow range. Small amounts of contamination from other TM species may not be readily observed in the absorbance spectrum. However, small shifts in the observed peak maxima may occur. The variability of the reported λ_{max} values is therefore an indicator of the use of impure samples. So now the question arises, who, if any of them, are right? Further examination of the methods that each of them used to determine these values is warranted.

Muller et al. were the first to isolate (except TM1) and characterize the TM series [35]. Initially, the identity of the TMs was determined by crystal structures and infrared (IR) spectroscopy. The shortcomings of IR spectroscopy and x-ray crystallography will be discussed in section 1.5.1.4. From here, the UV-visible spectra were measured and the molar absorptivities were determined. These results served as the standard for TM purity until only recently even though the purity of their samples were not accurately established. Also, the primary focus of Muller et al. was on structural aspects of the TMs. As such, the absorptivities were not determined to the high level of accuracy required for quantitative analysis. This is demonstrated by the fact that most of their values are known only to one significant figure. These molar absorptivities are therefore in question because of the uncertain initial purity of the compounds and the limited accuracy of the results.

Clarke and Laurie first established the purity of their synthesized TMs by elemental analysis and infrared (IR) spectroscopy [25]. The shortcomings of IR spectroscopy will be discussed in section 1.5.1.4. To some degree as well, purity was based on inspection of the UV-visible spectra as they state that these were "satisfactory". It is unclear, however, what this is relative to. Also, this list is incomplete due to the absence of TM1 absorptivities. The molar absorptivities from this work fall into question based on the uncertainty of the original sample purity.

Brule et al. determined molar absorptivities, primarily, for TM2 and TM4 [6]. The quality of the values they produced were deemed satisfactory based on agreement with literature values including those of Muller et al. Furthermore, this agreement was, at best, to the first significant figure in all cases. This list is incomplete as TM3 was not characterized. Also, curiously, the TM4 peak at 316 nm not was measured and only a minor TM1 band at 319 nm was recorded. The results from this work are uncertain since quality was based on comparison to other uncertain works.

Erickson and Helz determined molar absorptivities from Beer's Law curves using synthesized samples [30]. The resulting absorptivities were then compared to literature values in order to establish quality. The TM1 spectrum was characterized during its formation in solution [36]. These workers do acknowledge that the absorbance at 290 nm will be due "mostly" to TM1 and that the small peak observed at 314 nm may be due to small amounts of TM2. These results are uncertain based on the uncertainty of the initial TM purity.

Quagraine was the first to look at characterizing the UV-visible spectra of the TMs with no assumption as to the initial sample purity [24]. This method is discussed briefly in section 1.7.2. Quagraine used a non-linear least squares approach in which calculated absorbances were fit to the experimental ones. TM absorptivities at six wavelengths, along with the molar fraction of the TMs expected to be present, were optimized using the "goal seek" method in Microsoft Excel®. The fit was considered optimized when the total difference between the calculated and experimental absorbances were at a minimum. The limitation with this method is that each parameter is optimized individually. With each new adjustment, previously adjusted parameters can be further optimized and so forth. The endpoint of this fit is somewhat subjective as the value of each parameter is dependent on all the rest. This method provides the most certainty of those described but can be improved upon due to the method of fitting.

Overall, the characterization of the UV-visible spectra of the TMs has been limited by the initial uncertainty of TM purity in combination with extreme spectral

Table 1.1. Molar absorptivities (M^{-1} cm^{-1}) determined by various workers.

	Muller et. al. [35]		Clarke et. al. [25]		Brule et. al. [6]		Erickson et. al. [30]		Quagraine [24]	
	λ (nm)	ε	λ (nm)	ε	λ (nm)	ε	λ (nm)	ε	λ (nm)	ε
TM1	290	8000	288				290	7390	290	7000
	314	3000	392		319	2400	314	2900		
TM2	290	3000	288	2900	288	3800	290	3940	287	4100
	322	6000	322	6400	319	7900	322	6740	322	6800
	394	3000	394	2900	394	3500	394	3230	395	3200
TM3	312	6600	315	8400			312	7500	312	7800
	396	8700	398	8100			396	9030	396	9000
	462	2300	465	1400			462	2080	461	2100
TM4	318	18000	318	16600			318	16480	316	15900
	468	13000	470	11800	463	11800	468	11870	468	11700

overlap. As demonstrated by the work of Quagraine, though, modern computing technology provides new hope for precise, accurate characterization once and for all.

1.5.1.4 Other Methods

Infrared spectroscopy has been used to study the electronic structure of the TMs. The IR band positions of the TMs are summarized in reviews by Muller et al. [9] and Laurie [11]. Each TM has a characteristic spectrum. However, they differ only by the addition of one peak per added sulfur ligand with all other peaks appearing at the same point as the previous TM. In other words, the spectrum of TM2 would be completely enclosed within the TM3 spectrum. As such, it would not be feasible to use this as a method to determine the composition of a mixture.

The resonance Raman spectra of the tetraphenylphosphine salts of TM3 and TM4 are shown in a review by Muller et al. [9]. These spectra are nearly identical and as such would not be an effective means of distinguishing between TMs in a mixture.

Quagraine attempted to use electrospray mass spectrometry (ESMS) to ascertain the purity of TM samples [24]. The high temperatures (up to 350 ºC) caused the TMs to decompose, apparently into the lower TMs. This technique was unsuccessful for this purpose.

X-ray crystallography has also been used as an indicator of purity, particularly by Muller et al. [35]. Although, this is a useful technique for structural purposes, it does not unequivocally confirm the purity of a species. Thome used x-ray crystallography to determine TM structures [10]. Using the methods of Quagraine [24], it was determined, for example, that TM2 was 95 % pure and TM3 was 94 % pure. This technique is therefore inadequate for quantitative determinations of purity.

1.5.1.5 Other Separation-based methods

Size exclusion column chromatography has been shown to be of some use in purifying TMs [24]. Identification of the various species is facilitated by the difference in color. One limitation is the amount of time that the sample stays dissolved in water before it can be eluted from the column and isolated. In the case of TM4 and TM3, significant hydrolysis is not likely to occur but for TM2 and TM1, the purification is counteracted by hydrolysis that occurs during the process.

It is also possible that a sufficiently rapid separation-based method, such as Capillary Electrophoresis, could succeed for TM analysis. This has not been reported, however, probably since (see above) simple UV-visible analysis is perceived, rightly or wrongly, as giving satisfactory results.

1.5.2 Thiomolybdate Kinetics

As will be discussed in section 1.5.5, different TM species are known to interact differently with Cu *in vivo*. TM3 and TM4 are believed to be the major Cu antagonists while TM1 and TM2 are expected to have little effect [37-39]. TM3 and TM4 are, however, expected to be formed from the lower TMs, TM1 and TM2 [40]. Therefore, an understanding of the rates at which the various TM species form, interconvert and react with Cu is extremely important. This information can then be used to assist in the modeling of Cu speciation in the rumen (section 1.7).

As previously discussed (section 1.4), in the presence of sulfide, O ligands of the molybdate ion are successively replaced by S to form the final product of TM4. The factors that affect the extent that this process occurs were discussed previously in section 1.4.2. Conversely, in aqueous solution, TMs will hydrolyze at an increasing rate back to TM0. The complete TM interconversion scheme is shown below:

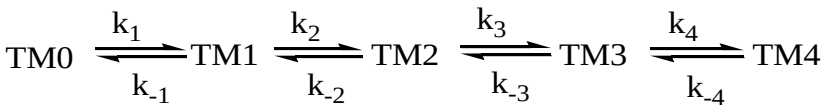

The kinetics of TM interconversions have been studied by a number of workers using UV-visible spectroscopy and under a variety of condition. However, there are four main problems that arise in the literature.

1. Kinetics have been performed on single, isolated processes. For example, k_3 would be measured by reacting TM2 with sulfide and monitoring TM3 formation. This was made necessary by the complexity of the reaction scheme. However, given the complexity of the reaction scheme, it is very unlikely that a single process can be isolated. This is especially the case when measuring the hydrolysis processes. Clarke and Laurie demonstrated that when TM2 is allowed to hydrolyze in aqueous solution, there is, in fact, some formation to TM3 that also occurs [25]. This assumption therefore limits the accuracy of the results.

2. TM interconversions have been monitored at a single wavelength. Because of the extensive overlap of the TM spectra (see Figure 1.5, section 1.5.1.3), it is difficult to find a suitable wavelength (if one exists) to monitor a specific process. Ideally, only the two TMs of interest (reactant and product) would absorb at the selected wavelength. Then knowing the absorptivities (see problem 4.) the concentrations could be calculated and the rate constant determined. If a secondary reaction occurs, though, there may be a third absorbing species which increases the error in the calculated concentrations (see section A1.1). If the third species absorbs elsewhere, the TM concentration represented at the measured wavelength is different from the initial TM concentration. It will also be unknown since the third species will not be quantified. Since the total TM concentration must be known to elucidate the concentration of each species, the concentrations would be in error. The rate constants determined from this data would also be in error.

3. The TM samples used in the kinetic experiments are of uncertain purity. If one is determining the various rate constants separately, pure TM starting materials are required. The successive nature of TM formation dogs the synthesis of pure TM samples (section 1.4.2). The presence of contaminants in the original sample will affect the result. In addition, new processes are introduced by the presence of other TMs. This issue relates to problem 1. in that if the synthesis of TMs under carefully controlled conditions inevitably results in cross-contamination, then surely under other conditions, multiple processes must be occurring.

4. The purity of the TM samples used was ineffectively determined. This issue was described in-depth in section 1.5 and ties in closely with problem 3. In this case, a sample may be considered pure based on the methods available. In fact, for the reasons discussed in section 1.5, this may not be true. TMs may falsely be considered pure but this uncertainty casts a shadow over the subsequent kinetic measurements.

TM kinetics have been studied by various groups in the literature. Each study contains one or more of the problems described above. Muller et al. first looked at TM kinetics in terms of their stability. In particular they looked at the rate of hydrolysis of TM4 at acidic pH at 463 nm [41]. Their results are shown in Table 1.2. TM4 is the most stable TM in solution (see section 1.4). Therefore, it will take the most time to hydrolyze. As TM3 forms it will rapidly hydrolyze (relative to TM4 hydrolysis) to TM2

Table 1.2. Rate constants of TM4 hydrolysis determined by Muller et al. [41].

pH	k (min^{-1})
4	1.6×10^{-3}
3	5.6×10^{-3}
2	1.8×10^{-2}

and so on. In this case, multiple reactions would be occurring. Also, a single wavelength was used at which both TM3 and TM4 absorb. The combination of unaccounted for reactions and single wavelength monitoring draws into question the validity of this study. The initial TM purity is not in question since TM4 can be easily synthesized in pure form.

The first comprehensive study of TM interconversion kinetics was performed by Harmer and Sykes [7]. It should first be noted that TM purity was determined by elemental analysis and by direct measurements of the UV-visible spectra. Therefore, the initial TM purity is in question. This study looked at a variety of TM interconversion processes under non-biological conditions. A summary of their results are presented in Table 1.3. The typical conditions used were as follows: pH = 8.2 – 10.2 using an NH_3/NH_4^+ buffer, I = 0.5 M and T = 25 ºC. The rate constants, k_1 and k_{-1} were determined by measuring the absorbance at 292 nm (TMO does not absorb here) until equilibrium was reached. TM1 concentrations were determined from observed molar absorptivities and the equilibrium constant was then calculated. The equilibrium rate constant was also determined from the rate of absorbance change until equilibrium was reached. Values for k_1 and k_{-1} were then calculated. This process relies heavily on the assumption that TM2 does not form. The authors claim that TM2 formation is denoted when the absorbance at 292 nm begins to decrease since it has a lower molar absorptivity at this point. A decrease in absorbance, though, would likely only occur when TM1 formation begins to slow. TM2 may still form and the absorbance at 292 nm would just increase at a slower rate. In fact, the TM1 spectrum presented in this paper shows a small peak at 395 nm. Erickson and Helz, suggested that a peak at 314 nm was likely due to TM2 [30]. It seems likely then that the peak at 395 nm is due to TM2 as well since this species absorbs here.

Harmer and Sykes also determined values for k_3 and k_{-3} by monitoring the absorbance at 393 nm, again, a single wavelength. The absorbance at 393 nm decreased toward equilibrium. The equilibrium constant and k_{-3} were determined and from these, k_3 was calculated. This experiment does not account for further hydrolysis beyond

TM2. It also requires the assumption that H_2S is not lost in the process which would drive the hydrolysis reaction forward. The k_4 and k_{-4} values were determined in two separate experiments. In the case of k_{-4}, further hydrolysis was not considered. The formation of TM4 from TM3 (k_4) requires a pure TM3 sample. The purity of TM3 is in question as described above.

Harmer and Sykes established a first order dependence on Mo for all reactions. For the formation processes and for k_{-3}, a first order H^+ dependence was observed as well. Also for the formation reactions a first order dependence on sulfide. The authors propose that HS^- is the likely form of sulfide since it would be the dominant species at the basic pH studied. Interestingly, a second order dependence on sulfide was seen for k_4 although the authors assumed that it was first order for calculations of the true rate constants. Table 1.3 shows the overall third order rate constants for the formation processes and first order rate constants for the hydrolysis steps. Finally, the authors propose an associative mechanism for the formation reactions. This mechanism was chosen because of the H^+ dependence.

Table 1.3. Rate constants of hydrolysis and formation from the work of Harmer and Sykes. The values are representative of the pH range 8.2 – 10.2 [7].

	Formation (M^{-2} s^{-1})		Hydrolysis (s^{-1})
k_1	4×10^{9}	k_{-1}	6.5×10^{-3}
k_3	1.2×10^{9}	k_{-3}	4.5×10^{-5}
k_4	1.6×10^{6}	k_{-4}	1.6×10^{-6}

Brule et al. studied the rate constants for the six processes between TM1 and TM4 [6]. This work first involved the determination of the three equilibrium constants, K_{12}, K_{23} and K_{34}, referring to equilibrium between TM1 and TM2, TM2 and TM3 and TM3 and TM4, respectively. These equilibrium constants were determined from ^{95}Mo NMR experiments. As discussed earlier, the determination of equilibrium constants

requires the assumption that no unwanted processes are occurring. In addition, the use of ^{95}Mo NMR is ineffective for quantitative TM analysis (see section 1.5.1.2).

The formation of TM4, k_4, was determined at a varying pH (3.88 or 5.70), ionic strength (0.26 or 0.43 M) and temperature of (15 – 45 °C). In this case, a pure TM3 sample is required. In section 1.5.1.3 it was discussed how TM purity was uncertain for these workers. The hydrolysis rate constant, k_{-4}, was then calculated from K_4 and k_4. Based on the suspect nature of K_4 and k_4, k_{-4} will also likely be in error. Similarly, k_{-3} and k_2 were calculated after experiments to determine k_3 and k_{-2} were performed. In both of these cases, the initial TM purity is in question. In addition, the presence of unaccounted for reactions leads to uncertainty. This is especially the case for k_{-2} where further hydrolysis to TM0 is inevitable.

As with Harmer and Sykes, all processes studied were determined to be first order with respect to Mo. A first order dependence for the k_2 and k_3 reactions was also observed for H^+ and sulfide. For k_4 a zero order result with respect to sulfide was observed. Also, a simple first order dependence on H^+ was also not observed. Table 1.4 shows a summary of the rate constants determined in this study. It should be noted that since k_4 has units of s^{-1}, k_{-4}, calculated from K_4 with units of M^{-2}, has units of M^2s^{-1}.

Table 1.4. Rate constants of TM interconversions determined at 25 °C by Brule et al. [6].

	Formation		Hydrolysis
k_2	6×10^8 M^{-2} s^{-1}	k_{-2}	1×10^{-3} s^{-1}
k_3	8×10^6 M^{-2} s^{-1}	k_{-3}	1×10^{-5} s^{-1}
k_4	2×10^5 s^{-1}	k_{-4}	2×10^{-16} M^{-2} s^{-1}

Brule et al. determined an activation entropy ($\Delta S^{\ddagger}$) of -244 J mol^{-1} K^{-1} at a pH of 3.88 and -197 J mol^{-1} K^{-1} at a pH of 5.70 for the k_4 process. For the k_{-2} process, $\Delta S^{\ddagger}$ was

determined to be -212 J mol^{-1} K^{-1} at a pH of 6.9. The magnitude of these values suggested to the workers an associative mechanism with three components in the transition state. The three components for both formation and hydrolysis were postulated as the TM, H_2O and H^+. The mechanism proposed by Brule et al. for k_4 is shown in equations 1.4 – 1.6. Curiously, H_2O is one of the components in the transition

$$MoOS_3^{2-} + H_2O + HA \underset{}{\overset{k_4}{\rightleftharpoons}} H_3MoO_2S_3^- + A^- \quad \textbf{(1.4)}$$

$$H_3MoO_2S_3^- + H_2S \overset{\text{rapid}}{\rightleftharpoons} H_5MoO_2S_4^- \quad \textbf{(1.5)}$$

$$H_5MoO_2S_4^- \overset{\text{rapid}}{\rightleftharpoons} MoS_4^{2-} + H_3O^+ + H_2O \quad \textbf{(1.6)}$$

state, whereas the sulfide reacts later to form a six-coordinate species. This seems implausible from a steric point of view but it is consistent with the zero order sulfide result. It is likely, though, that the zero order result is in error, especially considering Harmer and Sykes found a second order relationship.

The first TM kinetic study to closely mimic rumen conditions was performed by Clarke et al. [26]. Reactions were performed in a 0.1 M phosphate buffer with a pH of 6 – 8 and a temperature of 30 °C. For formation experiments, sulfide was in 100 - fold excess over TM. This is also the first recorded TM kinetic study in which the entire spectrum was monitored. However, rate constants were determined from single wavelengths. A summary of the observed first order rate constants for the processes studied in this work are shown in Table 1.5. The original purity of the TMs was determined by elemental analysis and UV-visible spectroscopy as described in a previous work by Clarke and Laurie [25]. Reasons for the uncertainty of the purity of these compounds were discussed in section 1.5.1.

This study was the first to consider multiple reaction steps simultaneously. The k_3 and k_4 constants were determined from the formation of TM2. Similarly, the hydrolysis of TM2 was monitored to give k_{-2} and k_{-1}. In this case, however, TM3 is

Table 1.5. Rate constants of TM interconversions as determined by Clarke et al. [26] at pH 7.0, and 30 °C.

	Formation (s^{-1})		Hydrolysis (s^{-1})
		k_{-1}	2.4×10^{-3}
		k_{-2}	1.5×10^{-5}
k_3	6.0×10^{-4}	k_{-3}	2.1×10^{-5}
k_4	1.9×10^{-5}	k_{-4}	$< 1 \times 10^{-6}$

known to form [25] but this was not accounted for. Values for k_{-3} and k_{-4} were also determined separately and no further processes were considered. Clarke et al. also support the proposal by Harmer and Sykes that HS^- is the likely nucleophile in the formation reactions.

Erickson and Helz studied TM kinetics under conditions relevant to sulfidic waters [30]. Typical reaction conditions included a temperature of 25 °C, an ionic strength of 0.8 – 2.2 M and a pH of 7.9 – 8.5. They first determined the equilibrium constants, K_{12}, K_{23} and K_{34}. From these, the rate constants were determined. The issues surrounding equilibrium constants were discussed earlier in this section. Furthermore, the uncertainty of TM purity in this work was discussed in section 1.5.1.3. It was also found that the formation reactions were all first order with respect to Mo and sulfide. No pH dependence was found over the admittedly narrow range studied.

These workers claim that a 10 – fold difference in consecutive formation rate constants allows each process to be studied separately. By studying the equilibrium, though, hydrolysis must be considered as well. The rate of hydrolysis must therefore be slow as well. Each consecutive hydrolysis step occurs at an increasing rate. It is therefore unlikely that a simple equilibrium will form between only the two TMs of interest.

By comparing the various kinetic studies, a few commonalities can be found. First, it is universally agreed that these reactions are all first order with respect to Mo and that k_2 and k_3 are first order with respect to sulfide. Also, it has been established that the rate constants of formation decrease with increasing substitution of sulfur while the rate of hydrolysis increases in the other direction.

Conversely, there are a couple of aspects that are still as yet unconfirmed. First, the order with respect to sulfide for the k_4 process has been found to be 0, 1 and 2 by three different workers. Secondly, the form of sulfide in the formation reaction is speculated to be HS^-. This has been generally accepted although Tossell showed computationally that H_2S was most likely [42]. There has been no concrete experimental evidence to confirm this.

The kinetic studies discussed here each contained some of the four main problems outlined above. In particular, single reactions were generally considered despite the inevitability of further processes occurring. In doing so, pure TM samples were required though an accurate means of determining purity was not used. Because of the resulting uncertainty in these works, TM kinetics must be revisited. A new method for establishing TM purity is discussed in section 3.1 while an accurate TM kinetic analysis is presented in section 3.2.

1.5.3 Copper-Thiomolybdate Interactions and Structures

It has been known for some time that TMs, especially TM3 and TM4, are responsible for copper deficiency in ruminants [37, 43] (see also section 1.5.5). However, detailed studies involving interactions between Cu and TMs *in vitro* have only begun relatively recently. These reactions are of interest for their implications toward copper deficiency but also because of similarities with the Fe-Mo-S cluster of the nitrogenase enzyme [44] and the possible use of TM4 as a treatment for Wilson's disease [45].

Studying these interactions has not proved to be a trivial matter. There have been an array of S:Mo ratios reported as well as varying oxidation states of the metal centers. Small changes in reaction conditions greatly affect the product and so there is a plethora of structures reported in the literature. A cross-section of the variation of conditions and the resulting structures will be presented later in this section. For an overview of synthetic aspects of Cu-Mo-S systems as they pertain to copper antagonism in biological systems, see the review by Sarkar and Mishra [46].

Clarke and Laurie were the first to take a detailed look at interactions between Cu and TMs in aqueous solution [47]. They mixed TM4 with Cu in a variety of forms including $Cu^{2+}_{(aq)}$, $Cu(His)_2$, $Cu(EDTA)^{2-}$ and Cu(Albumin). In all cases, except Cu(EDTA) which did not react, a 1:1 Cu:Mo ratio was observed. This was accompanied by a reduction of Cu(II) to Cu(I) as observed by ESR. Also, loss of the UV-visible spectra of TM4 and TM3 was observed, albeit at different rates depending on the form of Cu. The inclusion of a large excess of sulfide did not affect results.

Further study by Laurie et al. in 1986 produced some contradictory results [48]. In this study they claimed a 1.5:1 Cu:Mo molar ratio in the product. This was based on the amount of Cu required for complete spectral loss of TM4. They also discovered that two different compounds were formed depending on the ratio of reactants used. When Cu and Mo were mixed in a 1:1 ratio, a microcrystalline solid with formula NH_4CuMoS_4 was attained. In this case Cu was present as Cu(I) and Mo as Mo(VI). The second compound resulted from the mixing of higher Cu:Mo ratios. The result was an amorphous solid with the formula $CuMoS_4O_x$, where x = 2-3. The oxygen was absorbed from the air after the product was isolated. In this case, Cu(I) was still present but Mo now appeared as Mo(V).

Clarke et al. then looked at the reaction of thiomolybdates with copper in the presence of bovine serum albumin and metallothioneins [49], the primary Cu transport and storage proteins in bovine. They found that TM4 can bind directly to albumin with no Cu present. This binding is weak, however, as no change in the TM4 UV-visible

spectrum is observed. When TM4 was reacted with Cu-albumin there was a loss of the TM4 spectrum and a concomitant loss of the Cu(II) ESR signal. The product was found to be 1:1 in Cu:Mo and no precipitate formed. Reactions with TM4 and Cu(I)-thionein produced the same loss of UV-visible spectrum. In this case, though, a 2:1 Cu:Mo ratio was found. When TM2 or TM3 were used, a 1:1 ratio was found.

This study indicates that Cu antagonism by TM4 occurs despite Cu being bound to carrier proteins. A similar study was performed by Sarkar and Mishra who indicated that CuS would form long before TM4 could be formed from TM0. Their studies showed that TM4 solubilized CuS and reformed as a Cu-TM4 moiety [50]. This was isolated as a triphenylphosphine salt.

When examining the black amorphous precipitate that results from the Cu(II) reaction with TM4 by EXAFS, Ecclestone et al. found a 1.6:1 ratio [51]. This product was not soluble in common solvents which led these workers to suggest a polymeric species. EXAFS analysis also confirmed the Cu(I) and Mo(V) oxidation states found by ESR and also found S radical centers. This is the first report, though, to show that TM4 is not retained in the final structure. Instead an MoS_3 moiety was found.

These studies by the Laurie and his coworkers provided the first *in vitro* look at Cu-TM interactions in regards to copper deficiency in ruminants. They demonstrate the variability of the products and difficulty in ascertaining concrete results with the system.

Another area in which there is interest in Cu-TM interactions is the treatment of Wilson's disease. Wilson's disease is caused by copper poisoning resulting from a disruption in copper transport [45]. Treatment for this disease is typically by chelators. TM4 is gaining promise for this purpose because of its high affinity for Cu. A series of studies were done on rats with Wilson's disease [52-54]. TM4 selectively removes Cu bound to metallothionein and is excreted into the bile and blood. The molecular basis of

this Cu sequestration has been examined by George et al. using EXAFS [55]. This study is discussed in more detail below.

Aspects related to Cu-TM adducts under rumen-like conditions are summarized in a review by Laurie [11]. In general, under these conditions the Cu:Mo ratio is thought to be between 1:1 and 2:1 with the metal centers being Cu(I) and Mo(V). Typically, these adducts form a black precipitate that is believed to result from polymerization [51]. Some possible structural motifs are shown in Figure 1.6.

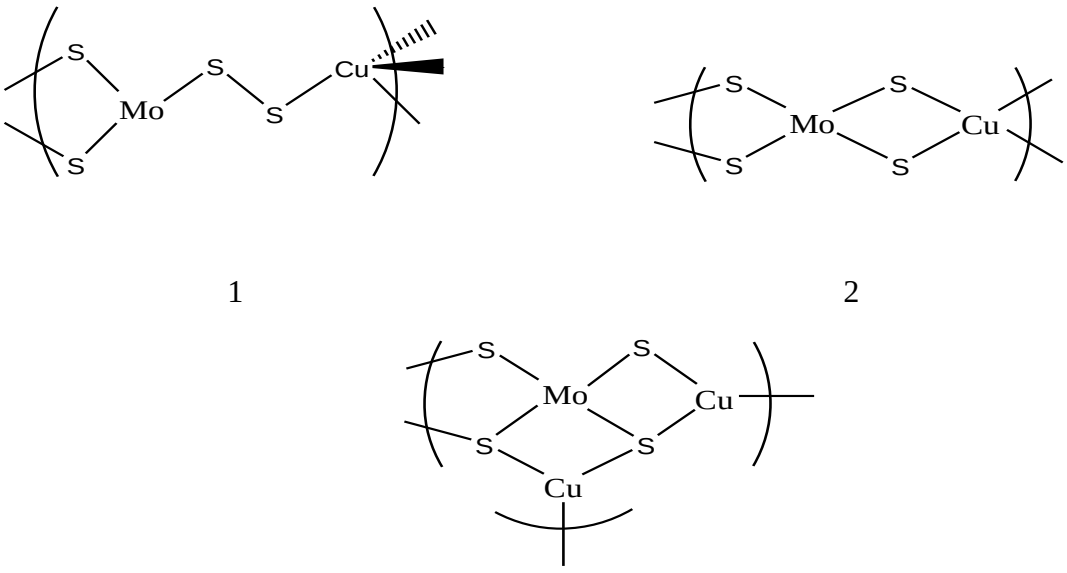

1 2

3

Figure 1.6. Some possible Cu-Mo adduct structures. Structure 1 reproduced from [51]. Structures 2 was adapted from [46]. Structure 3 was obtained from [55].

Under different conditions, however, the products can change drastically. Such conditions include the use of a Cu(I) starting material, different starting Cu:Mo ratios or the use of various organic ligands. A vast array of Cu-TM adducts have appeared in the literature.

In the previous section, structures related to Cu-TM interactions in the rumen were described. These involved the use of Cu(II) starting materials as this is the typical form of copper ingested. A couple of other examples of Cu(II) starting materials are provided by Muller et al. [56] and Gheller et al. [57].

Muller et al. mixed TM3 in a 2:1 ratio and TM4 in a 1:1 ratio with $CuCl_2$, both in the presence of triphenylphosphine (PPh_3). This resulted in a variety of products including $(Cu_3MoS_3Cl)(PPh_3)_3X$ and $Cu_4Mo_2S_6(PPh_3)_4X_2$ cage compounds, where X = O or S. They also found the linear products; $(PPh_3)_3Cu_2MoS_4$ and $(PPh_3)_4Cu_2MoS_4$ [56]. These products are very diverse in terms of structure and Cu:Mo ratio, further exemplifying the complexity of this system.

Gheller et al. reacted Cu(II)MoS_4 with KCN in a 1:1 ratio in the presence of n-Pr_4N_4Br to give $(n\text{-}Pr_4N_4)_2[(CN)CuS_2MoS_2]$ and in a 2.5:1 ratio with Ph_4AsBr to form $(Ph_4As)_2[(CN)CuS_2MoS_2Cu(CN)]\cdot H_2O$ [57]. It is interesting to note that in this case the Cu:Mo ratio changed due to the increase in KCN excess and not as result of changing the reagent Cu:Mo ratio. A similar reaction involving TM3 and $CuSO_4\cdot H_2O$ with one equivalent if KCN in the presence of Et_4N produced $(Et_4N)_2[(CN)CuS_2MoOS]$.

Many other studies involve the use of Cu(I) starting materials or Cu(II) compounds in conjunction with a reducing agent [58]. In this case, $Cu(NO_3)_2$ was the copper source and Et_4NBH_4 was added as a reagent. Often times, the Cu:Mo ratio of the product resembles the ratio of Cu:Mo in the reaction mixture. For example, Zhang et al. mixed Cu and Mo in a 4:1 ratio [59] and in a 3:1 ratio [60] and obtained $\{[Et_4N]_2[MoS_4Cu_4(CN)_4]\}_n$ and $[MoOS_3Cu_3(4\text{-pic})_6]Br$, respectively. Similarly, Sadr et al. used a 4:1 ratio with different ligands to give a $(NEt_4)_2[MoS_4(CuBp)_4]$ product [61]. Li et al. focused on TM3 structures by reaction with $CuSBu^t$. A 2:1 starting ratio gave a 2:1 butterfly structure while a 3:1 mixture gave a double incomplete cubane of Cu:Mo 3:1. A second 3:1 structure resulted in an attempt to incorporate Cd. This was an overall 9:3 cluster compound [62].

Some other examples do not show this same continuity between input and product S:Mo ratios. Guo et al. reacted copper and TM4 in a 2:1 ratio with Cu(I)Br and $(n\text{-}Bu)_4NBr$ to give $[(n\text{-}Bu)_4N]_4[Mo_4Cu_{10}S_{18}O]\cdot H_2O$, a 2.5:1 ratio [63]. The use of TM3 gave a similar result. An atypical example was provided by Hou et al. in which TM2 was the Mo source. This was reacted with CuCN in a 2:1 ratio with pyridine (py) containing small amounts of benzene. The result was $\{[MoOS_3Cu_3(CN)(py)_3]\cdot 0.5C_6H_6\}_n$ containing a 3:1 ratio [64]. The curious result here is that despite a TM2 reagent, there is a TM3 moiety present in the final structure. The most extreme example of ratio inequality was displayed by Wu et al. who produced the cluster compound, $(Et_4N)_4[MoS_4Cu_{10}Cl_{12}]$ from a 4:1 mixture of CuCl and TM4 with Et_4NCl [65].

An example of *in vivo* structural determination was provided by George et al. [55]. LEC rats with Wilson's disease were treated with TM4. The livers were then examined by EXAFS to elucidate the adduct structure. The product, $[(HSCu)_3S_4Mo]^{2-}$, was found with the external ligands being assumed to be HS^- groups. This example provides evidence for TM4 selectively sequestering Cu and the 3:1 ratio helps provide information about the efficiency of TM4 as a drug for Wilson's disease. Finally, it shows the value of EXAFS for providing detailed information from complex, untreated sample.

Commonly, the organic ligands terminate the growth of these adducts. In rumen studies, it seems likely that polymeric compounds form. Many of these studies result in the formation of single units. None-the-less they provide some insight as to the possible structures that may form. Recently, work in our lab on these adducts under rumen-like conditions was performed by Slamova and will be discussed in section 1.7.4.

1.5.4 Molybdenum Antagonism of Copper in Ruminants

Scouring, today, is known to be a symptom of Cu deficiency and carries with it conditions like diarrhea and paleness of coat. This connection was made by Brouwer et

al. in 1938 when they found that a Cu containing supplement prevented and cured scouring [66]. Mo was first linked to Cu deficiency by Ferguson et al. in 1943 [67]. Herbage from two different farms both contained similar, sufficient levels of copper. Still, cattle on one farm scoured while cattle on the other were healthy. An analysis of the feed showed high Mo content in the feed from the pasture containing the scoured cattle and very low Mo levels in the other.

Dick later confirmed the effect of Mo on Cu levels in the liver [68]. Further study, though, showed that two groups of cattle fed different feeds but with the same amount of Cu and Mo supplemented (Cu and Mo were not present in the feed), had different liver Cu levels. They postulated that there was a third factor that contributed to Cu deficiency. Analysis of the feeds suggested that the third factor was sulfate and further feed studies confirmed this [69]. This is the first mention of a three-way link between Cu, Mo and S.

Confirmation of the cause of copper deficiency prompted studies on cattle in areas showing symptoms. These studies correlated clinical signs with the composition of herbage in the area, particularly Cu and Mo [70-72]. Other studies focused on the effects of Cu supplementation to deficient animals [73-76]. Supplementation of Cu often results in complete recovery and removal of symptoms. Another area of study involved monitoring Cu distribution and metabolism in the animal as Mo and S intake changed [77-80].

Copper-molybdenum antagonism was examined in non-ruminants such as rats [81, 82], rabbits [83] and guinea pigs [84]. Relative to non-ruminants, much lower dietary levels of Mo were required for ruminants to experience adverse effects. Dowdy and Matrone in 1968 confirmed from a comparison of sheep (ruminant) and chicks (non-ruminant) that indeed ruminants were far more susceptible to Mo induced Cu deficiency than non-ruminants [85]. During their study, the formation of a Cu-Mo complex *in vitro* was observed. Job's method experiments showed a 4:3 Cu:Mo ratio but a structure was not obtained. Further studies by Dowdy and Matrone using radio-

labeled Cu and Mo showed that the formation of the Cu-Mo complex rendered Cu unavailable for ceruloplasmin synthesis [86].

The Cu-Mo complex created by Dowdy and Matrone contained no S despite the fact that SO_4^{2-} has been shown to play a role *in vivo*. A greater focus on the role of S was necessary. In the rumen, microorganisms reduce inorganic sulfur to sulfide. It has been proposed that sulfide affects the availability of Cu [87]. By using active rumen microorganism suspensions, Huisingh and Matrone were able to show that MoO_4^{2-} inhibits the reduction of sulfate to sulfide [88]. This appears to be in contradiction with evidence supporting Mo and S induced copper deficiency. But a later study by Huisingh et al. showed that while sulfate reduction decreased, reduction of methionine increased. Also, over time, sulfide production gradually recovered [89]. Gawthorne and Nader later confirmed the effects of MoO_4^{2-} on sulfate reduction in an in-depth study of S conversion and flow in the rumen. However, despite the rate of sulfide production decreasing, the sulfide concentration in the rumen increased [90]. Despite the initial apparent benefit of Mo on Cu deficiency, the overall effect is that Mo is still a contributor to it.

The effect of sulfur on Cu was further examined by Suttle under the hypothesis that insoluble CuS forms, Cu becomes unavailable for absorption [91]. Organic and inorganic S were both effective in reducing plasma Cu (indicative of reduced absorption). In addition, Cu given as CuS did not improve blood Cu levels but Cu as $CuSO_4$ did. CuS being insoluble would never be available for absorption while $CuSO_4$ is soluble allowing labile Cu species to exist in the aqueous phase. Also, dietary S did not affect the Cu status when the rumen was bypassed. This indicates that reduction to sulfide is necessary for Cu levels to be depleted. Suttle and Field followed this up by showing the effectiveness of Cu supplements given by injection instead of through the diet [92].

Much of the work done to this point is culminated in review by Suttle [93] and it is apparent that a great deal of uncertainty remained. Dick et al. then proposed in 1975,

for the first time, the formation of thiomolybdates as a precursor to Cu deficiency [43]. Thiomolybdates and their interactions with Cu had been studied previously in other fields (see section 1.5.3). In this study, they were now applied *in vivo*. Supplementing synthesized thiomolybdates produced the same effects on blood Cu as Mo and S fed separately. They therefore proposed that thiomolybdates formation must occur first followed by complexation with Cu to form the insoluble Cu-TM product. To this day, this is the universally accepted mechanism for Mo induced Cu deficiency.

1.5.5 *In vivo* studies

1.5.5.1 Evidence for the formation of thiomolybdates *in vivo*

The formation of an insoluble Cu:Mo complex as suggested by Dowdy and Matrone (section 1.5.4) does not account for the role of S in Mo induced Cu deficiency. Similarly, the formation of insoluble CuS does not coincide with the fact that S and Mo together produce a compounded effect. The thiomolybdate theory established by Dick et al. [43] reconciles these discrepancies in the literature [94]. In 1981, Mason then suggested the mechanism for this antagonism: that once thiomolybdates form in the rumen they will react with Cu to form insoluble complexes that are excreted in the feces. Remaining thiomolybdate can absorb into the blood and tissues where they can further disrupt Cu functions [95]. This may occur due to TMs binding with various proteins thereby creating unnatural binding sites for Cu [96].

The discovery by Dick et al. that thiomolybdates are a necessary precursor to the Cu-Mo-S antagonism relied heavily on blood Cu analysis [43]. Normally, Cu found in blood plasma is associated with the carrier protein ceruloplasmin. This Cu can be recovered from ceruloplasmin *in vitro* by dissolving it in trichloroacetic acid (TCA). However, in blood drawn from animals fed MoO_4^{2-} and SO_4^{2-}, Cu is largely found in the TCA insoluble fraction. Similarly, if thiomolybdates are added *in vitro* to plasma, Cu is increasingly found in the TCA insoluble fraction. Addition of MoO_4^{2-} and SO_4^{2-} separately to plasma has no effect on solubility. A similar experiment performed in vivo

showed that TM4 given intravenously increased amount of Cu in the TCA insoluble fraction while MoO_4^{2-} given intravenously did not have this effect. Therefore, TMs and MoO_4^{2-} affect Cu availability by reducing the amount of Cu complexed with ceruloplasmin.

Further indirect evidence for the presence of thiomolybdates was provided by Grace and Suttle [97]. They found that varying S intake affected the metabolism and absorption of Mo. When high levels of S and Mo were supplemented, a poorly exchangeable Mo complex was formed that was poorly absorbed and poorly excreted. This complex is presumed to be thiomolybdate.

The rumen was suggested to be the locale for thiomolybdate formation since Cu-Mo antagonistic effects are reduced when it is bypassed [93]. Dick et al. showed that when TM4 was administered directly into the duodenum (downstream of the rumen) the TCA insoluble Cu fraction increased. On the other hand, when MoO_4^{2-}, with or without SO_4^{2-}, was added to the duodenum there was no effect on blood Cu [43]. These findings indicate the importance of the rumen to Cu antagonism.

The specificity for thiomolybdate induced Cu deficiency in ruminants was advanced by comparisons with non-ruminants. Rats were fed diets of either MoO_4^{2-} and SO_4^{2-} or Mo as thiomolybdate. The rats fed thiomolybdate showed the same scouring seen in ruminants with Cu deficiency while rats fed only the Mo and S precursors showed no symptoms [43]. Non-ruminants do not have the same capacity as ruminants for reducing various forms of S to sulfide. This reduction, which occurs in the rumen, must be necessary for thiomolybdate formation *in vivo*.

To establish more directly that thiomolybdates form in the rumen, MoO_4^{2-} and SO_4^{2-} were added to a solution containing rumen micro-organisms. From this solution the absorbance spectra of TM2, TM3 and TM4 were observed [43]. This indicates that first, SO_4^{2-} must be reduced to sulfide, as HS^- and H_2S, and second, that thiomolybdates are formed in the rumen. Mills et al. made a similar observation but were only able to

observe TM2 and TM3. They estimated that TM4 would only be detected at unreasonably high Mo levels [98]. Based on *in vitro* solution studies that did not contain rumen micro-organisms, Clarke and Laurie concurred that TM4 is unlikely to form significantly unless high S:Mo ratios were used and after long reaction times [25]. Bray et al. did, however, observe the formation of TM4 in rumen cultures. In fact, as much as one third of the Mo was present as this species with less than a 10:1 S:Mo ratio used [99]. This suggests that results may vary when rumen micro-organisms are or aren't used. Another limitation is that these studies focused on the aqueous phase while *in vivo* rumen Mo is predominantly found in the solid phase [97]. The make-up of the solid phase is discussed in section 1.6.2.

Although Dick et al. and Bray et al. reported the formation of TM4 in their experiments, it is unclear how long it took to form. Mills et al. showed that TM4 was detected after 18 hours of incubation. If similar time spans were used in these other studies, this may be the reason for TM4 being observed. Regardless, TM2 and, especially, TM3 are typically present in the greatest amounts and must be formed before TM4 [100].

The first direct evidence of thiomolybdate formation in vivo was produced by Mason et al. [101]. Sheep were fed a diet of elemental S and MoO_4^{2-}. The increase of TCA-insoluble Cu occurred as described previously. Mo in the insoluble fraction was isolated from the protein complexes that were present. Size exclusion gel chromatography was used to separate the thiomolybdate species which were then identified by their UV-visible spectra. TM2 and TM3 were identified but TM4 was not. Control studies were also performed in which TM4 was infused directly into the rumen or injected intravenously. In this case, TM4 and some TM3 (presumably due to hydrolysis of TM4) were observed. These observations show that thiomolybdates are indeed formed in the rumen and also indicate that TM3 is the dominant TM species formed.

1.5.5.2 Effect of thiomolybdates *in vivo*

Thiomolybdate studies are typically carried out using TM4 since it is the easiest to synthesize in pure form and is the most stable in aqueous solution. Mason et al. infused ^{99}Mo-labelled TM4 into the duodenum of sheep to study the effects on ceruloplasmin diamine oxidase activity and plasma Cu [39]. As expected, the inclusion of TM4 caused an increase in Cu as well as a relative amount of ^{99}Mo in the TCA-insoluble fraction. The addition of TM4 also caused a reduction in the diamine oxidase activity of ceruloplasmin that corresponded to the increase in Cu and ^{99}Mo in the TCA-insoluble fraction.

Clarke and Laurie expected TM2 and TM3 (not TM4) to be the most abundant species under rumen pH and S:Mo ratios [25]. In 1982, Mason and coworkers therefore carried out an identical study to the one just described but infused TM2 and TM3 instead [38]. TM3 produced similar effects as those seen with TM4. Cu and ^{99}Mo appeared in the TCA-insoluble fraction of the plasma. Correspondingly, ceruloplasmin diamine oxidase activity was inhibited. ^{99}Mo from TM2, on the other hand, was not as abundant in the TCA-insoluble fraction. It also had only a minimal and short term effect on ceruloplasmin activity.

Contrary to the work of Mason, Mills and his coworkers subscribe to TM4 as the dominant antagonist. Mills et al. showed that TM4 given to rats drastically increased plasma Cu, most of which was TCA insoluble. It also significantly reduced ceruloplasmin activity. When MoO_4^{2-} and S^{2-} were given separately (although in higher concentrations), the same effects were observed [102]. Similar experiments using TM2 and TM3 showed a proportionally decreased effect with each added O ligand [103]. However, rats, like humans, are monogastric. Therefore, the pH in the rat stomach will be highly acidic. This will cause rapid decomposition of TM2 and TM3 which may cause their limited effects. When MoO_4^{2-} and S^{2-} are added separately, the lower pH may lead to a greater extent of TM formation than would be seen in ruminants (see

section 1.4.2). This could lead to a greater formation of TM4 in rats versus TM3 in ruminants as seen by Mason.

Further support for the formation of TM4 was presented by El-Gallad et al. Incubation of *in vitro* rumen cultures produced TM4 as seen by UV-visible spectroscopy. Difference spectra with added Cu confirmed the presence of TM4 [104]. Similar to previous findings by Mills et al. [98], though, high Mo concentrations and long incubation times (18 hours) were used. In addition, strong background absorption may have limited the detection of TM3 or other TMs as these have weaker absorption bands than TM4. Furthermore, the experimental method may play a role. This study employed a batch culture while Bray et al. used a continuous culture and found a predominance of TM3 over TM4 [99, 105].

Suttle and Field also looked at the formation of TM4 and its role in sequestering Cu activity. Mo was fed to lambs as TM0, TM2 or TM4 with low (1 g/kg DM) or high (4.1 g/kg DM) levels added S. When low S was given, TM4 still caused an increase of TCA-insoluble Cu while TM0 and TM2 were ineffective. When high S was given, TM0 and TM2 produced the same effects as TM4 [40]. This suggests that TM4 is the primary participant in Cu antagonism. However, in light of the finding by Mason that TM3 and TM4 produce the same effects on Cu, TM3 may still have been largely formed from TM0 and TM2.

It has been established that TM3 and TM4 both cause disruptions in Cu utilization. However, little was known about the mechanism of the antagonism or how TMs were metabolized. Mason et al. began studying TM metabolism by injecting intravenous injection of ^{99}Mo-labelled TMs [23]. Single doses of TM2, TM3 or TM4 were injected and monitored over time. Initially the usual results (decreased ceruloplasmin activity and increased TCA-insoluble Cu) were observed. However, after 15 minutes, Cu in the TCA-soluble fraction began to increase. Correspondingly, extensive hydrolysis toward TM0 was also observed. These results are counter to typical feed studies in which TCA-insoluble Cu does not solubilize.

Further study by Hynes and coworkers was carried out using radio-labeled TM2 and TM3 [106]. Injections of high levels (50 mg) of TM3 resulted in rapid hydrolysis but lower doses (1.5 mg) were much more stable. In addition, TM2 and TM3 can be absorbed from the rumen in protein bound form. The stability of these complexes prevented hydrolysis [107]. This demonstrates that the systemic effects caused by the TMs are not necessarily caused by the TMs alone but protein binding also contributes. These factors must therefore be considered when attempting to mimic said effects.

Cu in plasma that is not bound to ceruloplasmin is largely bound to albumin, specifically, bovine serum albumin (BSA) in cattle. Cu normally binds to BSA (~ 66 kDa) at the N-terminus. The Asp-Thr-His-Lys motif at the N-terminus provides a specific binding site for Cu. The histidine residue is crucial for binding Cu which has an affinity for the imidazole N. This binding is affected by the presence of TM3 as shown by Woods and Mason [108]. UV-visible spectral changes observed during the reaction of Cu and TM3 were also observed when Cu was added to TM3 bound BSA. Evidence that TM3-Cu-BSA binding did not occur at the usual N-terminus was obtained via comparison with canine serum albumin (CSA). CSA differs from BSA in that the histidine residue near the N-terminus in BSA is replaced by tyrosine. Addition of Cu to TM3 bound CSA produced the same spectral changes seen with BSA. Furthermore, the affinity of Cu to BSA was enhanced by the presence of TM3. TM3 appears to disrupt the natural binding of Cu with BSA. The creation of TM-protein complexes provide new ligands for binding Cu that can alter its distribution in tissues [109, 110].

1.6 BOVINE PHYSIOLOGY

1.6.1 The digestive tract

The material in this section is largely summarized from the reviews of Underwood and Suttle [111] and Church [112]. Digestion in ruminants occurs via mechanical, chemical and microbial means as contents pass along the digestive tract. The organs that comprise the digestive tract are shown in Figure 1.7. This system has

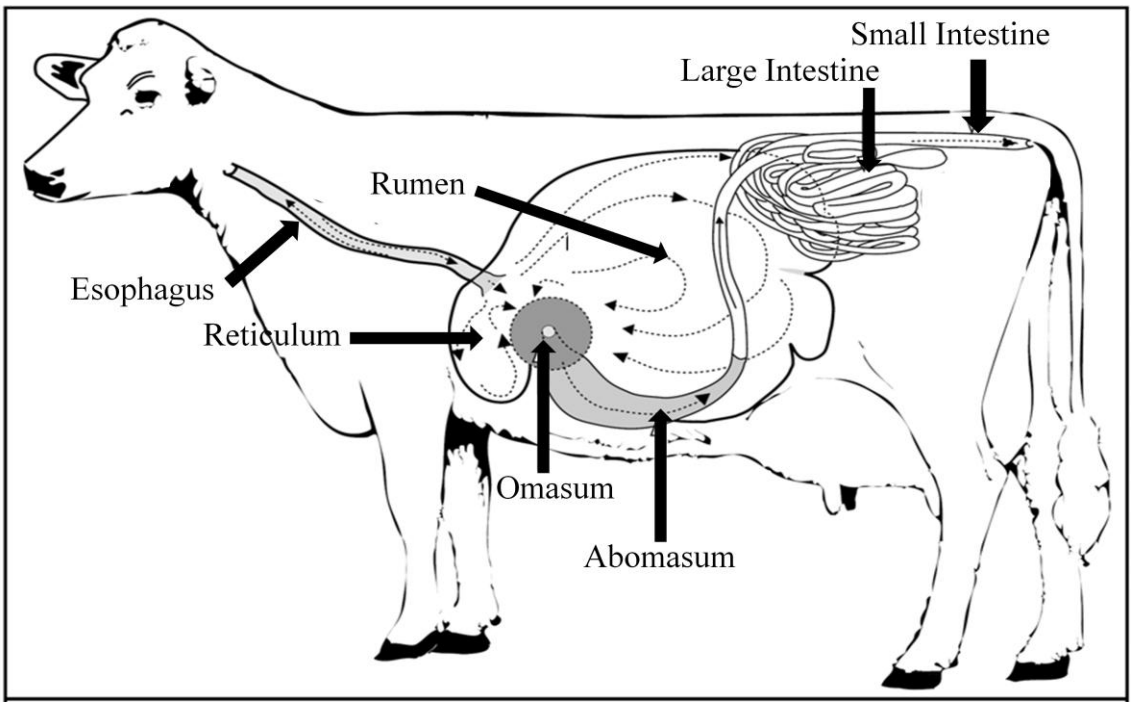

Figure 1.7. The ruminant digestive system. Adapted from [113].

evolved to effectively deal with the high cellulose diet of these animals. The ability to break down plant matter cell walls and convert them to energy is the primary difference between ruminants and non-ruminants.

Initially, food taken into the mouth is mixed with copious amounts of saliva. The food at this point is incompletely chewed. The saliva meanwhile helps to soften plant material and acts as a lubricant to facilitate swallowing. Upon swallowing, the contents pass through the esophagus down to the stomach.

The ruminant stomach consists of four chambers; the reticulum, the rumen, the abomasum and the omasum. There is no obvious separation between the reticulum and the rumen they are thus often referred to collectively as the reticulo-rumen. The reticulo-rumen is by far the largest of the stomachs. It comprises about 85 % of the total stomach volume and can have a capacity of up to 100 L [112]. The ruminant stomach is responsible for digestion and absorption.

The rumen is the first of the stomach chambers along the digestive tract. It is also the key distinguisher between monogastric and ruminant animals. Chiefly, the rumen provides optimal conditions for a large microbial population to thrive. The ruminant benefits from this symbiotic relationship as the microbial byproducts comprise about 20 % of the nutrients absorbed. A main source of these nutrients is the cellulose that makes up the plant cell wall. Without the rumen, cellulose would be indigestible as in monogastric animals.

When food, mostly comprised of cellulose, hemicelluloses, starch and water soluble carbohydrates, and water enter the rumen, it is broken down chemically by enzymes. These enzymes are produced from the large microbial population in the rumen. The primary fermentation products are acetic, propanoic and butanoic acids, also known as the volatile fatty acids (VFAs). The gaseous products CH_4 and CO_2 are also produced. The VFAs are mostly absorbed through the rumen wall. This is facilitated by papillae which line the rumen wall.

Proteins are hydrolyzed into peptides and amino acids. Some amino acids are further converted to organic acids (VFAs), NH_3 and CO_2. Micro-organisms in the rumen use amino acids and ammonia to synthesize proteins. These proteins can then be utilized by the animal.

A unique feature of ruminants is the ability to ruminate. Initially, food is only partially chewed and partially digested. This would result in a massive loss of potential resources. Rumination allows previously unused nutrients to be obtained. The process of rumination first involves the regurgitation of rumen contents back into the mouth. These contents are then remixed with saliva and re-chewed to form boluses. These boluses are then swallowed for further digestion. Some of this quantity will be passed from the rumen while some will likely go through the rumination process again. A bovine may spend about eight hours per day ruminating. However, this will vary with the type (for example, hay versus grass) and quantity of food taken in.

Semi-liquid contents are passed from the rumen to the omasum. The omasum is comprised of a series of folds that serve as a filter for the digesta. Here, dehydration occurs as about 40 % of the moisture is lost. The remaining contents then move on to the abomasum. The abomasum is similar to the monogastric stomach in terms of conditions and the mode of digestion. Undigested food and microbial cells are broken down in the acidic environment and digested by secreted enzymes.

Partially digested food is then passed to the small intestine where it is mixed with secretions from the duodenum, liver and pancreas. Absorption occurs via villi which line the wall of the small intestine. The small intestine is the main site for digestion in the ruminant. Some further digestion occurs in the large intestine where extensive microbial activity occurs. However, this is much less effective than in the rumen because of the short residence time. All remaining unabsorbed products of digestion are excreted.

1.6.2 Rumen Contents and Conditions

Conditions in the rumen are such that bacteria and protozoa can thrive. The microbial population is comprised mostly of species that survive in anaerobic conditions. A small portion, however, are oxygen scavengers and serve to maintain the anaerobic environment. The micro-organisms are present as a wide variety of species and serve to break down a wide array of components from various diets.

The contents of the rumen are not uniform even though muscular contractions cause constant mixing. Rumen contents consist of solid, liquid and gaseous phase components. The solid phase is comprised of undigested feed and other insoluble compounds. Approximately 10 – 15 % of the rumen content mass is in the solid phase.

The liquid phase is made up of water and water-soluble compounds like VFAs. The liquid phase of great importance because solubility is required for absorption to occur. Acetic acid is the most abundant VFA followed by propanoic and butyric acid.

Small amounts of isobutyric and valeric acid can also be found. VFAs are also produced from the protein digestion. Amino acids are the source of most short chained VFAs.

Saliva is excreted in the mouth and is then passed into the rumen to join the liquid phase. Saliva contains a variety of anions, cations, non-electrolytes, amino acids, proteins, carbohydrates and lipids. The large quantities of saliva that are produced, which can range from 40 – 190 L/day, serve to maintain the conditions in the rumen. This mainly includes liquid volume, pH and ionic strength. Of primary importance, phosphate and bicarbonate buffer the saliva at a pH between 5.5 and 8. In addition, alkaline salts which contain Na^+ and K^+ ions help to keep fermenting digesta in suspension which facilitates digestion.

The gaseous phase is made up mostly of CO_2 and CH_4. CO_2 is formed via the acid-base chemistry of bicarbonate. It is also a byproduct of bacterial fermentation. CH_4 is one of the VFA's produced in cellulose digestion. However, its presence in the gas phase means that it is wasted energy. Overall, CO_2 makes up about 65 % of the gaseous phase products while methane comprises about 25 %. Other components of the gas phase include N, mostly as NH_3 (7 %) and H, O and H_2S which are all present in trace amounts.

Total sulfur intake may range from 0.5 to 5.0 (or higher) g S/kg of dry matter depending on the type of feed. During feed studies, about 3 g S/kg dry matter, usually as Na_2SO_4, is typically given [23, 109]. Rumen microbes then reduce all forms of sulfur to H_2S. The extent to which this reduction occurs was studied by Gawthorne and Nader [90]. They determined that about one third was converted to sulfide leaving about 1 g S/kg DM. If this is compared to a typical Mo intake of 0.1 to 20 mg/kg dry matter [111], S:Mo ratios of 50:1 up to 1000:1 might be expected. This is of relevant primarily to the work presented in section 3.2.

The temperature in the rumen is maintained at 38 – 40 °C. This, however, can be as high as 41 °C or may be lowered with the intake of water. The pH is maintained by

carbonate and phosphate buffers from the saliva between 5.8 and 6.8. Variation depends on the accumulation of VFAs or the alkalinity of the saliva. The rumen environment is highly reducing with a potential of -360 to -420 mV [114]. As such, there is very little O present in the rumen. These conditions provide an optimum environment for the growth of micro-organisms and allow fermentation to occur. Fermentation is further enhanced by the long residence time of solids in the rumen. A large quantity (about 40 - 100 L) of rumen contents is maintained at all times [115]. Also, food may remain in the rumen for 9 – 12 hours. This gives time for slower processes to proceed to a greater extent.

1.6.3 Copper Metabolism

From the time Cu is ingested, it undergoes myriad interactions. As such, it is found almost exclusively in complexed form and not as free Cu(II) which is poisonous. However, in the absence of other ligands, Cu(II) is likely to be present as $Cu(H_2O)_6^{2+}$. Upon absorption as soluble complexes it is circulated to cells and tissues where it is exchanged with apoproteins and utilized. Systemically, Cu can be distributed amongst a wide array of fractions, the identity of which dictates its function. The primary site for Cu metabolism in the ruminant is the liver. Liver concentrations best reflect the Cu status of the animal.

Cu can exist in low molecular mass (LMM) or high molecular mass (HMM) fractions within the contents of the rumen. LMM ligands include the VFAs, amino acids, small peptides, carbohydrates and nucleotides. The role of the LMM fraction is to transport Cu between biological binding sites. They may also serve as temporary storage pools until exchange with proteins can be made.

The HMM fraction would contain complexes with proteins, nucleic acids, polysaccharides and lipids. HMM complexes can either be exchangeable (loosely bound) or non-exchangeable (tightly bound). The chief exchangeable protein is bovine serum albumin (BSA). It therefore acts as a Cu buffer as it can occupy excess Cu or

release Cu in times of deficiency. It also serves as a transport protein and a detoxifier. Ceruloplasmin is the primary non-exchangeable protein. Its purpose is targeted transport between the liver and tissues.

Cu absorption occurs primarily in the small intestine although some absorption occurs at all points of the gastrointestinal (GI) tract. The rate of Cu absorption is relatively slow but is affected by a multitude of factors. For example, the pH affects absorption because it can affect solubility. Also, the rate of absorption may increase during times of deficiency and decrease in times of excess.

Absorption occurs by via a two step process. The first step involves uptake into mucosal cells while the second results in transfer across membranes to the blood and tissue. The biochemical mechanism of absorption is not fully understood but it is believed that it is regulated by the need of the animal and that metallothioneins play a role [116]. Two possible mechanisms were suggested by Cousins [117]. The first is by simple diffusion from areas of high Cu concentration to areas of low concentration. The second, when Cu concentrations are low, is by active transport whereby Cu is carried across the membrane by proteins with Cu binding sites.

Once in the blood, Cu is transported mostly to the liver and, to some extent, the kidney. Transport to the liver is carried out by two main transport proteins, bovine serum albumin and transcuprein. Both of these are exchangeable. From the liver to the cells and tissues, transport is achieved by ceruloplasmin. This is a non-exchangeable protein that selectively releases Cu only into the tissues.

Cattle are somewhat resistant toward fluctuations in Cu levels. Exchangeable proteins like metallothionein and bovine serum albumin sequester excess Cu. The cells are protected from poisoning by excess Cu as it is kept intracellularly in the plasma. Excess plasma Cu can then be utilized during times of deficiency to help maintain normal functions. As mentioned earlier, the rate of Cu absorption also adjusts with Cu levels. This buffering ability is the reason why Cu deficient animals may not show

symptoms initially. The onset of symptoms would then suggest a chronic deficiency as opposed to an acute deficiency.

Cu levels are maintained by excretion which offsets intake. The primary mode of excretion systemically is in the bile. Since the liver is the main storage site for Cu, the bile is considered to be the main excretory route. Cu may also be eliminated via the urine or the feces post-digestion. Whereas dietary protein generally enhances the bioavailability of Cu, the formation of complexes with sulfide or thiomolybdates may trap Cu in the solid phase of the digesta. In this case, fecal loss will occur.

1.6.4 Effects of Copper Deficiency in Ruminants

Cu is found in a large number of proteins and enzymes in bovine. Each of these performs a specific function in the body. However, when the supply of Cu is low, whether it is due to a primary or secondary deficiency, the activity of these enzymes begins to decline. This leads to the symptoms that are commonly associated with Cu deficiency. As mentioned in section 1.6.3, cattle are somewhat resistant towards deficiencies and so symptoms may not manifest themselves initially. Other factors that affect the onset of symptoms include age, sex, severity and duration of the deficiency and the environment that the animal is a part of.

Typically, a bovine is considered hypocupremic when blood Cu levels drop below 20 ug/dl [112] even though overt symptoms may not be present. Overt symptoms may include diarrhea, rough hair coat, leg abnormalities, swayback, growth retardation and infertility. Regardless of the clinical symptoms, lesions in the skeletal and cardiovascular systems occur. Serious deficiencies may result in sudden cardiac failure, also known as falling disease, which can be fatal.

Ceruloplasmin is an important Cu containing enzyme involved in Cu transport to the tissues (see section 1.6.3). Ceruloplasmin, however, also plays a role in the oxidation of Fe^{2+} to Fe^{3+}. Reduced ceruloplasmin activity hinders this process thereby

affecting Fe transport. As a result Cu deficiency may lead to anemia, thus giving rise to reduced Fe containing enzyme activities.

Lysyl oxidase is involved in the cross-linkages in connective tissue [111]. Its depletion may lead to a weakening and reduced stability of bone collagen and impair the formation of cartilage. Therefore a Cu deficiency may cause joint disorders and fragile, easily broken bones. Clinical signs of bone disorders are enlarged bone ends and a beading of the ribs [112]. Cattle may acquire a pacing gait due to leg stiffness. As well, the onset of osteoporosis leads to the bowing of the forelegs, particularly in sheep.

Swayback may occur in cattle after chronic Cu deficiency. Although the pathology of swayback is not fully understood, it is known to be a nervous disorder. However, cytochrome c oxidase and Cu-Zn superoxide dismutase activities are found to be lower in the brain and brain stem, respectively, in ataxic lambs [111]. Swayback is characterized by uncoordination and a partial paralysis of the hind quarters. Muscle tremors, teeth grinding and pupil dilation may also occur [112].

The most common symptom of Cu deficiency is diarrhea. This has been correlated with muscular atrophy in the small intestine. This, combined with a decrease in cytochrome oxidase activity, results in poor absorption. This leads to decreased food conversion and diarrhea.

The Cu containing enzyme, tyrosinase, is found in the hair of cattle and wool of sheep. Reduction of its activity results in loss of pigmentation. Tyrosinase is involved in melanin formation. Melanin provides pigment to hair and skin in humans and other mammals. In sheep, wool also loses its crimp and begins to resemble hair. Pigment can be regained when Cu levels return to normal.

Infertility is known to result from Cu deficiency although possibly only when it is Mo induced. The release of luteinizing hormone was impaired when Mo induced Cu deficient heifers but not when the deficiency was Fe induced. It was thought that this

may be a result solely of Mo toxicity but it was later found that Cu deprivation was required [111].

1.6.5 Methods of Diagnosing Copper Deficiency

The identification of Cu deficiency is impaired by the delay in the onset of symptoms. Cu levels are known to drop below acceptable levels before symptoms appear [118]. In fact, ruminants can withstand temporary or seasonal periods of deficiency without any apparent detriment [119]. Effective diagnosis and treatment at this stage is obviously desirable. A variety of methods have been explored in attempt to achieve this goal.

The liver is the main storage organ for Cu in the ruminant, so liver tissue is likely to provide the most accurate measurement of Cu status. However, tissue sampling procedures are invasive [120]. Also, during minor deficiencies, liver Cu stores are depleted in favor of maintaining plasma Cu levels. This may lead to an overestimation of Cu deficiency even if the animal is healthy [121].

The most common biomarkers for Cu status in ruminants are plasma or serum Cu. Blood Cu levels can give a reasonable estimation of Cu status and is easy to collect and assay. These results can be misleading, however, because all blood Cu is not necessarily bioavailable. As discussed in section 1.5.5, the presence of thiomolybdates increases blood Cu levels but it is present in a TCA insoluble fraction that is not of use to the animal.

Serum Cu analysis was used as the basis of a survey of Cu status of cattle across the United States [122]. The simpler serum Cu analysis allows a larger population to be studied than would liver Cu tests. Comparison of serum Cu to liver Cu, though shows poor correlation between the two methods. In addition, it was found that a threshold value of serum Cu could be used to rule out Cu deficiency but low serum Cu results were inadequate to confirm Cu deficiency [123].

Cu enzyme activities provide another means of monitoring Cu levels. Ceruloplasmin activity has often been used. It is closely related to plasma Cu levels but has a distinct advantage. When Cu deficiency is the result of high dietary Mo, plasma Cu levels increase but ceruloplasmin activity decreases as would be expected [119]. Unfortunately, ceruloplasmin activity (as well as plasma Cu) can be affected during times of stress and inflammation [120].

The Cu enzyme plasma diamine oxidase has shown promise as an effective Cu biomarker. Results from diamine oxidase activity are consistent with other methods but is expected to have fewer confounding factors [120]. Currently the limitation with this method is that there is inadequate sensitivity.

Blood and tissue analyses are likely to give the most accurate view of Cu status in a given animal. However, multiple animals in the herd must be studied in order to gain a legitimate understanding of the steps required to improve the overall health. This can be very time consuming and expensive. Methods of predicting the Cu status of animals in a region *a priori* would allow a more efficient application of quantitative methods.

Analysis of feed and water can help diagnose Cu deficiency if low Cu concentrations are discovered. This will provide circumstantial evidence at best. Suttle proposed creating hypothetical models based on real data. This involves logging the results of dose-response trials [124]. The limitation with this is that it does not address the instance of at risk animals showing no symptoms.

Work in the Reid lab has focused on predicting Cu deficiency based on mathematical models. This would provide a rapid, inexpensive method of identifying at risk regions as well as assisting in the improved efficiency of Cu supplementation. By acquiring some basic information about animals in a particular region, for example the levels of S, Mo and Cu in the feed, the Cu speciation could then be determined. From the results, herds that are more likely to suffer from copper deficiency can be identified.

In this case, more direct animal testing could be performed. This would be especially useful where Cu deficient conditions exist but the animals are not showing clinical signs. On the other hand, expensive, time consuming test could be bypassed for herds that are not in an at risk environment. The work that has been done toward this goal was discussed in section 1.7.

1.6.6 Feeding Habits

In order to determine the long term effects of Mo intake (and thus thiomolybdate formation) on the Cu status of a bovine, reactions that mimic natural feeding habits must be performed (section 3.3.5). This is especially important because of the relatively slow formation of thiomolybdates. Fresh intake of starting materials will often occur before the previous materials are completely reacted. A realistic estimation of the feeding (and excretion) patterns of the bovine are therefore needed.

Naturally, feeding habits will vary from animal to animal. In addition, other factors such as the height of the food (ground level versus above the ground), climate, condition of the teeth and competition may alter an animal's regular habits [125]. However, some general observations can be made.

Cattle typically feed between 6 and 11 times per 24 hour period [125, 126]. Most grazing (85 %) is done during the day leaving one or two feeding events to occur at night. Total food intake over this period is typically between 14 and 25 kg. Water intake may total 65 – 93 L/day in as few as four drinks. However, the number of drinking events tends to increase if the quantity of the drinks is low [127].

About 10 each of defecations and urinations occur over a 24 hour period [125]. Since the overall rumen volume remains somewhat constant, the total amount excreted will be about equal to the amount taken in over a period of time.

1.7 PREVIOUS STUDIES IN THE REID GROUP

1.7.1 Copper(II) Speciation Modeling

The work presented in this thesis is part of an ongoing study in the Reid group. Previous workers have followed one of two main research paths toward the final goal of modeling Cu in the rumen. The first path involves the modeling of copper in the presence of small molecules commonly found in the rumen. The second path involves the study of thiomolybdates and their role in copper antagonism.

Mohammed Attaelmannan was the first to study and model rumen Cu [128]. His work developed from discrepancies in the literature as to what was the best form of Cu for supplementation. The belief was that chelated Cu complexes were more effective than inorganic salts like $CuSO_4$. The higher stability constant of the chelated species was expected to keep the complex intact through the stomach and into the intestinal tract. However, conflicting evidence from *in vivo* studies prompted an *in vitro* and theoretical speciation study to try to clarify the matter.

Formation constants of Cu (II) complexes with lysine, histidine and glycine were determined using a gravimetric autotitrator at 25 and 38 ºC [129]. From these formation constants, it is possible to develop a computer simulation for Cu speciation as it passes through the digestive tract. Initially, the speciation within the saliva was determined. The concentrations and formation constants concerning the components of McDougall's solution (synthetic bovine saliva) were included in the simulation. McDougall's solution is comprised of $NaHCO_3$, Na_2HPO_4, KCl, NaCl, $MgSO_4$ and $CaCl_2$. Bovine saliva contains high concentrations of CO_3^{2-} and PO_4^{3-}. Despite the high formation constant of the chelated copper compounds, speciation models suggest that Cu(II) will largely be bound to CO_3^{2-} and PO_4^{3-} species, regardless of the form of the supplement.

The results of the Cu(II)-lysine speciation in McDougall's solutions were then confirmed by ^{1}H NMR [130]. The chemical shifts of lysine protons as a function of pH were measured. However, each resonance is actually a weighted average of a particular group of protons based on the fractional abundance of the species present. The species fractions were calculated using the acid dissociation constants and the true chemical shift of each species was determined by regression analysis. A similar experiment was then performed using increasing concentrations of Cu(II) added to lysine. This resulted in the chemical shifts of various Cu(II)-lysine species being determined. The chemical shifts extracted here were used to predict the chemical shift expected as lysine is added to McDougall's solution. This resulted in good agreement with experiment.

The speciation model was then expanded to include common low molecular mass rumen components. This included the volatile fatty acids (VFA's); acetic, propanoic and butanoic acids as well as other components like NH_3, CH_4, H_2S and CO_2. The results showed that Cu(II) was not significantly bound to the VFA's. Instead, most copper was found bound to NH_3. It is likely, though, that at lower pH values the Cu-VFA and Cu-lysine fractions will increase.

The results of the rumen simulation were confirmed using ^{1}H NMR experiments. The VFA's within a rumen fluid sample were monitored with and without the addition of Cu(II) in a similar fashion as the lysine experiments described above. Simulations of the chemical shifts agreed well with experiments.

Finally, the chemical shift of acetate protons in the rumen sample were measured and simulated with increasing amounts of lysine. Experimental and theoretical shifts matched well at low lysine concentrations (0.8 mM). At moderate lysine concentration (4 mM), there was a large shift indicating that acetate was being stripped from Cu(II). The fit was still good at this point. At high lysine concentration (20 mM), however, deviations occurred between measurement and calculation. This deviation was later addressed by Essilfie-Dughan and will be discussed later in this section.

1.7.2 Thiomolybdate Interactions with Copper(II) and Other Ligands

Emmanuel Quagraine was the first to begin looking at thiomolybdates in the Reid group [24]. Much of the literature involving TMs in terms of Cu antagonism in the bovine rumen comes from feed studies. The relatively small amount of *in vitro* TM work is hindered due to the reasons discussed in section 1.5.1. This prompted Quagraine to first develop a method for synthesizing all four TMs. This was accomplished using a common synthetic route with $(NH_4)_2S$ as reagent instead of H_2S. The reaction was controlled by adjusting the temperature, pH, S:Mo ratio and reaction time. This was the first time that TM1 had ever been isolated in solid form. ^{1}H NMR standard addition experiments were used to determine the level of hydration.

The issue of inevitable cross-contamination (section 1.5.1) was dealt with by the development of a multivariate regression analysis program using Microsoft Excel®. The absorbance at selected wavelengths was calculated using Beer's Law. Since the absorptivities and actual molar TM fractions were unknown, they were adjusted using the goal seek function until the calculated absorbance matched the experimental absorbance. This process was repeated as necessary for each wavelength studied. The absorptivities and sample composition were considered optimized when the sum of the deviations between experimental and calculated absorbances at all of the studied wavelengths was minimized. From here, a variety of experiments looking at the stability of TMs in solution and their formation from TM0 was performed using UV-visible spectroscopy. The new method of analysis allowed the TM composition to be determined at any given time.

Quagraine also studied the reactions between the various TMs and Cu(II) [131]. He found that at acidic pH the TM4 UV-visible spectrum was lost when one equivalent of Cu(II) was added indicating a 1:1 Cu:Mo ratio. At neutral pH, 1.5 equivalents of Cu(II) were required to eliminate the TM4 spectrum. The excess Cu(II) was thought to be necessary to drive the reaction forward and the ratio was still considered 1:1. A similar result was found when TM3 was used.

The Cu-TM products are known to form precipitates in aqueous solution [47]. This precipitation was shown to occur faster at lower pH and higher ionic strength. Also, in unbuffered solution, no precipitation occurred, indicating that other factors are involved in the complexation. Further interactions involved the inclusion of EDTA. The Cu-TM complex was highly stable as EDTA could not strip Cu. On the other hand, S^{2-} did compete with TM4 for Cu(II) binding. If Cu(II) was first mixed with S^{2-} and then TM4, the TM4 spectrum was observed whereas without S^{2-} it was completely lost.

The next set of experiments involved bovine serum albumin (BSA), a Cu transport protein. First, direct interactions between the TMs and BSA were studied. As the pH was lowered from 8 to 6, BSA-TM4 binding was shown to increase. As the pH was lowered further, the extent of the binding decreased. With TM3, maximum binding occurred at pH 7. With TM1 and TM2 there was no conclusive evidence of binding with BSA.

Tripartite interactions were then performed between Cu(II), TMs and BSA. Evidence supports the presence of a three-way interaction. Of note, the product is soluble. This was the case if the TM (namely, TM4 or TM3) were added to Cu(II)-albumin or if Cu(II) was added to TM-albumin. If the insoluble Cu-TM product was previously formed, BSA did not dissolve it.

To further examine how Cu(II) interacts with the binding site of BSA, peptide models were used [132]. The N-terminal binding site was mimicked using peptides such as His-Lys, Thr(Ac)-His-Lys and Thr-His-Lys. ^{1}H NMR was used to provide information about the binding of Cu(II) at this site. This was done first by monitoring the peptide chemical shifts as the Cu(II) concentration was increased. Secondly, the chemical shifts of 1:1 Cu(II)-peptide solutions were monitored with changing pH.

As Cu(II) is added to the peptide solution, broadening of the peaks will occur due to the paramagnetic nature of Cu(II). Due to the distance between various protons being monitored, though, the peaks will broaden at different concentrations based on

where Cu(II) is bound. It was found that the peaks due to the β-CH_2 and immidazole protons of His were the first to be affected. On the other hand, Lys protons were less affected indicating broadening due to proximity as opposed to direct binding.

Increasing the pH of a 1:1 Cu(II)-His-Lys solution results in signal loss as a function of pk_a and the complex formation constant. The loss of a signal indicates the displacement of a proton at a particular site with Cu(II). In general, the His protons disappear at very low pH while the Lys protons begin to broaden later. This corroborates the results of varying Cu(II) and suggests that binding occurs primarily at the His.

This work was then extended to include the TMs by studying the interactions between Cu(II), TM and the His-Lys peptide model. The presence of a three-way product was deduced by UV-visible spectroscopy and further inferred by line broadening studies with ^{1}H NMR. The mixing of Cu(II) with the peptide resulted in line broadening. As TM4 was added, the peaks reappeared and become sharper. Before and after differences in chemical shift refute the idea that Cu(II) is simply stripped from the peptide to form a Cu(II)-TM complex. The chemical shift continued to change up to about 1.2:1 Cu:Mo. It was again suggested that the product ratio was actually 1:1 with the excess Cu(II) required to push the reaction to completion.

Further evidence for the existence of a three-way product was shown by measuring NMR peak areas after reaction with Cu(II) and TM4. After the insoluble product had formed, the remaining solution concentration was less by about 1 equivalent. This suggests that the peptide is present in the insoluble product. This was confirmed by elemental analysis. The empirical formula determined from elemental analysis was approximately 1 peptide:3 Cu:2 Mo. This ratio was different than that determined from solution studies.

1.7.3. Copper(II) Speciation in the Thiomolybdate Contaminated Rumen

The work of Joseph Essilfie-Dughan largely extends that of Attaelmannan. The primary focus of his work is computer modeling of Cu under various conditions [113]. He first looked at modeling speciation of Cu with CO_3^{2-}, a primary component in bovine saliva. This was a computer model based on mass balances of the Cu(II) and CO_3^{2-} species. It included CO_3^{2-}, HCO_3^-, H_2CO_3, H^+, Cu^{2+}, $CuCO_3$ and $[Cu(CO_3)_2]^{2-}$ and all species were defined in terms of free Cu and HCO_3^-. The complexity of the model made an iterative approach necessary to determine the concentrations of the individual species. This model differed from that of Attaelmannan's, however, in that it contained a "smart" iterative process. After each iteration a correction factor was determined and applied to the resulting concentration to create a new initial concentration for the next iteration. Another feature of this method is that it uses only multiplication and division operations. The use of addition and subtraction could lead to the loss of significant digits.

This model was then expanded to include other low molecular mass ligands. For example, the VFA's were included in order to model Cu(II) speciation in the rumen. It was found that Cu(II) is largely present as $Cu(CO_3)_x$ species. At a more acidic rumen pH (5.8) the $Cu(PO_4)_x$ and $Cu(OAc)_x$ species were also present in significant quantities. Further inclusion of HS^-, Mg^{2+} and Ca^{2+} into the model did not produce an effect. Results from this model were in excellent agreement with results obtained from the commercial speciation program, Hyperquad Simulation and Speciation (HySS).

The speciation of various Cu(II)-amino acid complexes (Cu-Lys, Cu-Met and Cu-Gly) was examined in McDougall's solution. At pH 5.5 the dominant species were the $Cu(CO_3)_x$ and $Cu(PO_4)_x$ species. As the pH was raised, CO_3^{2-} dominated the speciation. The Cu-amino acid species ranged from about 5 to 15 % of total Cu(II) depending on the amino acid and the pH. However, if Cu-His or Cu-EDTA were used, these species were maintained at over 90 % abundance.

A similar experiment was then performed using the same Cu-amino acid species under rumen-like conditions. The results showed that these species are essentially lost while the acetate and carbonate species dominate. Again Cu-His and Cu-EDTA were the exception as they remained largely intact. Similarly, the use of the peptide models mentioned earlier resulted in the Cu-peptide species being the dominant fraction.

^{1}H NMR studies were then performed to study Cu speciation in the rumen. In this case, a simulated rumen fluid consisting mainly of the VFA's was used. From the chemical shift changes with added Cu(II), regression analysis produced the chemical shifts of all species present. Using this information, a computer simulation was performed to predict the chemical shift with changing Cu(II). These results were in good agreement with experiment.

To test the robustness of the model, lysine was added in varying amount. At low lysine concentrations (0.8 mM), there was little deviation between simulation and experiment. As the lysine concentration was increased (up to 20 mM), the model overestimated the amount of Cu-Lys present where as experiment suggest a much larger Cu-acetate fraction than expected. This issue arose earlier in the work of Attaelmannan. However, the discrepancy was adequately accounted for by the inclusion of a mixed ligand complex involving acetate and lysine. The same results were achieved when this experiment was performed in actual rumen fluid, confirming the importance of the mixed ligand complex.

The importance of TMs in the rumen prompted the simulation of their kinetically controlled formation. Analytical expressions for the multistep formation were obtained using the Laplace Transform method. Simulation results matched well with experiments. In order to extend the simulation to include reaction with copper, the rate constant for the reaction of Cu(II) with TM4 was first established. This was found by monitoring the reaction with a Cu(II) ion selective electrode. Once the rate constant was obtained, the simulation was expanded to include this step. This work will be discussed in more detail in section 3.3.

To complete the overall model, the kinetic model involving Cu-TM4 formation had to be combined with the thermodynamic equilibrium model. This was performed by allowing the kinetic model to run over a small time increment (usually one minute). Then the thermodynamic model was applied and a new time increment was implemented. This process was continued for 107 min, the mean residence time of sulfide in the rumen [90]. This method is made possible by the relatively slow reaction kinetics compared to the rapid thermodynamic processes. Results from this model show that despite the variety and concentration of other ligands present, most Cu will be present with TM4.

1.7.4 Other Work Performed in the Reid Group

Some other studies have been performed in regards to rumen Cu modeling. Mildred Korateng extended the ^{1}H NMR and potentiometric studies on Cu-mixed ligand complexes [133]. Dean Thome established the structures of the various TMs using X-ray crystallography [10]. Darina Slamova is currently studying the structures of the Cu-TM adducts using EPR and EXAFS [134].

1.7.5 Approach to This Study

The work presented in this thesis is presented in three distinct sections that correspond with the goals of the study outlined in section 1.2. The first area of study (section 3.1) focuses on the determination of the UV-visible spectra of the pure TMs. This is then extended to determine the composition of TM mixtures in solution.

Section 3.2 focuses on the kinetics of thiomolybdate interconversions. Kinetic experiments were carried out from a TM0 starting point under biologically relevant conditions. Curve fitting methods were used to determine which interconversion processes occur under these conditions. Also, rate constants for each of the processes that are occurring were determined simultaneously.

Section 3.3 describes the work that was done regarding interactions between Cu(II) and the TMs. The UV-visible spectra of the various Cu-TM reaction products were characterized. This information was then used to study the kinetics of reactions between Cu(II) and the TMs, particularly TM3 and TM4. Thiomolybdate formation experiments were then carried out in the presence of Cu(II). These were extended in order to mimic the effects of bovine feeding. Finally, computer simulations were carried out using the various rate constants determined in this study. These simulations monitored TM and Cu(II) speciation while mimicking bovine feeding habits.

2. EXPERIMENTAL

2.1 SOURCES OF CHEMICALS

The thiomolybdates; mono-, $Cs_2MoO_3S\cdot 1/2H_2O$, di-, $(NH_4)_2MoO_2S_2\cdot 2H_2O$, tri-, Cs_2MoOS_3, and tetra-, $(NH_4)_2MoS_4$ were synthesized based on the methods developed by Quagraine as discussed in section 1.4. The syntheses are described in detail below.

Water was purified to a resistivity of 18.2 MΩ·cm using a MilliQ Gradient water purification system and deoxygenated with Ar before use. All other chemicals were of reagent grade and used without further purification. Sodium sulfide nonahydrate ($Na_2S\cdot 9H_2O$), sodium dihydrogen phosphate (NaH_2PO_4), sodium hydrogen phoshate (Na_2HPO_4), ammonium sulfide (minimum 20 % ($(NH_4)_2S$), Sephadex G-25 and $Cu(NO_3)_2\cdot 2.5H_2O$ were purchased from Sigma-Aldrich (St. Louis, USA). Sodium molybdate ($Na_2MoO_4\cdot H_20$), cesium chloride (CsCl), aqueous NH_3 solution (28 - 30 %), anhydrous diethylether ($C_4H_{10}O$) and concentrated HCl were obtained from BDH (Toronto, Canada). Anhydrous ethanol (C_2H_5OH) was purchased from Commercial Alcohols Inc. (Brampton, Canada). Ar was purchased from Praxair Canada Inc. (Mississauga, Canada).

2.2 SYNTHESIS

2.2.1 TM1 $(Cs)_2MoO_3S\cdot 1/2H_2O$

$Na_2MoO_4\cdot H_20$ (1.0 g, 4.13 mmol) was dissolved in a solution of water (1.2 ml) and 8 ml of aqueous ammonia (28 - 30 %) and placed in an ice bath to reduce the temperature to ~5 °C. 2 ml of $(NH_4)_2S$ solution (20 %) was also cooled in an ice bath

and was added to the molybdate solution. The reaction mixture (~ pH 13) was mixed and allowed to stand for 10 minutes before a CsCl solution (2.8 g, 16.63 mmol in 2 ml of water) was added. The reaction mixture was added to a previously cooled mixture of 15 ml diethyl ether and 5 ml ethanol, shaken, and left stand to precipitate for about 15 minutes. A fine yellow precipitate (1.39 g, 75 % yield) formed. This precipitate was filtered and washed 3 times with 10 ml of ethanol then twice with 10 ml of diethyl ether. The pale yellow, crystalline $Cs_2MoO_3S \cdot 1/2H_2O$ was dried and stored under an inert atmosphere. The level of hydration was determined by x-ray crystallography.

2.2.2 TM2 $(NH_4)_2MoO_2S_2 \cdot 2H_2O$

$Na_2MoO_4 \cdot H_20$ (1.0 g, 4.13 mmol) was dissolved in 1.2 ml of water and 5 ml of aqueous ammonia (28 - 30 %) and cooled in an ice bath. 4.8 ml of cold $(NH_4)_2S$ solution (20 %) was added, mixed and allowed to react in an ice bath for 10 minutes. Precipitation occurred by adding 20 ml of a cold 1:1 ethanol/ether mixture followed by 20 ml of ether then 12 ml of ethanol. The mixture was allowed to stand for another 15 minutes before the fluffy yellow-orange precipitate was filtered out. This precipitate turned brown in air so precipitation was performed in a filter flask attached to a Schlenk line with thorough washing with ethanol followed by ether. The dried TM2 was quickly transferred to a storage vial and stored under inert atmosphere. The product was amorphous making x-ray crystallography ineffective.

2.2.3 TM3 Cs_2MoOS_3

$Na_2MoO_4 \cdot H_20$ (0.5 g, 2.07 mmol) was dissolved in 1 ml of water and 1ml of aqueous ammonia (28 - 30 %). To this was added 5 ml of $(NH_4)_2S$ solution (20 %). To avoid precipitation of $(NH_4)_2MoO_2S_2 \cdot 2H_2O$ before the addition of CsCl neither solution was pre-cooled and the mixture was mixed with gentle swirling. The mixture was then allowed to stand at room temperature for 8 minutes before a CsCl solution (1.4 g in 2 ml water) was added. Deep orange precipitate formed immediately and 10 ml of 1:1 ethanol/ether was added to improve the yield (71 %). The product was washed with 10

ml of cold water, twice with 10 ml of ethanol and twice with 10 ml of diethyl ether, dried, and stored under inert atmosphere. The addition of non-polar solvents to the filtrate caused the product that was dissolved by the water to precipitate. This product is of higher purity and was filtered, washed with ethanol and ether, and stored under inert atmosphere.

2.2.4 TM4 $(NH_4)_2MoS_4$

$Na_2MoO_4 \cdot H_20$ (1.0 g, 4.13 mmol) was dissolved in 2 ml of water and to it was added 15 ml of $(NH_4)_2S$ solution (20 %). The contents (~ pH 10) were stoppered, shaken and allowed to stand in a 35 °C water bath. After about 3 hours dark green rod-like crystals began to form but the mixture was allowed to stand for at least 4 hours to ensure completeness of reaction. 10 ml of a cold mixture of 1:1 ethanol/ether was added, shaken vigorously and left in an ice bath for 30 minutes to improve the yield (79 %). The precipitate consisted of fine dark red crystals with a green shimmer as well as the rod-like crystals that had formed previously. The product was filtered and washed with 10 ml of cold water, 10 ml of 1:1 ethanol/ether, and 10 ml of ether before storing under inert atmosphere. As with TM3, a second precipitate formed in the filtrate. This was filtered and washed with 10 ml of 1:1 ethanol/ether and twice with 10 ml of ether to obtain a red scaly precipitate (22 % yield). This product was also dried and stored under inert atmosphere.

2.2.5 Cross-Contaminated Thiomolybdate Samples

TM1 was synthesized to include contamination with TM0 using the procedure outlined in section 2.2.1 but with a couple of changes. 10 ml of aqueous NH_3 was used and the reaction was allowed to proceed for only 8 minutes before adding the CsCl solution.

TM2 was synthesized to contain TM1 contamination by making the following changes to the procedure in section 2.2.2. 4 ml of aqueous NH_3 was used and the reaction was allowed to proceed for only 8 minutes.

TM3 was synthesized to contain TM4 contamination using a modified version of the procedure outlined in section 2.2.3. In this case, no aqueous NH_3 was used and instead a total 2 ml of H_2O were added. The reaction was then allowed to proceed for 12 minutes. These TM samples are discussed further in section 3.1.2.

2.3 EXPERIMENTAL PREPARATION

2.3.1 Characterization of Thiomolybdate UV-Visible Spectra

TM0 (0.01 - 0.02 g) was weighed into clean, dry 1 L or 500 ml volumetric flasks and dissolved in water. Solutions were made to ensure that the concentrations could be known to three significant figures. This was the benchmark for the lowest concentration used. The greatest concentration used did not produce a UV-visible absorbance above one in the measured range. Concentrations of the solutions varied between 4.1×10^{-5} M and 8.2×10^{-5}M. These solutions were used for the experiments described in section 3.1.4.

Twenty TM4 solutions were made with the same considerations as TM0. In this case, between 0.01 g and 0.015 g of the salt were weighed into 1 L volumetric flasks to obtain final concentrations between 4.0×10^{-5} M and 5.5×10^{-5}M.

A minimum of ten impure TM1 (0.01 – 0.018 g), TM2 (0.01 – 0.017 g) and TM3 (0.01 – 0.02 g) samples (see section 3.1.2) were weighed separately into volumetric flasks and dissolved in water. For TM1 and TM3, 500 ml and 250 ml volumetric flasks were used. For TM2, 1 L and 500 ml volumetric flasks were used. All solutions were known to three significant figures and did not produce a UV-visible absorbance over one in the measured range.

Test solutions (see section 3.1.5) consisted of the following TM mixtures: TM0 and TM1, TM and TM2, TM2 and TM3 and TM3 and TM4. The TMs were weighed into clean, dry 1 L volumetric flasks and dissolved in water. Five solutions of each mixture were made with varying composition. The absorbance of all solutions was kept below one.

2.3.2 Kinetics of Thiomolybdate Interconversions

0.1 M phosphate buffers of pH 7.20, 7.00, 6.80, 6.60 and 6.40 were made as follows. For the pH 7.20 buffer, 4.2800 g of KH_2PO_4 and 12.1575 g of K_2HPO_4 were weighed into a clean, dry 1 L volumetric flask and dissolved in water. The pH was adjusted to 7.20 with HCl. The final ionic strength was calculated to be 0.24 M. The remaining buffers were made using the same procedure except that KCl was added to each of these solutions to obtain a final ionic strength of 0.24 M. These buffers were used for the work described in section 3.2.4.2.

Buffers with varying ionic strengths were prepared as follows. A stock phosphate buffer was made by dissolving 10.0766 g of KH_2PO_4 and 25.9996 g of K_2HPO_4 into 4.00 L of water. The pH was adjusted to 7.20 with HCl and a final ionic strength of 0.131 M was calculated. Buffers with ionic strengths if 0.15, 0.20, 0.25 and 0.30 M were created by adding the appropriate amount of KCl to 1.00 L of stock buffer solution. Experiments involving varying ionic strength are described in section 3.2.4.1. The phosphate buffer described here with an ionic strength of 0.15 M and a pH of 7.20 was used for studying the effects of temperature (section 3.2.4.3).

MoO_4^{2-} solutions for the TM kinetic experiments (section 3.2.4) were made by diluting $Na_2MoO_4 \cdot H_2O$ (0.1 – 0.11 g) with the appropriate phosphate buffer in a 200 ml volumetric flask. The concentration of the MoO_4^{2-} solution was typically about 2×10^{-3} M.

Na_2S (0.23 – 0.27 g) was dissolved in a 100 ml volumetric flask with the same phosphate buffer as the corresponding MoO_4^{2-} solution. The pH was then adjusted to the original buffer pH with HCl before being made up to the mark with buffer. The final sulfide solution concentration was typically between 9.7×10^{-3} M and 1.1×10^{-2} M.

Reaction mixtures were prepared by first weighing 2.2 – 2.5 g of Na_2S stock solution into a clean, dry quartz cuvette. The cuvette was then sealed and placed in the UV-visible spectrometer cell holder for temperature equilibration (see section 2.4). The volume of TM0 stock solution required to give a 250:1 S:Mo ratio was calculated (0.05 – 0.08 ml) and a mechanical pipette was calibrated to deliver this amount. The reaction was then initiated by pipetting the TM0 solution of the same pH and ionic strength into the sulfide containing cuvette, mixing and commencing measurements. These experiments were performed at either 25, 30, 38 or 45 °C. Section 3.2.4 discusses these experiments further.

2.3.3 Characterization of Cu-Thiomolybdate Product UV-Visible Spectra

A pH 5.5 phosphate buffer solution with an ionic strength of 0.15 M was made using the procedure described in section 2.3.2. Five separate pH 5.5 $Cu(NO_3)_2 \cdot 2.5H_2O$ solutions were prepared with concentrations ranging from 6×10^{-5} M to 6×10^{-4} M. This was done by weighing an appropriate amount of salt into a 100 ml volumetric flask. This was first dissolved in a small amount of water before making up to the mark with buffer to prevent precipitation.

Five TM4 solutions with concentrations ranging from 5×10^{-5} M to 4×10^{-4} M, corresponding to the five $Cu(NO_3)_2 \cdot 2.5H_2O$ solutions, were prepared. The TM4 salt was weighed into a 100 ml volumetric flask and made to the mark with pH 5.5 phosphate buffer. This procedure was repeated for TM1, TM2 and TM3.

From each pair ($Cu(NO_3)_2 \cdot 2.5H_2O$ solution and corresponding TM solution) three mixtures were created. The first mixture was created by pipetting 4.00 ml of TM

solution and 8.00 ml of the Cu solution into a flask. The second mixture was comprised of 3.00 ml of the TM solution and 9.00 ml of the Cu solution. The third mixture contained 2.00 ml of the TM solution and 10.00 ml of the Cu solution. The Cu:Mo ratios of the three mixtures were 2:1, 3:1 and 5:1, respectively. In total 15 mixtures were created, each with a final volume of 12.00 ml. Each solution was allowed to react for about 3 minutes before the UV-visible spectrum was taken. See section 3.3.2 for a discussion of this experiment.

2.3.4 Kinetics of Reactions Between Copper(II) and Thiomolybdates

$Cu(NO_3)_2 \cdot 2.5H_2O$, TM4 and TM3 stock solutions were prepared in the following manner. 0.0020 – 0.0025 g of $Cu(NO_3)_2 \cdot 2.5H_2O$ was added to a 200 ml volumetric flask and made up with water. This gives a final Cu concentration of about 5×10^{-5} M. TM4 (0.033 – 0.038 g) or TM3 (0.057 – 0.065 g) was added to 100 ml volumetric flasks and made up to the mark with water for final TM concentrations of 1.2×10^{-5} M – 1.5×10^{-5} M.

2.3 – 2.5 g of $Cu(NO_3)_2 \cdot 2.5H_2O$ solution were weighed into a clean, dry quartz cuvette, sealed and placed in the UV-visible spectrometer cell holder for temperature equilibration (see section 2.4). The required volume of TM0 stock solution to give a 1:1 Cu:Mo ratio was then calculated (~ 0.1 ml). A mechanical pipette was calibrated to deliver this amount. The reaction was initiated by pipetting the TM0 stock solution into the cuvette with the Cu solution and mixing. Spectral acquisition was immediately commenced. These experiments are described in detail in section 3.3.3.

2.3.5 Thiomolybdate Formation in the Presence of Copper

Phosphate buffers of pH 6.0, 6.4 and 6.8 and an ionic strength of 0.15 M were prepared by the method described in section 2.3.2. Na_2S stock solutions were then prepared in phosphate buffer as described in section 2.3.2 to give a final concentration of 1×10^{-2} M. However, a sulfide concentration of 8×10^{-2} M was used for pH 6.0

solutions. A Cu stock solution was made by dissolving 0.1 g of $Cu(NO_3)_2 \cdot 2.5H_2O$ in water up to 200.0 ml. The final concentration was about 2.1×10^{-3} M. A TM0 solution was made by dissolving the appropriate amount of TM0 (about 0.1 g) in a 200 ml volumetric flask to give an equal concentration as the Cu solution. TM0 was dissolved in an appropriate buffer solution.

The Na_2S stock solution (2.3 – 2.5 g) was weighed into a clean, dry quartz cuvette. This was then sealed and placed in the UV-visible spectrometer cell holder for temperature equilibration (see section 2.4). The volume of TM0 required to give a S:Mo ratio of 150:1 was then calculated and a mechanical pipette was calibrated to deliver this amount. To initiate the reaction, the TM0 solution was pipetted into the sulfide solution in the cuvette and mixed. Immediately, the same volume of Cu solution was added to the mixture to give a 1:1 Cu:Mo ratio. This solution was then mixed and the measurements taken. For a 2:1 Cu:Mo ratio, two pipette volumes of the Cu solution were added to the cuvette. See section 3.3.4 for more on these experiments.

For the experiments mimicking bovine feeding habits (see section 3.3.5), sulfide stock solutions of pH 6.8 were prepared with a concentration of 2×10^{-2} M. TM0 and $Cu(NO_3)_2 \cdot 2.5H_2O$ stock solutions of pH 6.8 were both made with a final concentration of 2.5×10^{-4} M. The ionic strength of all solutions was 0.15 M. Initially the reaction was initiated as just described. The temperature for this experiment was 38 °C.

At predetermined time intervals, a portion of the reaction mixture was removed by pre-calibrated mechanical pipette. This was typically between 5 and 10 % of the volume in the cuvette. This volume was replaced by fresh stock solutions of Na_2S, $Cu(NO_3)_2 \cdot 2.5H_2O$ and TM0. The added solutions contained a 1:1 Cu:Mo ratio and a S:Mo ratio of at least 50:1. In order to increase the Cu:Mo ratio in the reaction mixture, input Cu:Mo ratios were as high as 5:1. Table 2.1 shows a schedule of cycling events including the various input ratios and the resulting ratios in the reaction mixture. Twice, cycles 8 and 18, only fresh sulfide was added in order to increase the excess of sulfide in the reaction mixture.

Table 2.1. Schedule for mimicking bovine feeding.

	Time	Ratio of Reagents Added		Ratio Left in Solution		V Exchanged
Cycle	(hr:min)	S:Mo	Cu:Mo	S:Mo	Cu:Mo	(ml)
1	0	200.6	1.00	200.6	1.00	N/A
2	1:30	8.4	1.00	130.4	1.00	0.0761
3	3:10	69.9	1.00	123.6	1.00	0.1405
4	3:40	237.8	1.00	129.3	1.00	0.1363
5	6:02	158.4	1.00	130.7	1.00	0.1012
6	8:30	80.6	1.00	123.4	1.00	0.1576
7	10:00	159.8	1.00	126.0	1.00	0.1515
8*	11:40	N/A	N/A	142.2	1.00	0.1511
9	14:00	159.8	2.00	143.6	1.08	0.1765
10	18:00	136.4	4.00	143.3	1.20	0.2269
11	22:00	136.4	4.00	143.0	1.32	0.2269
12	24:00	129.5	5.00	142.4	1.49	0.2269
13	26:00	129.5	4.00	141.8	1.60	0.2269
14	29:00	131.8	4.00	141.3	1.72	0.2269
15	29:30	66.4	1.00	134.3	1.65	0.2015
16	30:00	67.0	0.50	123.3	1.46	0.1765
17	32:00	132.9	1.00	124.0	1.43	0.1515
18*	33:00	N/A	N/A	135.1	1.43	0.1008
19	34:00	67.0	0.50	124.9	1.29	0.1765
20	36:00	79.3	0.50	118.5	1.18	0.1765
21	39:00	157.3	1.00	121.2	1.17	0.1515
22	46:00	77.8	0.50	115.7	1.09	0.1765
23	47:30	154.5	1.00	118.2	1.03	0.1515

* Volume exchanged with sulfide only to increase S:Mo ratio

2.4 UV-VISIBLE SPECTROSCOPIC MEASUREMENTS

All UV-visible measurements were acquired with a Beckman DU 640 diode array spectrophotometer. Background corrections were made using an appropriate solvent (water or phosphate buffer). Except where specified otherwise, all spectra were collected at a scan rate of 1200 nm/min. Absorbance measurements were acquired with a precision of ± 0.0001 absorbance units. The accuracy was known to ± 0.5 nm.

Absorbance measurements were never above one in order to minimize stray light errors. A 1 cm pathlength quartz cuvette was used for all measurements. Where applicable (see sections 3.2 and 3.3), temperature was controlled to ± 0.1 °C. This was done using temperature controlled water bath continuously flowing through a water jacket around the cell holder. The temperature in the cuvette was determined manually and the water bath temperature was adjusted as required. For all temperature controlled experiments, the temperature of the solution in the cuvette was allowed to equilibrate for at least 15 minutes before use.

2.4.1 Characterization of UV-Visible Spectra

Spectra were acquired over a range of 275 to 500 nm for solutions containing TM4, TM3 and TM2. When measuring TM0-contaminated TM1 samples, a range of 200 to 500 nm was used. See section 3.1 for further discussion on these experiments.

UV-visible spectra of the products obtained from reactions between Cu(II) and the TMs were collected between 275 and 500 nm. This work is discussed in section 3.3.2.

2.4.2 Kinetic Experiments

Spectra for the thiomolybdate kinetic experiments were collected between 275 and 500 nm. The first scan was collected immediately after the reaction was initiated. Spectra were then collected at 1 minute intervals for 12 minutes. After this, 12 spectra were collected at 3 minute intervals. This gave a total of 24 spectra over a 45 minute period. These experiments are discussed in section 3.2.

For the kinetics of Cu(II) interactions with TM4 and TM3 a spectral range of 390 – 470 nm was used with a scan rate of 2400 nm/min. The first spectrum was collected immediately after mixing. After this 11 more spectra were collected at 15 second intervals for a reaction time of 2 minutes 45 seconds. At 3 minutes 15 seconds, a

set of 12 spectra were collected at 1 minute intervals. The total reaction time was 14 minutes 15 seconds. See section 3.3.3 for further discussion of these experiments.

TM formation in the presence of Cu was monitored over a spectral range of 285 – 485 nm. The first spectrum was collected immediately after the addition of the Cu solution (section 2.3.5) and then at 30 second intervals for a total of 5 minutes 30 seconds. After this, spectra were obtained at 1 minute intervals for a total reaction time of 17 minutes 30 seconds. These experiments are discussed in detail in section 3.3.4.

For the experiment mimicking bovine feeding habits, a spectral range of 285 – 485 nm was used. At the beginning of each cycle, the first measurement was taken immediately after the addition of fresh reagents and then at 1 minute intervals. After 12 scans the intervals were increased. This interval was typically either 10 or 15 minutes but ranged from 5 to 30 minutes. For shorter cycles (Table 2.1), shorter intervals were used. For longer cycles, longer intervals were used. The results of this experiment are discussed in section 3.3.5.

2.5 DETERMINATION OF MOLAR ABSORPTIVITIES

Molar absorptivities for the pure salts of TM0 and TM4 were determined from the slope of the Beer's Law plots at the desired wavelengths. Since a 1 cm path length was used, plots of absorbance vs. concentration give a slope numerically equivalent to ε. The standard deviation of the slope was calculated using least squares regression. The molar absorptivities of TM1, TM2 and TM3 were determined using curve fitting methods (see section 2.6). See section 3.1.4 for the results of these experiments. The molar absorptivities of the Cu(II)-TM reaction products were also determined by Beer's Law plots. This work is discussed further in section 3.3.2.

2.6 CURVE FITTING

2.6.1 Characterization of Thiomolybdate UV-Visible Spectra

The molar absorptivities of TM1, TM2 and TM3 were found using the non-linear curve fitting function in Origin7® software. The fitting equations used were based on Beer's Law and the principle that absorbances (A) are additive (equation 2.1).

$$A_\lambda = \sum(\alpha_x \varepsilon_x)\ (c_m/Fm) \qquad \textbf{(2.1)}$$

These equations were fit to absorbance data by optimizing either the molar absorptivities (ε) or the molar fractions (α). Fm is the average formula mass of the sample and c_m is the TM concentration in g/L. The absorbance data was collected as described in section 2.3.1 using samples that were synthesized as described in section 2.2.5. The fitting method will be described in detail in section 3.1.3.

2.6.2 Determination of Composition of Thiomolybdate Mixtures

The fractional composition of TM mixtures was found by curve fitting using Origin7® software. Absorbance spectra were fit using equation 2.2. ε_S and c_S are the

$$A = (\Sigma(\alpha_{TMx}\varepsilon_{TMx})c_{TM} + \varepsilon_S c_S) \qquad \textbf{(2.2)}$$

molar absorptivities and concentration of sulfide, respectively. Absorptivities were determined as described in section 2.6.1. The α's were then determined by iteration.

2.6.3 Kinetics of Thiomolybdate Interconversions

Absorbance data for the kinetics of TM interconversions was collected as described in section 2.3.2. TM concentrations were found as described in section 2.6.2. Rate constants were determined via non-linear least squares fitting using Origin7® software. Fitting equations for the reaction scheme presented in equation 2.3 were developed using the Laplace Transform method (see A2.5.1 for the development of these equations). This method is also discussed in general terms in section A2.3. For a detailed discussion of the kinetics of TM interconversions see section 3.2.

$$TM1 \underset{k_{-2}}{\overset{k_2}{\rightleftharpoons}} TM2 \xrightarrow{k_3} TM3 \xrightarrow{k_4} TM4 \qquad \textbf{(2.3)}$$

2.7 COMPUTER SPECIATION SIMULATIONS

Simulations were performed using Microsoft Excel® 2007. TM formation was simulated using the integrated rate equations developed in section A2.5.1. The initial TM1 concentration was set at 1.5×10^{-5} M while the other initial TM concentrations were set to 0. The observed pseudo-first order rate constants were used. These were determined as discussed in section 3.2. From the rate constants, values for f, g and h were determined using the "Goal Seek" method in Microsoft Excel®. The f, g and h values are non-linear expressions consisting of the rate constants (see A2.5.1). The theoretical concentrations of the various TMs were then calculated as a function of time. The total TM concentration was determined at each time interval after the TM concentrations were calculated. Deviations from the initial TM concentration were corrected for before concentrations were calculated at the next time interval.

The reaction of Cu with TM4 was incorporated after the TM concentrations were determined at each time interval. It was assumed that Cu reacted only with TM4 and that the product formed in a single elementary step. The rate constant used was based on the k_1 value determined in section 3.3.3. The initial concentration of Cu was

set at 1.5 x 10^{-5} M for 1:1 Cu:Mo simulations or 3.0 x 10^{-5} M for 2:1 simulations. Using the appropriate integrated rate equation, new concentrations of Cu, TM4 and Cu-TM4 were calculated. This process was repeated for further time intervals. These simulations are discussed in detail in section 3.3.3.

The effects of bovine feeding on TM and Cu species concentrations were also simulated. The simulations were performed initially as described above. When the next "feeding" event occurred, all concentrations were adjusted to account for a volume of the reaction mixture being removed and made up with fresh TM1 and Cu solutions. The simulation was then carried out until the next "feeding". A schedule similar to that shown in Table 2.1 was used. Feeding cycles were repeated until all species concentrations equilibrated. Cu:Mo ratios of 1:1 and 2:1 were simulated.

The effects of changing Cu:Mo ratios were then simulated. Once the 1:1 Cu:Mo situation had reached equilibrium, the input concentrations were adjusted to increase the Cu:Mo ratio to 2:1. Feed cycles were simulated under these conditions until equilibrium was reached. The reverse case was also performed.

2.8 COMPUTATIONAL INSTRUMENTATION

All computations were performed with a computer equipped with an AMD Athlon 64 X2 Dual Core Processor 4400+ running at 2.30 GHz and containing 1.93 GB of RAM. The operating system used was Windows XP Pro®, version 2002. Microsoft Office® 2007, including Microsoft Excel® and Microsoft Word®, was obtained from Microsoft Corporation, Seattle, WA, USA. Origin7® is a product of Originlab®, Northampton, MA, USA. Maple10™ mathematical software was obtained from Maplesoft, Waterloo, ON, CAN.

3. RESULTS AND DISCUSSION

3.1 UV-VISIBLE CHARACTERIZATION

3.1.1 Introduction

The inevitability of cross-contamination of TM samples (section 1.4.1) makes it necessary to have an effective means of elucidating the composition of the sample. UV-visible spectroscopy is a useful technique for analyzing TMs [25, 30], but it is limited by the great deal of overlap in the TM spectra (section 1.5.1.3) [135]. The limitations of initially assuming TM purity were also discussed in section 1.5.

To use UV-visible spectroscopy effectively for speciation, molar absorptivities of each pure species must be determined. Extensive spectral overlap and uncertainty of the original sample purity complicate this. Initially, the composition of the synthesized samples and the respective absorptivities must be determined simultaneously. Accurate determination of the absorptivities can then be used to provide a means for determining the composition of all TM mixtures in solution thereafter.

Origin7® software contains a curve fitting tool that can be used to optimize a large number of parameters simultaneously. In this case, absorptivities at multiple wavelengths for each TM that is present. The benefits of multiple wavelength measurements were discussed in section A1.2.

In theory, mixtures of all five TMs could be measured and the absorptivities of all TMs could be determined simultaneously. However, in practice, this is an excessive number of parameters and the effectiveness of the fitting routine becomes limited. Instead, each TM was characterized individually from samples contaminated with

previously characterized TMs. The potential for compounding error was outweighed by the improved results from limiting the number of parameters.

3.1.2 Synthesis

TM4 is the final product in the series to be formed. Therefore, forcing the reaction toward the products will exclusively form TM4. This reaction can be driven to completion by increasing the S:Mo ratio, decreasing pH, increasing the temperature, and allowing a longer reaction time. Attempts to force the reaction further, i.e. even greater S:Mo ratios, resulted in no changes to the UV-visible spectrum indicating the presence of uncontaminated TM4. Also, no peak at 395 nm, indicative of the presence of TM3 [25], was observed.

Each subsequent TM was carefully synthesized to contain contamination only by already characterized TMs (see section 2.2.5). "TM3" was synthesized to contain TM4 but no TM2. This was done by increasing the S:Mo ratio typically used in the synthesis and also allowing the reaction to proceed for a longer time to favor TM4 formation. The UV-visible spectrum of this product showed a distinct peak at 468 nm indicating the presence of TM4. In the absence of TM4 a plateau would be expected (see Figure 1.5 in section 1.5.1.3). The presence of TM2 should produce a shoulder at 321 nm. Since no shoulder was present, TM2 was assumed to not be present. Small amounts, however, could go undetected during this inspection. Therefore, TM2 was accounted for in all analyses as a precaution but was not detected in this sample. This will be discussed further in 3.1.4.

"TM1" was prepared such that it contained only TM0 as a contaminant. TM0 is commercially available in high purity and could be easily characterized. This synthesis was performed by decreasing the S:Mo ratio and shortening the reaction time from that described in section 2.2.5. The presence of TM2 in the TM1 sample was ruled out by the absence of a peak at 322 nm. Since TM1 does not absorb at this wavelength, even small amounts of TM2 would have been obvious in the spectrum.

The contamination in the "TM2" sample was not crucial since TM2 would be the only uncharacterized TM at this point. None-the-less, TM2 was synthesized to favor contamination with TM1. The greater difference in the TM1 and TM2 spectra, compared to the TM2 and TM3 spectra, makes fitting this mixture more reliable. Contamination by TM1 was identified by a shift in the peak at 286 nm as well as an increase in its expected absorbance. This is because TM1 absorbs strongly (more strongly than TM2 in this region) at 290 nm. These changes were identified in this sample. On the other hand, contamination by TM3 should be evident at 461 nm. At this wavelength, the TM3 plateau would appear while TM2 does not absorb. TM3 was not observed in this sample. However, due to the weak TM3 absorbance at 461 nm, small concentrations may be difficult to detect. TM3 was therefore included in the characterization of TM2 as a precaution.

3.1.3 Development of the Fitting Routine

The absorbance at a given wavelength is defined by Beer's Law (equation 3.1).

$$A_\lambda = \Sigma(\alpha_x \varepsilon_x)c \qquad \textbf{(3.1)}$$

A_λ is the total absorbance at wavelength λ, α_x is the mole fraction of species x, ε_x is the molar absorptivity of species x, and c is the total molar concentration of all species of interest.

Since the synthesized samples are of unknown concentration, the molar TM concentration, c, is not known. Equation 3.1 must therefore be adapted to equation 3.2. The TM concentration, c_m, is in units of g/L and is determined from the mass of the synthesized sample used in each solution. Fm is the average formula mass of the synthesized sample.

$$A_\lambda = \sum(\alpha_x \varepsilon_x)\ (c_m/Fm) \qquad \textbf{(3.2)}$$

In equation 3.2, there are two sets of unknown values, the α's and the ε's. There is not enough known information to fit both sets of unknowns together. Instead, two separate fitting routines are needed. To do so, equation 3.2 is utilized in a slightly different fashion for each set of unknowns. The α's can be found using equation 3.3 while the ε's can be determined using equation 3.4.

$$A_{sol} = \sum(\alpha_{TMx"y" TMx})\,(c_{TM"y"}/Fm_{TM"y"}) \quad \textbf{(3.3)}$$

$$A_{\lambda} = \sum(\alpha_{TMx"y"}\,\varepsilon_{TMx,\lambda})\,(c_{TM"y"}/Fm_{TM"y"}) \quad \textbf{(3.4)}$$

Equation 3.3 is utilized in the following way: The wavelengths used in the fitting routine are listed in the first column of an Origin7® worksheet (see section A1.3). The absorbance values of the various solutions at these wavelengths are listed in consecutive columns and are labeled as A_{sol} (The absorbance at the corresponding wavelength in that particular solution sample). These are declared as the dependent variables in the fitting program. The ε's for each TM are listed in adjacent columns to the absorbances and declared as the independent variables. Concentrations and average formula mass are included as constants. The α's (all TM fractions that may be present in the sample) are included as parameters. The data is then plotted as A_{sol} vs. λ. This gives a separate curve for each solution that resembles its UV-visible spectrum. Fitting equation 3.3 to each of these curves is accomplished by simultaneously optimizing the α's.

Equation 3.4 makes use of the same data as equation 3.3 but in a modified format. In this case, the independent variables are the solution concentrations. These are listed in the first column of a new Origin7® worksheet. The corresponding solution number and absorbance data is then listed in adjacent columns which represent each of the selected wavelengths (see Figure 3.1). These are the independent variables. In other words, the absorbance data in each horizontal row would be identical to a vertical column in the previous fitting routine. The absorptivities at each measured wavelength of the TMs that have already been characterized are input as constants. The average

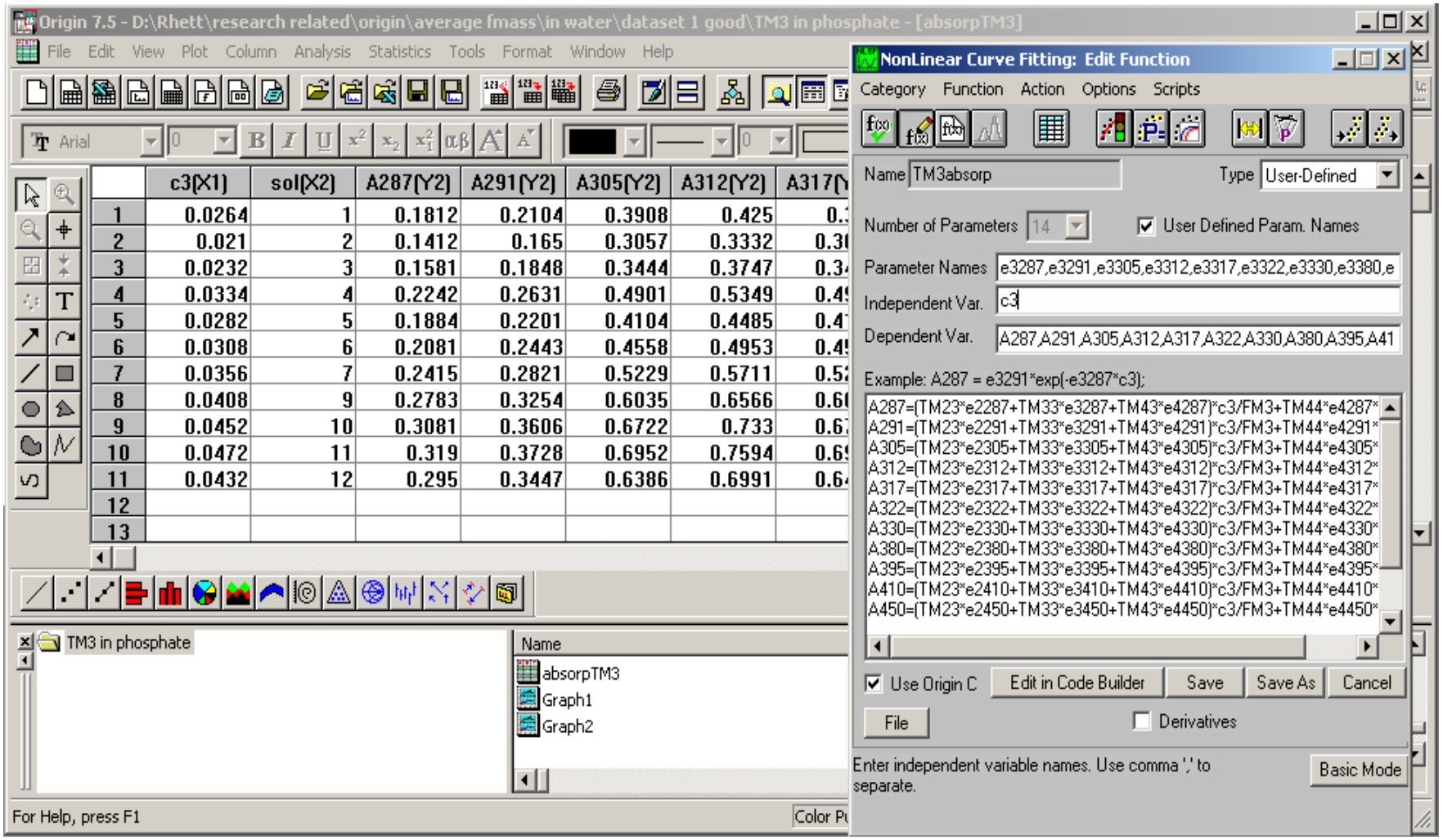

Figure 3.1. Screen shot of Origin7® worksheet and nonlinear curve fitting window set up for fitting with equation 3.4.

formula mass is calculated from the results of the fitting with equation 3.3 and is also set as constant. The absorptivities of the TM to be characterized are included as the parameters. The data in the worksheet is then plotted as A_λ vs. solution #. This produces a separate curve for the array of absorbances at each wavelength. Fitting of equation 3.4 to these curves is then performed by simultaneously optimizing the molar absorptivities.

3.1.4 Determination of Composition and Absorptivities

The wavelengths selected for use in the fitting routine are shown in Table 3.1 along with the absorptivities for each TM. These wavelengths were carefully selected in order to maximize the accuracy of the results. This list includes all peak maxima for each TM in the wavelength range studied. It also includes a selection of other wavelengths. Each peak that appears in the UV-visible spectrum of the individual TMs (Figure 1.5, section 1.5.1.1) was represented by at least three wavelengths. Wavelengths were selected so that there was variability of TM absorptivities at each point. Increased variability improves the likelihood that two species can be discriminated from one another and thus unique absorptivities can be established (see section A1.2). Therefore,

Table 3.1. Molar absorptivities (M^{-1} cm^{-1}) of the TMs at selected wavelengths.

λ (nm)	TM0	TM1	TM2	TM3	TM4
287	0	8410	4280	3190	683
291	0	8560	4090	3740	1030
305	0	4920	4990	6870	8920
312	0	2870	6960	7330	15500
317	0	1930	8100	6650	17300
322	0	1370	8460	5500	15100
380	0	45.4	3250	6170	251
395	0	23.5	3790	9550	114
410	0	12.2	2930	6860	172
450	0	0	302	1920	7390
461	0	0	130	1860	11800
468	0	0	80.0	1780	12800
480	0	0	37.1	1540	9630

isosbestic points are not effective for this work. Also, an effort was made to find wavelengths that best represented each TM. In other words, at each wavelength a different TM was the dominant absorbing species. This helped to ensure that one TM was not biased over another.

Molar absorptivities of TM0 and TM4 were determined via Beer's Law curves at the selected wavelengths. Since these species could be obtained in pure form, direct measurements could be used for their characterization. A plot of absorbance vs. concentration at a constant wavelength resulted in a slope of εl, where l is the path length. Since the path length in this case is 1 cm, the slope is numerically equal to the molar absorptivity. A sample plot is shown in Figure 3.2. Molar absorptivities for TM0

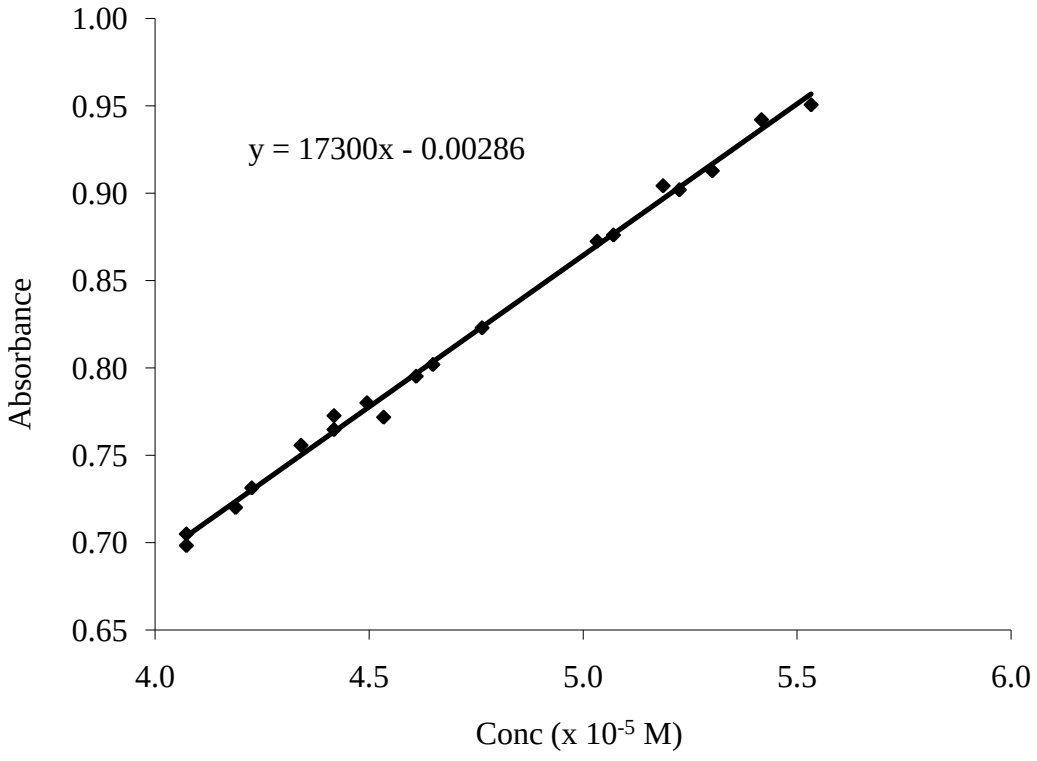

Figure 3.2. Beer's Law curve of TM4 solutions at 317 nm to determine the molar absorptivity.

and TM4 serve as anchors for the characterization of the other TMs. The accuracy of these absorptivities were therefore paramount and so were meticulously determined using a large number of solutions.

The absorptivities for TM1, TM2 and TM3 were all determined by curve fitting. As discussed earlier, TM1 and TM3 were synthesized to contain only TM0 and TM4 as contaminants, respectively. TM3 or TM1 absorptivities were thus left as the only unknowns. This reduced the number of variables and improved the quality of fit. Following TM1 and TM3 characterization, TM2 was characterized with all other TM absorptivities fixed. It should be noted that initially all TMs were included in the fitting routine. This was done to account for any unexpected TM contaminants. Once the TM2 absorptivities were known, the fitting of the TM1/TM0 and TM3/TM4 data was repeated with TM2 included. This was done to ensure that TM2 was indeed not present in these samples as well as to double check the quality of the previous analyses.

The first fitting stage involves the use of equation 3.3 to determine the sample composition. The absorptivities were set to reasonable starting values as determined either from the literature or by estimation from a synthesized sample. The average formula mass was calculated from an assumed initial composition.

Because the TMs were synthesized with different counterions, the formula mass depended on the target TM. For example, when synthesizing TM3, the target would be Cs_2MoOS_3 and so any TM4 that forms would be Cs_2MoS_4 as opposed to the ammonium salt that would be produced by TM4 synthesis.

Running the fitting routine produced a best fit once the optimized composition values were reached. From this composition, an improved formula mass could be calculated. Using this value, the fitting routine was initiated again. This sequence was re-executed using improved formula masses until there were no further improvements to the composition. Figure 3.3 shows the quality of fit obtained when determining the TM composition. Six of the selected wavelengths have been removed for clarity.

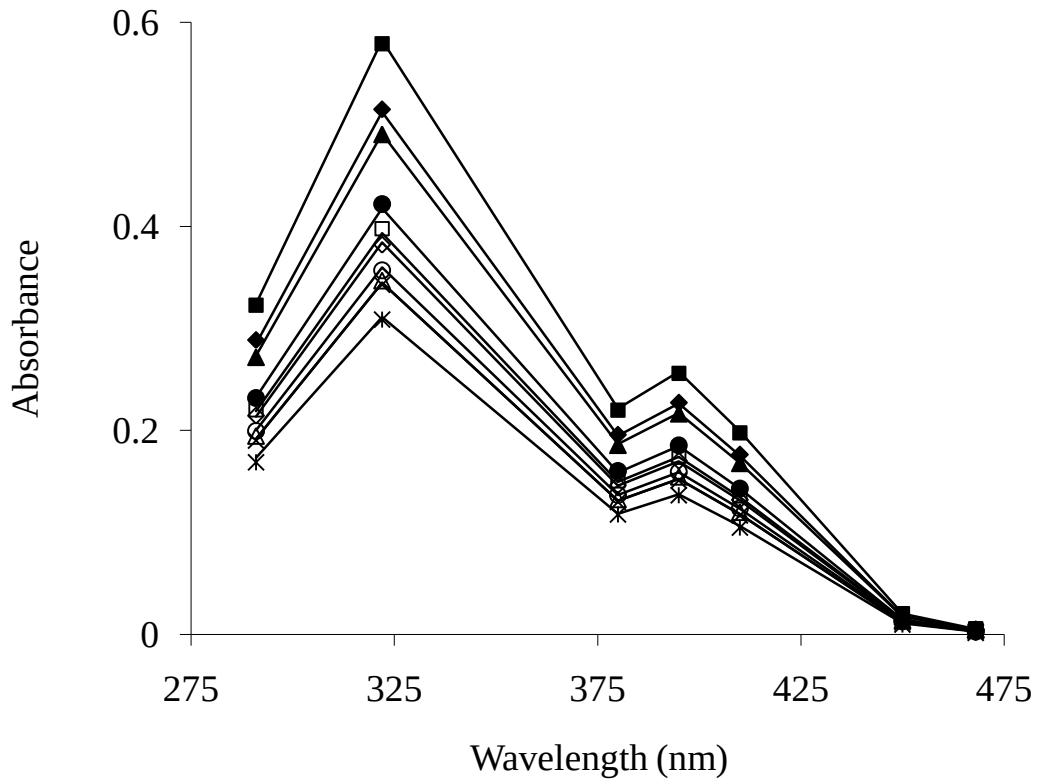

Figure 3.3. Origin7® fit to find TM composition in an impure sample. The data points are the solution absorbances at the selected wavelengths used in this study, the solid lines represent the fit.

By fixing the absorptivities, only the TM fractions were unknown. These unknowns can be reliably fit because the limited number of unknowns reduces the degrees of freedom. Each spectrum was measured from solutions of varying concentration but constant composition. Therefore, there was a single, unique value for each unknown fraction that allowed all datasets to be fit. The overall quality of the fit, however, was limited by the accuracy of the absorptivities used. As the absorptivity values were improved, the fit improved.

For the second fitting stage, the fractional TM composition and corresponding formula mass were fixed as the values calculated in stage 1. Execution of the fitting routine produced a set of absorptivities at the selected wavelengths for the unknown TM

in the sample. Figure 3.4 illustrates the quality of fit obtained for absorptivity determination. Six of the selected wavelengths have been removed for clarity.

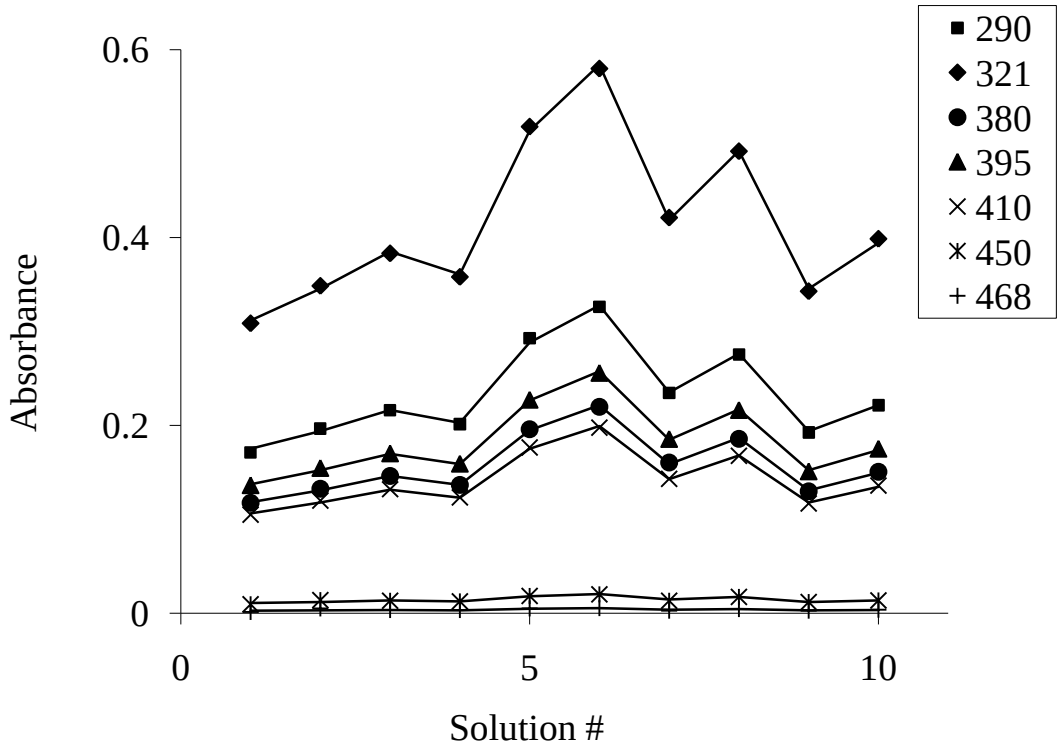

Figure 3.4. Origin7® fit to find TM molar absorptivities in an impure sample. The data points are the absorbances at selected wavelengths used in this study, the solid lines represent the fit.

With the composition and average formula mass fixed, the absorptivities could be exclusively determined. This was found to be more effective when the absorptivities of a single TM were being optimized. Early attempts to determine multiple sets of absorptivities proved unsuccessful because of the large number of unknowns. Whereas the TM fractions influence the absorbance at all wavelengths, the absorptivities apply to only a single wavelength. This affects the ability to find multiple absorptivities at each wavelength. This increases the linear dependence of the absorptivities on each other and reduces the likelihood of a unique set of values being found. In other words, there may be more than one combination of absorptivities that can make up that particular

absorbance. Instead, if a single absorptivity is sought at each wavelength, a single unique result can be obtained for each wavelength (see section A1.2).

The two fitting stages were repeated alternately by continually inputting the ever improved results until all parameters (α's and ε's) could be improved no further. Knowing the composition of the samples, the complete spectra of the pure TMs could be extrapolated. The spectra of the pure TMs as determined from this study are shown in Figure 3.5.

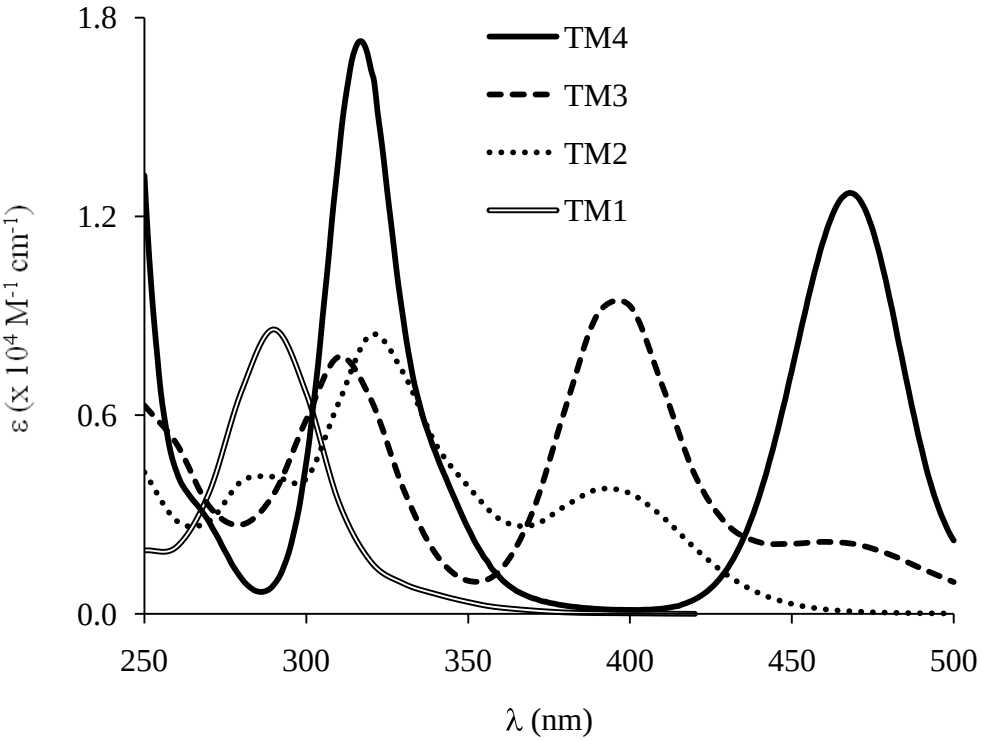

Figure 3.5. UV-visible spectra of the pure TMs.

As mentioned earlier, the wavelengths selected included peak maxima. These were simply observed from the synthesized spectra. Further investigation, though, showed that some peak maxima did not coincide with the true λ_{max}. This is likely due to the presence of other TMs in the synthesized samples. For example, the synthesized

TM2 sample had a peak maximum at 287 nm. This sample was contaminated with TM1 which has a strong absorbance at 290 nm. Contamination with TM1, therefore, could result in the peak maximum shifting slightly toward the λ_{max} of TM1. The true λ_{max} were determined by including the wavelengths on either side of the peak maxima in the fit, in this case 286 and 288 nm. All previously determined absorptivities were fixed and the new absorptivities were determined. In the case of the synthesized TM2 sample, a λ_{max} at 286 nm was found. This process was repeated for all peak maxima and for each TM in order to effectively determine the λ_{max} values.

There are some significant discrepancies between absorptivities achieved in this work compared to other works (Table 3.2) [6, 30, 136]. This is likely due to the

Table 3.2. Molar absorptivities (ε in M^{-1} cm^{-1}) at λ_{max}. Errors for TM0 and TM4 are standard deviations of the slope of the Beer's Law curves. All others are RMS deviations as determined from the fit.

	This Work			Erickson 2000 [30]			Muller 1969 [41]	
	λ_{max}	ε	±	λ_{max}	ε	±	λ_{max}	ε
TM0	207	10100	200				208	8400
							231	2800
TM1	290	8600	50	290	7390		288	8000
				314	2900		314	3000
TM2	286	4300	50	290	3940	40	288	3000
	321	8470	60	322	6740	60	318	6000
	395	3790	30	394	3230	50	394	3000
TM3	312	7330	40	312	7500	40	313	6600
	396	9550	80	396	9030	80	392	8700
	461	1860	20	462	2080	10	465	2300
TM4	317	17300	300	318	16480	190	317	18000
	468	12800	200	468	11870	150	467	13000

characterization methods (see section 1.5.1), in conjunction with potentially impure samples that were assumed to be pure. Differences in λ_{max} may also be a result of shifts caused by contamination. By determining the composition concomitantly with the absorptivities, values are not dependent on the purity of the synthesized sample.

In the case of TM1, the absorptivity obtained in this work at 290 nm is greater than from other works. Because TM1 had not previously been isolated, this value was obtained by monitoring its formation in solution [137]. During formation there is not likely to be a point at which only TM1 is present because of the rapid formation of TM1 and TM2. It is likely that TM2 will begin to form while TM0 is still present. The presence of TM2 accounts for the second small peak that was often recorded around 314 nm [7, 30, 137]. Being able to synthesize and isolate the TM1 salt was paramount to being able to properly characterize TM1 and subsequently TM2.

It is difficult to identify contamination in a TM2 sample by inspection of the UV-visible spectrum. This is because the TM2 spectrum is completely overlapped by the TM1 and TM3 spectra. TM3 does absorb around 461 nm, however, the absorbance is weak and so small amounts of TM3 may still not be obvious. Large amounts of TM3 would lead to increased absorbance in the peak at 395 nm but this would also be apparent at 461 nm. Contamination with TM1 would explain the differences in λ_{max} for the peak at 286 nm. In this case, though, an increase in absorbance and thus absorptivity might be expected. However, it also may be possible to have some contribution of TM0 in the sample, as well, which does not absorb in the studied region and would reduce the overall absorbance. The presence of undetected contaminants, generally, would lead to the lower absorptivities reported by Erickson and Helz [30] and Muller et al. [41] than were seen in this work.

The TM3 spectrum gives away the fewest clues about contamination. One method of attempting to quantify purity in the literature was to find a characteristic peak ratio between the peaks at 396 and 461 nm [20]. There has been very little agreement on this value in the literature, though [9, 20, 25]. The presence of TM2 will decrease both absorbances by a similar amount since the difference in absorptivities at both wavelengths is similar. This method is therefore a poor landmark for purity.

Qualitatively, one can identify the primary contaminant in synthesized "TM3". Around 461 nm TM3 has a plateau. The formation of a discernable peak indicates the

presence of TM4. If TM2 is the primary contaminant a shoulder should appear at 286 nm. This may be difficult to observe if there is only a small amount of TM2 present. Table 3.2 shows that the absorptivities at 461 nm are greater (and slightly shifted) in the literature examples. This is indicative of TM4 contamination.

The primary difference between the method of characterization described in this thesis and those attempted by others is that purity and absorptivities are determined simultaneously. Direct measurement of absorptivities may result in very good precision but the accuracy is intimately dependent on the initial purity of the sample. By fitting both absorptivity and composition together, the error in one is not propagated onto the other. This method also utilizes the mass of the sample and accounts for the actual formula mass and not that of the target species. This minimizes errors incurred by assuming molar concentrations.

3.1.5 Application of Absorptivities

The ultimate goal of this work is to be able to find TM concentrations from a mixture in solution. To test this, TM mixtures were created from the previously characterized samples and the theoretical concentrations calculated. The UV-visible spectra were then fit using equation 3.1. These fit results were then compared to the theoretical composition. Table 3.3 shows the theoretical composition and the results determined by fitting. Regardless of which TMs were expected to be present, all TMs were included in the fitting routine. This was done to ensure that artifactual concentrations of nonexistent TMs didn't appear.

TM solutions were created such that concentrations could be calculated to three significant figures. This allows the TM fractions to be optimized to 0.1 %. The ability to measure changes this small gives this method a great advantage over methods previously described in the literature (see section 1.5.1). This provides an increased level of confidence in the quantitative analyses of TM mixtures.

Table 3.3. Comparison of theoretical composition with results from fitting UV-visible data.

Theoretical % Mo					% Mo from fit				
TM0	TM1	TM2	TM3	TM4	TM0	TM1	TM2	TM3	TM4
56.5	43.5				56.5	43.5			
3.3	51.1	45.6			3.8	48.1	48.2		
			44.2	55.9				44.1	55.9
	5.7	57.4	35.5	1.6		5.2	56.4	36.9	1.5
	5.3	53.8	39.3	1.7		4.7	53.4	40.4	1.6

Differences between the theoretical and experimental values for TM0/TM1 and TM3/TM4 mixtures are quite small. These differences can be attributed to small errors in the respective absorptivities as well as errors incurred during the making of the solutions. In fact, it is easy to identify when the fit deviates due to solution concentration errors. If this is the case, the fit line parallels the experimental absorbance across the spectrum. The fit can then be optimized completely by adjusting the concentration. On the other hand, errors in the absorptivities would likely cause a random deviation between fit and experiment. Deviations of this kind are minimal. Because only one solution is being fit at a time the error in the fit is expected to be greater than is achieved from fitting multiple data sets (from multiple solutions) simultaneously.

Mixtures including TM2 seem to show the greatest discrepancy. The molar absorptivities of TM2 were the last to be determined. The error in the TM0 absorptivities would propagate into the TM1 absorptivities and then, finally into the TM2 values. Therefore, the errors in the TM2 absorptivities are expected to be the greatest. Perhaps more importantly, though, is how precisely the composition can be determined over time, i.e., how sensitive is this method to small changes in composition. Since this will be used to monitor concentrations in kinetic experiments

the initial accuracy is less important than the precision of the fitting since it is the rate of change that is of interest.

Hydrolysis experiments were used to examine the effectiveness of this method for following changes in solution. Figure 3.6 shows UV-visible spectra of a previously characterized "TM2" sample in water as hydrolysis occurs. For clarity some spectra in

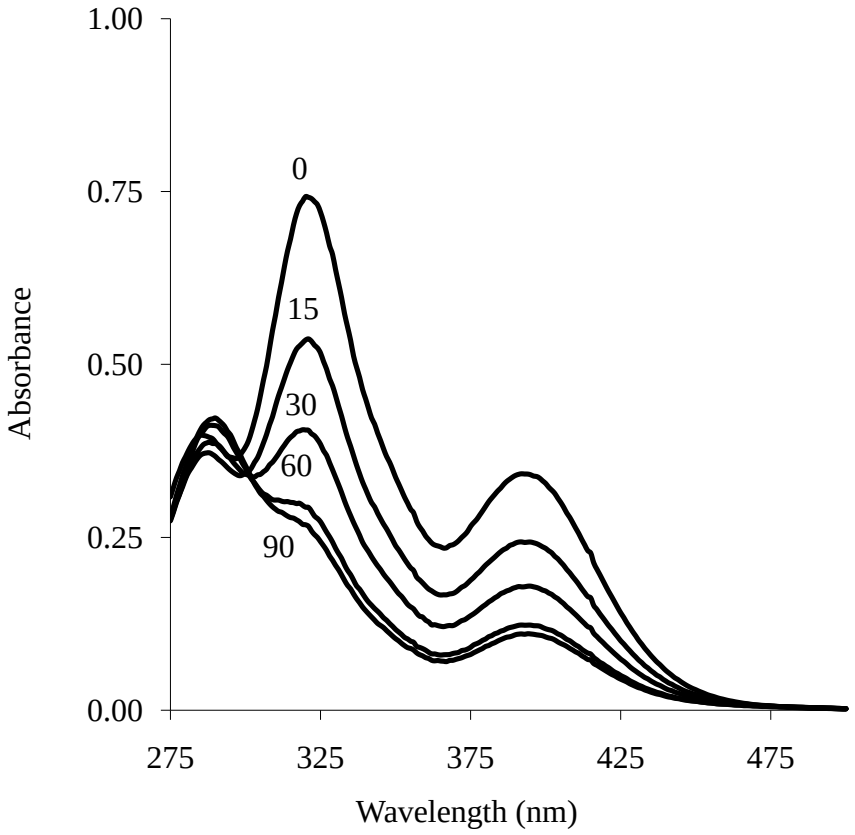

Figure 3.6. UV-visible spectra of a TM2 solution sample hydrolyzing with time. The numbers represent the incubation time in minutes.

the series have been removed. Figure 3.7 shows the percentage of each TM species present during each measurement as determined from Origin7® fitting. The smoothness of the concentration vs. time curves indicates a consistent response to changes in concentration of all TMs.

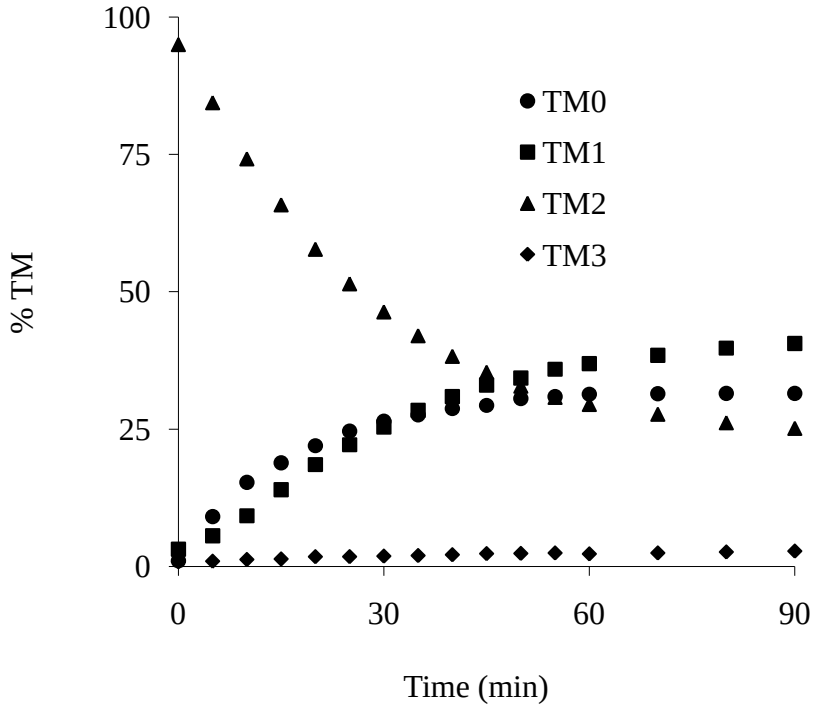

Figure. 3.7. TM composition over time obtained from Origin7® fit of UV-visible spectra shown in Figure 3.5.

The quality of the fit over time was very good. Only after long periods of time, especially when a particular species approached zero, did the quality of the fit began to degrade slightly. The reduction in the quality of fit, though, did not appear to affect the resulting concentrations at the 0.1 % level. The consistency of the results also did not appear to be affected. If this were so, increased scatter in the concentrations would be expected over time.

Some comparisons can be made between the UV-visible spectra in Figure 3.5 and the results shown in Figure 3.7 that support the validity of the results. The increase in absorbance at 461 nm indicates the formation of TM3. This was also seen in the fitting results. The decrease in absorbance at 321 nm and 395 nm indicates the loss of TM2. The peak at 286 nm increases with time and gradually shifts to longer wavelengths. This is expected for an increase in TM1 concentration since TM1 has a

λ_{max} at 290 nm. Also, TM1 absorbs more strongly than TM2 in this region prompting the increase in absorbance. Finally, after 90 minutes, it is apparent that the spectrum is losing many of its features and the magnitudes of the absorbances are generally decreasing. This is consistent with the conversion of the TMs to TM0 which absorbs at shorter wavelengths than were measured here. The fitting results are consistent with all of these observations.

Further hydrolysis experiments were performed with each TM with the same success as the TM2 case (data not shown). This shows that this method can be used to monitor TM mixtures in solution as the species interconvert. Percentages can be easily converted to TM concentrations for use in kinetic analyses.

3.2 THIOMOLYBDATE INTERCONVERSION KINETICS

3.2.1 Introduction

The complete TM interconversion scheme is rather complex. In order to overcome this complexity previous workers have isolated single processes and individually obtained rate constants. This first requires the synthesis of a pure starting material and secondly assumes that only that process of choice is occurring. The specifics of the work carried out previously and the limitations with these studies were described in section 1.5.2. The difficulties in establishing initial TM purity were discussed in section 1.5.1.

The focus in our lab is the computer modeling of Cu-ligand interactions in the bovine rumen. Thiomolybdates play a crucial role in Cu speciation because of their high binding affinity toward Cu. However, each thiomolybdate reacts differently with Cu. For example, TM1 and TM2 are thought to have little effect on Cu while TM3 and TM4 are the primary antagonists [37]. Compounding the issue is the relatively slow formation of TMs. And so, in order to properly determine the effect of TMs on Cu, accurate rate constants determined under biologically relevant conditions are required.

This means determining all necessary rate constants simultaneously without the assumption of isolated reactions.

This section describes the simultaneous determination of the kinetic parameters from reactions performed under biologically relevant conditions. This was done by fitting the integrated rate equations of the appropriate reaction scheme to the concentration vs. time data (see section 3.1.5). The integrated rate equations were developed using the Laplace Transform method and the fitting was carried out using Origin7® software. Rate constants at varying pH, ionic strength and temperature were then determined and a plausible reaction mechanism was proposed.

3.2.2 Reaction Order

TM formation experiments were carried out using the methods outlined in section 2.4.2. Figure 3.8 shows the progress of a typical formation experiment as monitored by UV-visible spectroscopy. TM concentrations were determined from the UV-visible spectra as described in section 3.1.5. Figure 3.9 shows the resulting TM concentration vs. time data. This information can then be used for calculating reaction rates and eventually in the fitting that produced the rate constants.

The order of reaction with respect to the various components was determined first. This was necessary since the Laplace transform method is only valid if all processes are first or pseudo-first order. Since sulfide concentrations were routinely in large excess, the prerequisite for using this method was that the reaction was first order with respect to Mo. Previous studies of reaction order consisted of monitoring individual processes [6, 7, 26]. Reaction orders were therefore determined using the methods described in this thesis in order to corroborate the results.

The balanced equation for a single formation and corresponding hydrolysis reaction can be nominally shown as in equation 3.5 for the TM1/TM2 case. This would suggest that a dissociative mechanism (with first-order kinetics) or an associative

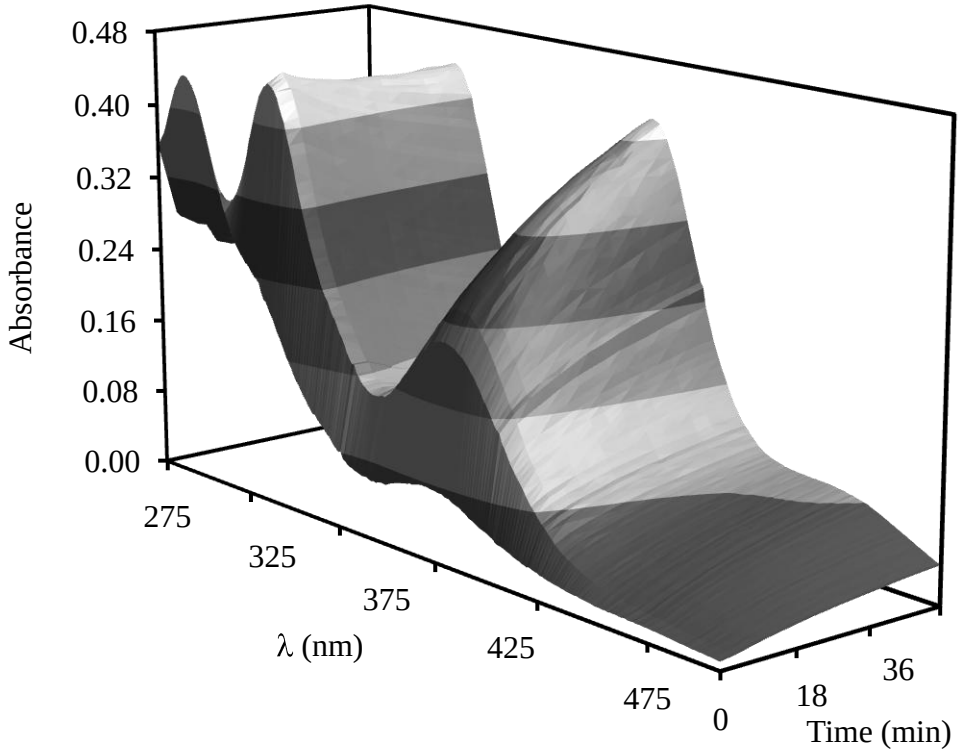

Figure 3.8. UV-visible spectra of TM formation over time.

mechanism (second-order) could be plausible. Actual proposed mechanisms will be discussed in section 3.2.4.4.

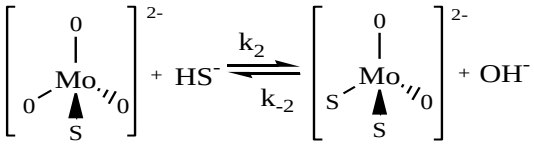

(3.5)

From equation 3.5, nominal rate laws for forward and reverse reactions can be written as shown in equations 3.6 and 3.7.

$$\text{rate} = k_2 [TM1]^m [HS^-]^n \quad \textbf{(3.6)}$$

$$\text{rate} = k_{-2} [TM2]^o [OH^-]^p \quad \textbf{(3.7)}$$

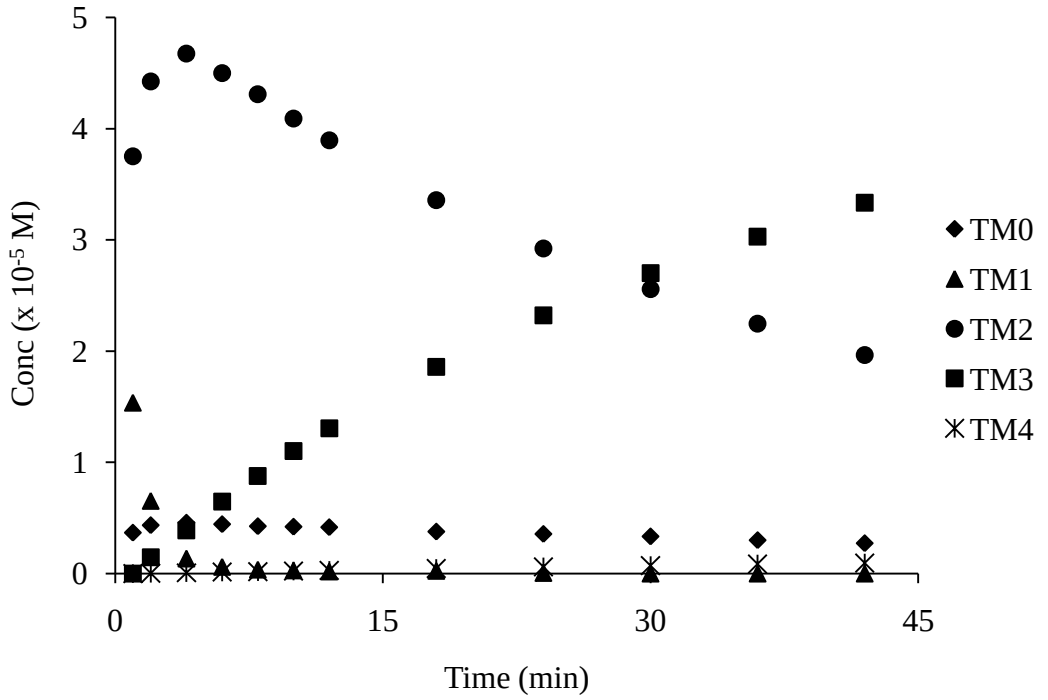

Figure 3.9. TM concentration vs. time for typical formation experiment.

The variables m, n, o and p are reaction orders with respect to the corresponding species. Since the formation experiments are being run with a large sulfide excess and in buffered solutions, equations 3.6 and 3.7 can be simplified to equations 3.8 and 3.9

$$\text{rate} = k_2' [TM1]^m \quad \textbf{(3.8)}$$

$$\text{rate} = k_{-2}' [TM2]^o \quad \textbf{(3.9)}$$

where k_2' and k_{-2}' are the pseudo-rate constants and are defined in equations 3.10 and 3.11.

$$k_2' = k_2 [HS^-]^n \quad \textbf{(3.10)}$$

$$k_{-2}' = k_{-2} [OH^-]^p \quad \textbf{(3.11)}$$

The order of k_2' and k_{-2}' depends solely on that of the TMs. Taking the log of equations 3.8 and 3.9 gives equations 3.12 and 3.13.

$$\log \text{rate} = \log k_2' + m \log [TM1] \quad \textbf{(3.12)}$$

$$\log \text{rate} = \log k_{-2}' + o \log [TM2] \quad \textbf{(3.13)}$$

Now it can be readily seen that plots of log rate vs. log [TM] will produce linear curves with the slope being equal to the order of the reaction with respect to TM.

The various TM concentrations were obtained at each time interval by the fitting methods described in section 3.1.5. The initial rate of TM2 formation and TM1 loss were then calculated. Initially, the formation of TM2 was the only measurable process occurring. TM0 had already reached a steady state concentration as of the first measured spectrum. The TM3 concentration increased very slowly at first and only became significant after a sufficient buildup of TM2.

The initial rate of TM3 formation could not be determined. Because TM2 was being rapidly formed from TM1, the rate of formation of TM3 would accelerate as TM2 was formed. Therefore, attempting to obtain the initial rate of formation of TM3 would result in an underestimation of the true rate. The rate of TM3 formation was therefore determined at a later time when the formation of TM2 was complete (TM1 had reached a steady state concentration). At this point, the only competing reaction would be the formation of TM4. The slow formation of TM4 would account only minimally to the error of the rate of TM3 formation.

Plots of log rate vs. log [TM] gave slopes of 1.0 ± 0.1 and 1.1 ± 0.1 for TM2 and TM3 formation, respectively. A sample plot of the formation of TM2 is shown in Figure 3.10. These values agree with those reported in the literature [7, 26]. These results indicate that the formations of TM2 and TM3 are obeying first order kinetics with respect to the TM.

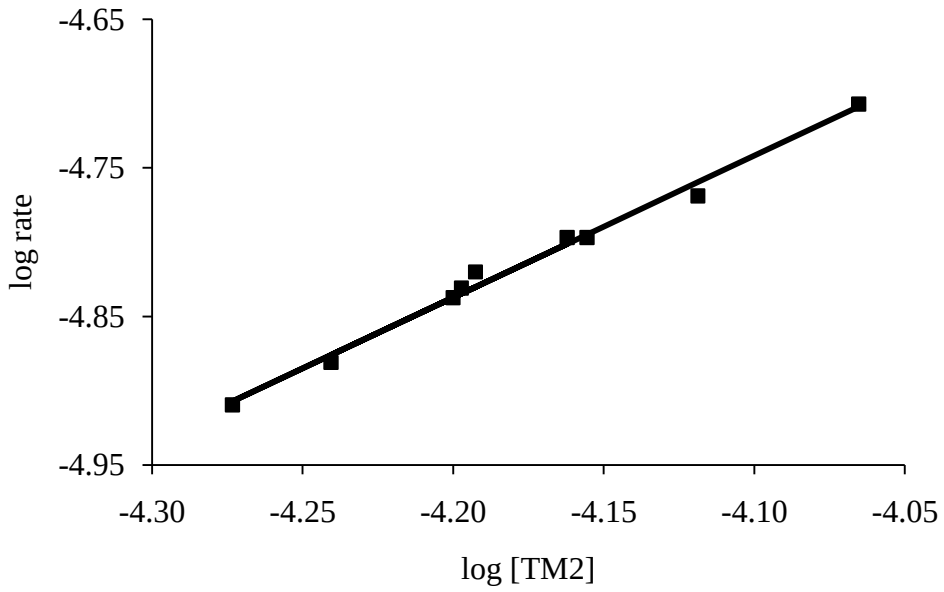

Figure 3.10. Order with respect to TM for the formation of TM2.

The order with respect to the TM for the formation of TM4 was more difficult to ascertain. The slow rate of initial formation made accurate rate determinations difficult. In fact, there was typically a lag of up to 5 minutes before any TM4 formation was observed as the TM3 concentration had to build up first. Also, with multiple reactions occurring simultaneously, the rate of TM4 formation is intimately tied to the progress of the other, faster, processes. In this case, TM4 formation is best monitored from a TM3 starting point as this reaction can be sufficiently isolated. Harmer and Sykes and Brule et. al. have shown a first order response with respect to Mo [6, 7]. Clarke et al. used TM2 for the starting material and achieved the same result [26]. The formation of TM4 will be considered first order with respect to TM.

The order with respect to sulfide for the formation reactions and hydroxide for the hydrolysis reaction can be determined using equations 3.10 and 3.11, respectively. By taking the log of equations 3.10 and 3.11, equations 3.14 and 3.15 are obtained. Details of how k' values were obtained are presented in section 3.2.3.

$$\log k_2' = \log k_2 + n \log [HS^-] \quad \textbf{(3.14)}$$

$$\log k_{-2}' = \log k_{-2} + p \log [OH^-] \quad \textbf{(3.15)}$$

Plots of log k' vs. log [S] for the formation of TM2 and TM3 gave slopes of 1.0 ± 0.1 and 0.8 ± 0.1, respectively, indicating first order responses. The errors are in terms of standard deviations of the slopes. Since these slopes are based on the pseudo-first order rate constants and not the rate, the occurrence of multiple simultaneous reactions would not be a source of error. Instead, the deviation of the formation of TM3 from the integer value may be due to slight errors in the kinetic fitting. However, this difference is not significant enough to prompt speculation of a more complicated mechanism.

The order with respect to S for the k_4 process has been reported in the literature as both zero-order [6] and, tentatively, as second-order [7]. In the present work, the slope of the log k' vs. log [S] is 0.13 ± 0.02. This would suggest that a zero-order result is more likely. Perhaps more telling, though, is that when it is assumed that the k_4 reaction is first-order with respect to H_2S, the resulting overall second order rate constant is constant with changing ionic strength or pH. This provides a strong indication that the k_4 process is first order with respect to S. In addition, the simplest scenario is that k_4 would be of the same order and hence the same mechanism as the other forward processes. For this work, a first order result with respect to S for the k_4 process will be assumed.

The near zero slope for the formation of TM4 is probably a result of its slow formation. In order to see a large change in k_4', there would have to be a large change in the sulfide concentration used. However, experimental considerations reduced the possible effective range of sulfide. If too large of a sulfide concentration was used in phosphate buffer, precipitation was induced. Conversely, if the concentration was reduced, the MoO_4^{2-} concentration also had to be reduced in order to maintain the requisite S excess. With lower MoO_4^{2-} concentrations, peaks such as the TM4 peak at 468 nm took longer to appear making it more difficult to accurately follow its

formation. The slowness of TM4 formation may also be the cause of the uncertainty in the literature.

In addition to TM4 formation being slow, there was very little change in TM4 concentration relative to changes in the other TMs. During the fitting process, small adjustments in k_4' (~ 1%) produced very small changes in the quality of the fit. Adjustment of the other three rate constants, however, produced much larger improvements. This may have created a bias toward the optimization of k_2', k_{-2}' and k_3'. Since optimization of these three rate constants results in a good quality of fit with a very low reduced chi^2 value, the quality of fit is improved only marginally by adjusting k_4. As a result, small changes that may be expected in k_4' as the S concentration is changed were not detected causing an erroneously low slope for the log k' vs. log [S] curve. Fortunately, this type of error in k_4' is not expected to significantly affect the other rate constants.

The k_{-2} process involves, nominally, the reaction of TM2 with OH^- to form TM1. The slope of the graph of log k_{-2}' vs. log $[H^+]$ was 0.8 ± 0.1 suggesting first order with respect to H^+. This is in apparent contradiction with the notion that the reaction involves OH^-. This issue will be addressed throughout section 3.2.

All four processes have been determined to be first-order with respect to the TM. All processes were also determined to be second order overall. By keeping the sulfide in large excess and the pH buffered in all cases, pseudo-first order conditions are maintained. Therefore, the Laplace Transform method can be utilized for determining the integrated rate equations necessary for the fitting routine.

3.2.3 Reaction Scheme and Determination of Rate Constants

The complete theoretical reaction scheme for TM interconversions is shown in equation 3.16. Integration of the appropriate rate equations would be extremely cumbersome and would likely require special training to solve. As was alluded to in section 3.2.2, however, the Laplace Transform method can be used in order to solve the

$$TM0 \underset{k_{-1}}{\overset{k_1}{\rightleftharpoons}} TM1 \underset{k_{-2}}{\overset{k_2}{\rightleftharpoons}} TM2 \underset{k_{-3}}{\overset{k_3}{\rightleftharpoons}} TM3 \underset{k_{-4}}{\overset{k_4}{\rightleftharpoons}} TM4 \qquad \textbf{(3.16)}$$

integrated rate equations without knowledge of advanced calculus. The rate constants can then be determined via non-linear least squares fitting of integrated rate equations to the experimental concentration vs. time data.

The fitting procedure, carried out using Origin7® software, involves iteration of the rate constants until the theoretical equations match the experimental data. The initial concentrations of each TM found from the first spectrum collected after mixing were input as constants (non-zero starting concentrations were incorporated into the equations). The TM concentrations were the dependent variables and the corresponding times were the independent variable. The rate constants were the optimized parameters.

The Laplace Transform method involves taking the Laplace transform of the fundamental rate equations thus converting the time domain equations to frequency domain equations. These equations are then solved using matrices before taking the inverse Laplace transform to get the time domain integrated rate equations. The details for the general use of this method are outlined elsewhere [138]. Laplace and inverse Laplace transform solutions are tabulated and can be found in the literature [139].

Even using the Laplace Transform method, it is rather cumbersome to determine the integrated rate equations for equation 3.16. Also, under the biologically relevant conditions studied, there is no evidence that all processes indeed occur. The true reaction scheme must therefore be determined before the rate constants can be determined. In fact, the inclusion of redundant parameters (in this case the rate constants) in the fitting routine can lead to meaningless results even with a good quality fit (see section A1.2). The true reaction scheme will therefore include the least number of parameters that allow a satisfactory fit.

In order to simplify the reaction scheme, some simple assumptions can be made. First, the k_1 and k_{-1} processes could not be observed. Analysis of the first spectrum in a typical formation experiment shows that TM0 has already reached a steady state concentration. Also, TM1 has already peaked and its concentration is in decline (Figure 3.9). It can therefore be assumed that TM1 is the starting point. Second, a large excess of sulfide is used in all experiments. Le Chatelier's principle suggests that this will force the reaction to the right and so the reverse reactions are assumed absent. The simplified reaction scheme will thus contain only the forward processes starting from TM1 (equation 3.17).

$$\mathrm{TM1} \xrightarrow{k_2} \mathrm{TM2} \xrightarrow{k_3} \mathrm{TM3} \xrightarrow{k_4} \mathrm{TM4} \qquad \textbf{(3.17)}$$

The Origin7® fit using this reaction scheme is shown in Figure 3.11. Overall, the fit is poor, suggesting that this model is incomplete. The most striking deviations of the fit

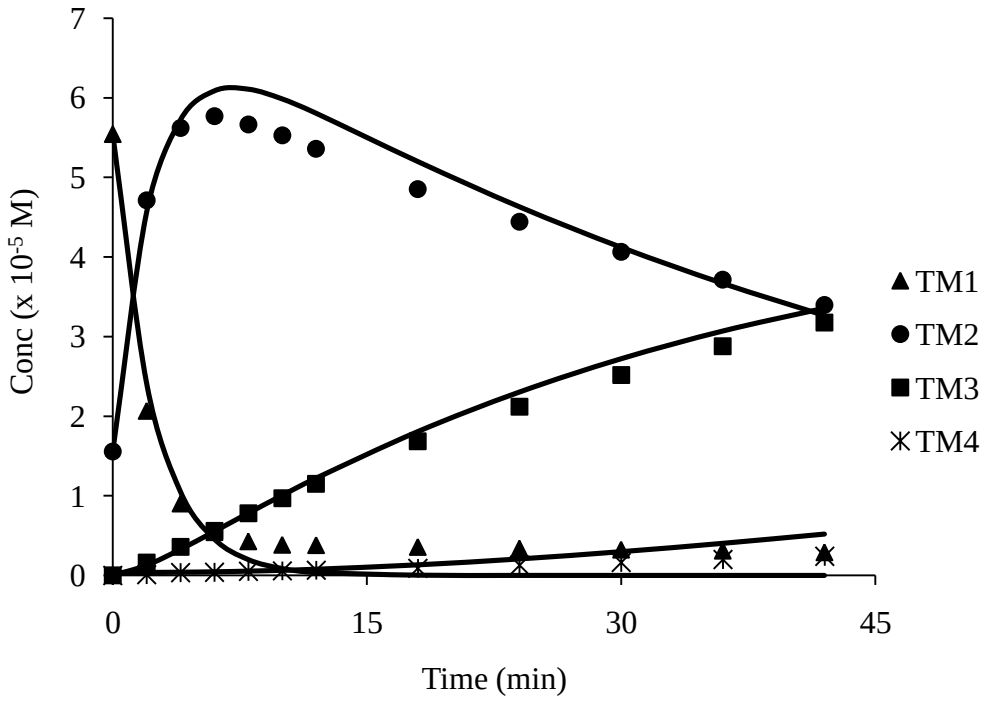

Figure 3.11. Origin7® fit (solid lines) of forward only reaction scheme (equation 3.17) to experimental concentration vs. time data (points).

from the data are seen in the TM1 and TM2 curves. The TM1 fit shows the complete loss of TM1 despite the actual TM1 concentration remaining at a non-zero level. This indicates that TM1 must in some way be regenerated throughout the reaction. Conversely, the fit of TM2 overestimates the experimental curve. Also, the deviation seen for TM1 appears to be of similar magnitude as that of TM2. It seems reasonable then that TM2 must be the source of TM1 regeneration. The k_{-2} process was therefore included to account for this discrepancy. The new reaction scheme is shown in equation 3.18.

$$\mathrm{TM1} \underset{k_{-2}}{\overset{k_2}{\rightleftharpoons}} \mathrm{TM2} \xrightarrow{k_3} \mathrm{TM3} \xrightarrow{k_4} \mathrm{TM4} \qquad \textbf{(3.18)}$$

New equations were developed from equation 3.18 and incorporated into the Origin7® fitting routine. The resulting fit is shown in Figure 3.12. The inclusion of k_{-2}

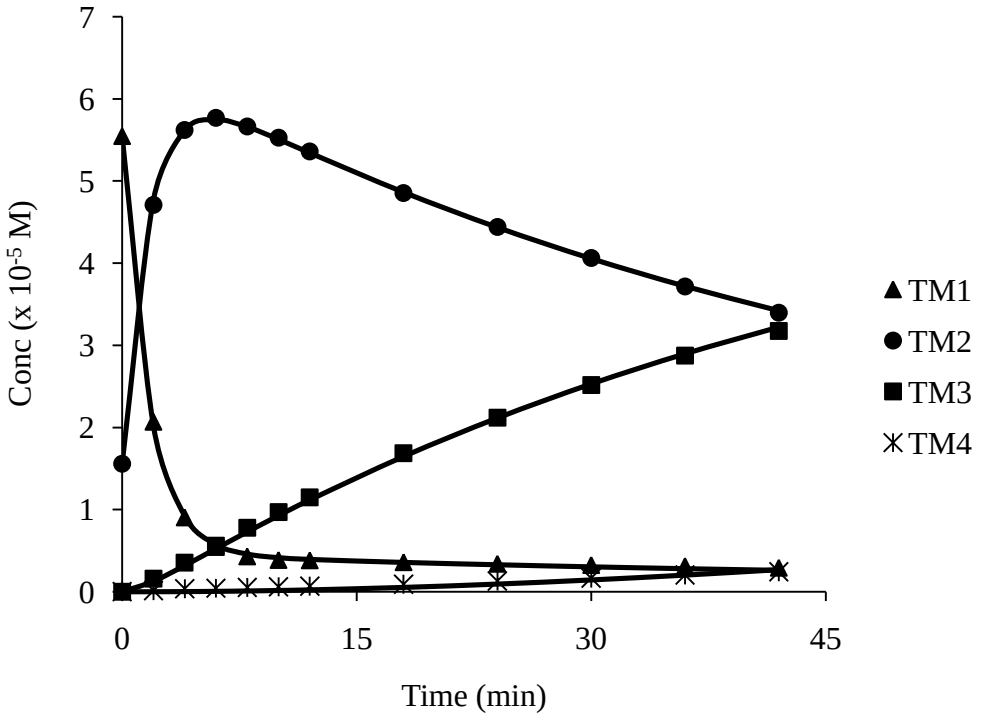

Figure 3.12. Origin7® fit (solid lines) of reaction scheme including k_{-2} (equation 3.18) to experimental concentration vs. time data (points).

clearly improved the quality of fit. This provides strong evidence that the k_{-2} process occurs significantly under the reaction conditions studied. It is unclear if the regeneration of TM1 from TM2 is a result of simple hydrolysis or of disproportionation of two TM2 molecules to form TM1 and TM3. Nonetheless, it is perhaps not surprising that this occurs even under excess sulfide condition. TM2 is relatively unstable in aqueous solution as demonstrated in section 3.1.5 and quickly begins to hydrolyze to form TM1 and TM0. Meanwhile, the formation of TM3 from TM2 is not a particularly rapid process. It thus stands to reason that an excess of sulfide will not fully restrict the k_{-2} process.

The k_{-3} and k_{-4} terms were also included to ascertain their possible occurrence. Neither of these, however, resulted in any further improvement in the fit. TM3 and TM4 are significantly more stable in non-sulfidic aqueous solution than TM2. TM3 is stable for over an hour while TM4 may be stable for up to a day. In these cases their formations are significantly faster. The presence of a large excess of sulfide would only favor the formation processes. It is therefore reasonable to conclude that the k_{-3} and k_{-4} processes do not measurably occur and so they were not included for any further analysis.

This is an example of how curve fitting can be used to determine the true reaction scheme for complex reactions. The true reaction scheme will be consistent with the model that accurately fits to the data. This has been seen elsewhere in the literature [140].

3.2.4 Effect of Varying Parameters

There are two main reasons for determining the rate constants under varying conditions. The first, and most important to this study, is to have reliable values for the Cu-ligand speciation model. In the rumen, there may be natural variations of ionic strength, pH and temperature. In order to accurately predict Cu speciation, TM formation rate constants that cover the appropriate ranges are necessary.

The second reason for varying reaction parameters is to gain mechanistic information. Although basic mechanisms have been suggested in the literature, there are some points of debate such as the specific identity of the sulfide species. Some of the inconsistencies in the literature may be related to the methods used to determine the rate constants. The improved methods described in this thesis should provide increased certainty about the mechanism.

3.2.4.1 Effect of Ionic Strength

In the literature the sulfide nucleophilic species has been referred to nominally as H_2S [6, 34]. It has been shown that the rate of formation increases with decreasing pH. The fraction of H_2S also increases under these conditions. Harmer and Sykes, however, alluded to HS^- being the likely nucleophile [7]. This is reasonable from a standpoint of TM synthesis which is carried out at pH 10-13. pKa_1 for H_2S is 7 while pKa_2 is 17 [141] leaving HS^- as the dominant species for *in vitro* synthesis. At the pH of the rumen, both H_2S and HS^- will be present in significant amounts.

Table 3.4 shows the second order rate constants at pH 7.2 at varying ionic strengths. The true rate constants were calculated using equations 3.14 and 3.15. The order with respect to sulfide, n, was 1 and the sulfide concentration was taken to be the

Table 3.4. Rate constants with varying ionic strength. T = 38°C, pH = 7.2. All rate constants are in $M^{-1}min^{-1}$. Numbers in parentheses are the standard deviation of the last significant digit.

I (M)	$k_2 \times 10^2$	$k_{-2} \times 10^5$	k_3	k_4
0.15	2.0 (1)	6.1 (9)	5.4 (5)	0.54 (4)
0.20	2.0 (1)	8 (4)	5.2 (2)	0.47 (7)
0.25	2.3 (2)	6 (1)	6.1 (4)	0.48 (6)
0.30	2.3 (2)	6.1 (1)	5.4 (6)	0.5 (1)

concentration of the H_2S fraction. The ionic strength of the rumen is typically around 0.15 M and so this served as a starting point for the ionic strengths studied. The ionic strength range studied was 0.15 – 0.30 M. Within this range, the activity coefficient is essentially constant and so concentrations and not activities can be used. Lower ionic strengths were not used because this would have required the use of a weaker buffer concentration and there is an increased risk of the pH changing.

The rate constant is related to the ionic strength by the Debye-Hückel limiting law (equation 3.19) where z_A and z_B are the charge of reacting species A and B, respectively. Plotting log k vs. √I therefore produces linear curves with slopes equal to $1.02z_az_b$ [142]. The identity of the reacting species may then be inferred.

$$\log k = \log k° + (1.02z_Az_B)\sqrt{I} \qquad \textbf{(3.19)}$$

Figure 3.13 shows the log k vs. √I plots for each process. The slopes obtained from the k_{-2} and k_3 values were -0.2 ± 0.5 and 0.2 ± 0.2, respectively. Using

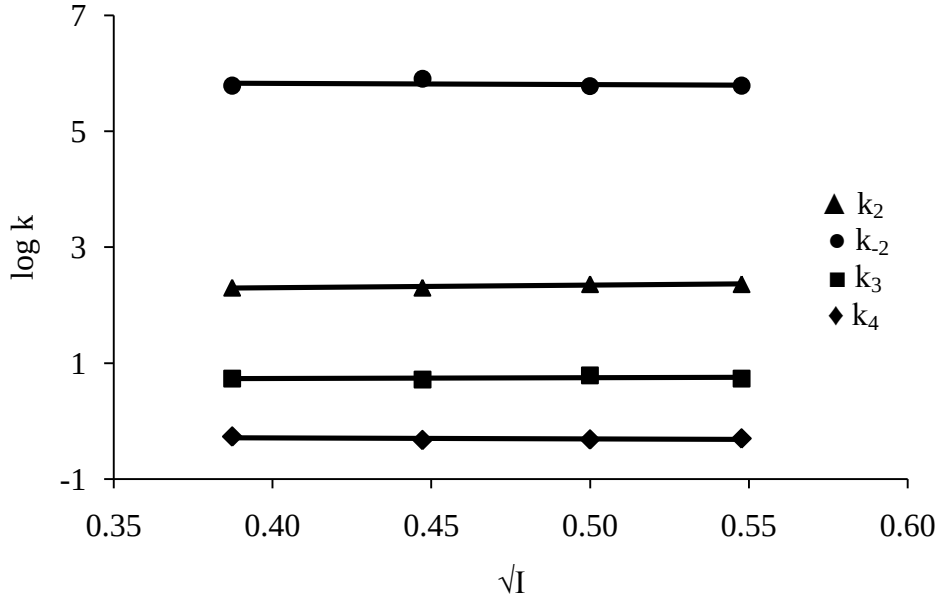

Figure 3.13. Plots of log k vs. √I. Log k values were calculated from second order rate constants with units $M^{-1}min^{-1}$. Data was obtained at pH 7.2 and T = 38°C.

standard deviations of the slopes, t-tests were performed and showed that neither of these were statistically different from 0 at a 99% confidence limit. From k_2 and k_4, the slopes were 0.5 ± 0.2 and -0.6 ± 0.4, respectively. Though the slope obtained using k_4 was closest to -1, this would not be a sensible result and so a slope of 0 is assumed. This slope is likely skewed because of the slightly higher value at an ionic strength of 0.20 M. The slope using k_2 was equally close to 0 and 1. However, looking closely at the data, there is no consistent trend that convincingly suggests a slope of 1. On the other hand, all other processes result in a slope of 0, this is assumed to be 0 as well.

The 0 slope indicates a neutral species in the rate determining step. This is likely to be H_2S, or H_2O in the case of k_{-2}. From the pKa's of H_2S (7) and H_2O (15), it is evident that there are significant concentrations of these species present at pH 7.2. On the other hand, pKa_2 for MoO_4^{2-} is estimated to be between 5.0 and 6.5 [143]. At the neutral to slightly acidic pH range studied, the unprotonated and singly protonated species will be dominant. There are no pKa's given in the literature for the TMs. However, based on the pKa's of H_2S and H_2O, we may qualitatively assume that the TMs have lower pKa's than TM0 or, at least, that they are a high estimate. We can therefore assume that the TMs are not likely fully protonated. The only neutral species present at significant concentration will be H_2S. It is likely that at higher pH values, such as those used for TM synthesis, that HS^- is still the nucleophile. Based on this data, though, H_2S (and H_2O for k_{-2}) appears to be the preferential nucleophile when it is present in sufficient quantity.

That H_2S is the nucleophile in the formation reactions is counter to what was expected by Harmer and Sykes [7]. However, if HS^- were the sulfide source, the electrostatic repulsion of the TM ions and HS^- would be unfavorable. Perhaps more importantly, it is difficult to rationalize the decrease in HS^- concentration with the increasing rate constant. Instead, it seems plausible that H_2S is the preferred nucleophile in the neutral to acidic pH range while HS^- is adequate at more basic pH's when it is the dominant sulfide species.

3.2.4.2 Effect of pH

The pH in the bovine rumen can range from 5.8 - 7.2 but is typically around 7 [115]. Under the conditions used in this study, however, the sulfide solution often became cloudy below a pH of 6.4. This effect was enhanced when the sulfide concentration was increased. Decreasing the sulfide concentration, though, means that the MoO_4^{2-} concentration must also be decreased. A pH range of 6.4 - 7.2 provided a suitable window in which precipitation could be avoided and a sufficiently strong UV-visible signal could be obtained.

Table 3.5 shows the pseudo-first order rate constants for all four processes studied. At pH 6.4 and 6.6 the k_2 and k_{-2} processes were too fast to measure using the

Table 3.5. Rate constants with varying pH. T = 38°C, I = 0.26M. All rate constants are in min^{-1}. Numbers in parentheses are the standard deviation of the last significant digit.

pH	k_2	k_{-2}	k_3	k_4
7.2	1.45 (6)	0.065 (2)	0.033 (1)	0.00186 (5)
7.0	2.68 (3)	0.084 (8)	0.059 (3)	0.0024 (2)
6.8	5.0 (3)	0.17 (3)	0.104 (6)	0.0033 (5)
6.6			0.161 (5)	0.0039 (3)
6.4			0.19 (1)	0.0039 (1)

current methods and so no values were obtained. In all cases the observed first order rate constant increased with decreasing pH. This is not unexpected for the forward processes as a decrease in the pH will result in an increased fraction of H_2S being present. The k_{-2} process has previously been shown to have a first order dependence on H^+ (section 3.2.2).

If the second order rate constants are now calculated using the H_2S concentration for the forward processes, k_2 and k_3 continue to increase with decreasing

pH. The second order rate constant for k_{-2}, calculated using the concentration of H^+, is constant. Figure 3.14 shows how the second order rate constants change with pH. The

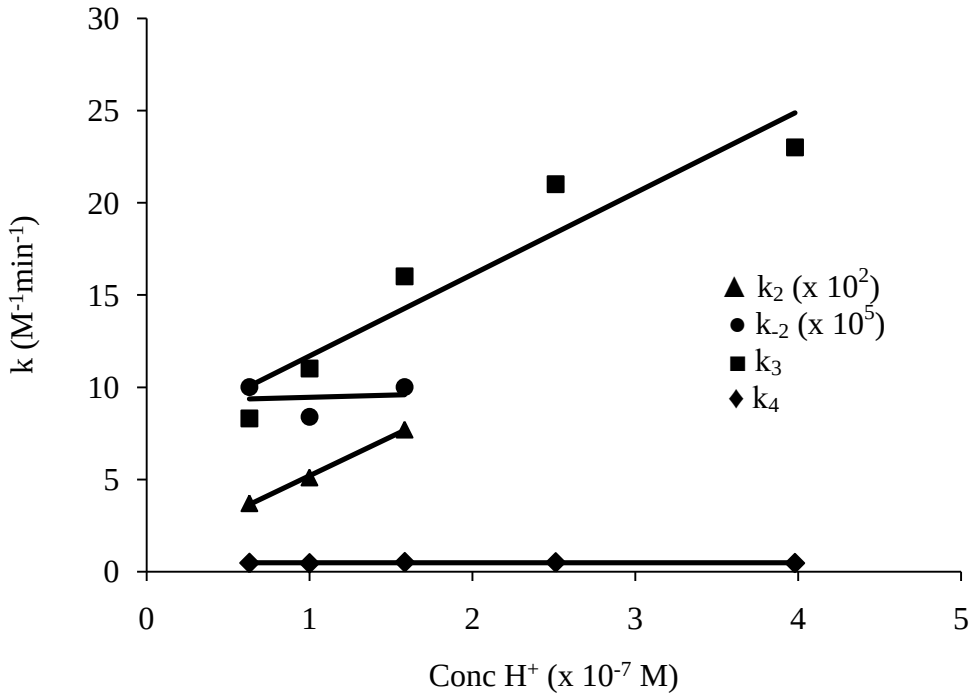

Figure 3.14. Second order rate constants as a function of pH.

rising values of k_2 and k_3 suggest that the pH is playing a greater role than simply creating a greater fraction of H_2S. The additional effect is probably protonation of O ligands. This would cause a weakening of the Mo-O bond thereby facilitating its cleavage. This is not noticed with k_4 although this may simply not be observed for reasons outlined previously (section 3.2.2). The fact that k_{-2} is constant as a second order rate constant corroborates first-order H^+ dependence.

The forward processes do not appear to depend in a simple first order manner on H^+ as is the case with k_{-2}. However, H^+ clearly causes an increase in the rate constant beyond what can be explained by an increasing H_2S fraction. Even still, the mechanism for this enhancement in both cases would seem to be pre-protonation. So why are the responses to H^+ quantitatively different? The excess of sulfide causes the forward

reactions to be kinetically favored. In this case H^+ is not be so much required for formation to occur. The O ligand is expected to have a greater pKa than the S ligand. As mentioned earlier, MoO_4^{2-} has a pKa_2 of 6.0. Therefore, over the pH range used in this study, there is likely to be significant protonation of O ligands. Decreasing pH, then, may simply further facilitate a favorable reaction, in a sense acting as a catalyst. H^+ will therefore not appear in the rate law despite its effect. Conversely, k_{-2} is not a favorable process under these conditions. In order for it to occur, pre-protonation may be required as opposed to being just a facilitator. The lower pKa of the S ligand would mean reduced protonation, especially in the presence of O ligands. In this case, decreasing the pH would result in protonation that is necessary for the reaction to occur. This would result in the observed first order dependence. In this regard it would appear as part of the rate law.

3.2.4.3 Effect of Temperature

Table 3.6 shows the second order rate constants and the corresponding activation energies (E_a) as determined from Arrhenius plots. A sample Arrhenius plot is shown in Figure 3.15. As expected, all rate constants increase with increasing temperature. The apparent exception is k_4 (see section 3.2.2).

Table 3.6. Rate constants with varying temperature. pH = 7.2, I = 0.15 M. All rate constants are in $M^{-1}min^{-1}$. E_a is in kJ mol^{-1} K^{-1}. Numbers in parentheses are the standard deviation of the last significant digit.

T (° C)	k_2 x 10^2	k_{-2} x10^5	k_3	k_4
25	1.4 (3)	1.1 (5)	4 (1)	0.27 (2)
30	1.6 (2)	0.7 (3)	4.1 (4)	0.27 (3)
38	2.1 (1)	4 (2)	5.5 (5)	0.23 (2)
45	2.4 (2)	8 (3)	6.2 (3)	0.3 (1)
E_a	22 (1)	92 (1)	19 (1)	N/A

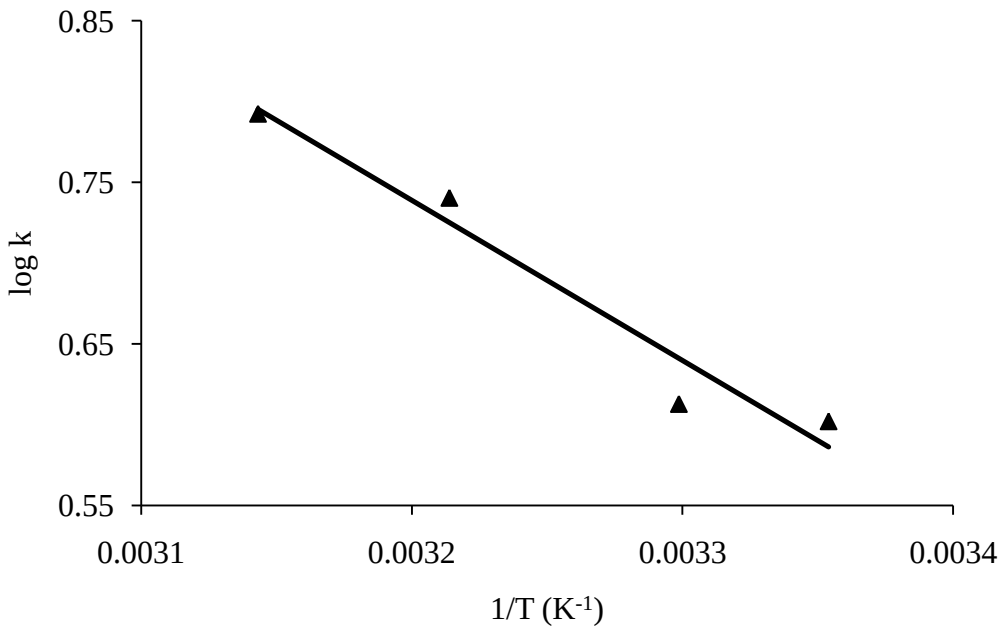

Figure 3.15. Arrhenius plot of k_3 process.

E_a for the k_2 and k_3 processes are very similar suggesting the same mechanism for both processes. However, the magnitude of k_2 is much greater than k_3. This equates to the pre-exponential factor for k_2 being greater. This indicates a greater reaction efficiency for k_2. This can be explained in terms of simple probability. With TM1, there are three potential sites for S substitution. Conversely, TM2 only has two possible sites.

The k_{-2} activation energy is significantly higher than those for the forward processes. Under the conditions studied, the reverse process is less favorable than the forward processes. So much so, in fact, that k_{-3} and k_{-4} are not observed. One reason for this may be the increased affinity of H^+ for O over S as demonstrated by the pKa's of H_2O and H_2S. If protonation favors O, the Mo-O bond will be more labile than the Mo-S bond. The high sulfide concentration increases the probability of O being substituted for S.

3.2.4.4 Mechanism

The rate laws for the forward and reverse reactions are shown in equations 3.20 and 3.21, respectively. The overall second order kinetics suggests an associative

$$\text{rate} = k\,[TM]\,[H_2S] \qquad \textbf{(3.20)}$$

$$\text{rate} = k\,[TM]\,[H^+] \qquad \textbf{(3.21)}$$

mechanism for all processes. A proposed mechanism for the TM formation reactions is shown in equation 3.22. The k_3 process is shown as an example. The proposed k_{-2} mechanism is shown in equation 3.23.

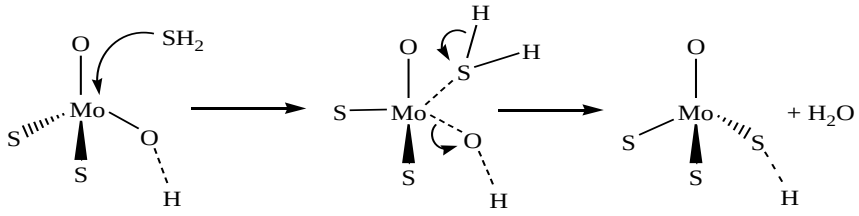

(3.22)

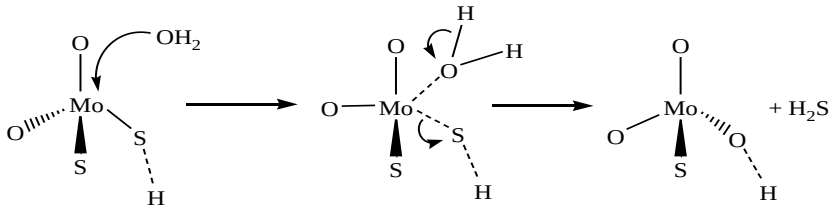

(3.23)

The ionic strength studies suggest that H_2S is the nucleophile in the pH range 6.4 – 7.2. The slope of zero from the log k vs. √I graph does not provide information as to the charge on the TM species. After calculating the second order rate constant using the H_2S concentration, though, it was apparent that H^+ continued to contribute positively to these reaction. This is likely due to the effects of pre-protonation. The mechanism therefore indicates pre-protonation of an O ligand which increases its

lability. Nucleophilic attack of H_2S will result in a 5-coordinate transition state. OH^- would then be released and likely reform H_2O with a proton from H_2S.

For k_{-2} a similar mechanism is proposed. H_2O was determined to be the nucleophile from the ionic strength studies despite the reaction being first order with respect to H^+. This indicates a required protonation of sulfide along with coordination by H_2O. This would create a 5-coordinate transition state consistent with an associative mechanism. HS^- would then be released and, depending, on the pH would likely reform H_2S.

3.3 INTERACTION BETWEEN Cu(II) AND THE THIOMOLYBDATES

3.3.1 Introduction

Very few *in vitro* studies have been performed that examine the non-structural aspects of interactions between Cu and the TMs [47-49, 131]. In section 1.5.5 an overview of previous *in vitro* Cu-TM studies was presented. In section 1.7.2, the work done by Quagraine was discussed. This laid the qualitative groundwork for the present study [24]. As well in section 1.7.3, the contributions of Essilfie-Dughan provided a first look at quantifying the rates of interactions between Cu(II) and TM4 under various conditions using a Cu^{2+} ion selective electrode (ISE). He also proposed a multistep reaction scheme for the formation of the heteronuclear adducts [113].

These interactions are complex and can be difficult to monitor. Typically, studies are performed using the synthesized TM of choice, typically TM4. However, in the rumen, TM0 is the species that is ingested. This is followed by sequential formation of the TMs. During this formation, all manner of interactions will occur, including with Cu. This is likely to affect the rate of formation as predicted from the TM kinetics. Also, interactions with TM1 and TM2 may be significant enough to alter the overall Cu speciation that one might expect from a direct reaction between Cu and TM3 or TM4.

This section will focus on studies done to further our understanding of Cu-TM interactions. This includes characterization of the UV-visible spectra of various Cu-TM products in solution, kinetic studies using UV-visible spectroscopy to complement the work done by Essilie-Dughan (section 1.7.3) and an attempt to monitor TM formation in the presence of Cu. Experiments meant to mimic Cu-TM interactions in terms of bovine feeding were also done *in vitro* as well as theoretically. These results are presented in this section as well.

The formation of Cu-TM4 adducts is very fast. The Cu^{2+} ion selective electrode (ISE) is well suited for monitoring these kinetics because of the speed of the measurement. A large number of data points can be collected within the 3 minutes or so during which the reaction is effectively completed. This is especially valuable when the reaction is first initiated. The ISE is also valuable because it is still effective in the presence of a precipitate, which the reaction of Cu and TM4 is prone to produce. Work using the Cu^{2+} ISE was carried out by Essilfie-Dughan [113].

On the other hand, the Cu^{2+} ISE comes with some distinct disadvantages. It is selective for labile (relative to complexes formed with the electrode itself) Cu in the 2+ oxidation state. Cu^{2+} that is reduced to Cu^{+} or Cu complexed with other ligands like OH^{-} or S^{2-} will not be detected. The measurements then are in terms of "free" Cu^{2+} loss and cannot necessarily be equated to Cu-TM4 adduct formation. Another potential shortfall is that S^{2-} is a common interfering ion with this electrode, S^{2-} being a by-product of TM hydrolysis. Fortunately, with TM4, hydrolysis will not occur appreciably over the time course of the experiment (section 1.4.1).

3.3.2 UV-Visible Characterization of Copper-Thiomolybdate Complexes

When using UV-visible spectroscopy to follow Cu-TM4 reactions, the rising Cu-TM adduct spectrum overlaps with the decreasing TM4 spectrum. As a result, the rate of TM4 concentration loss cannot be measured directly. There must be some

knowledge of the molar absorptivities of the Cu-TM4 spectrum to properly elucidate the various species concentrations. This applies to interactions between any TM and Cu.

Cu-TM solutions were created as described in 2.3.3. In each case, Cu was added to the TM in an excess of no less than 2:1. Each solution was allowed to react for 2 to 3 minutes before the UV-visible spectrum were taken. Given enough time, however, all of these Cu-TM mixtures will form precipitates. The time it takes until precipitation occurs, though, depends on conditions such as pH and the ionic strength [24]. Precipitation was also found to occur faster when the reagent concentrations were increased. Solutions were therefore examined closely before measurement to ensure that no precipitation had occurred. If there was any visual evidence of precipitation, the solution was discarded. The resulting spectra are shown in Figure 3.16. Beer's Law plots were then created in order to extract the Cu-TM molar absorptivities. A sample Beer's Law plot is shown in Figure 3.17.

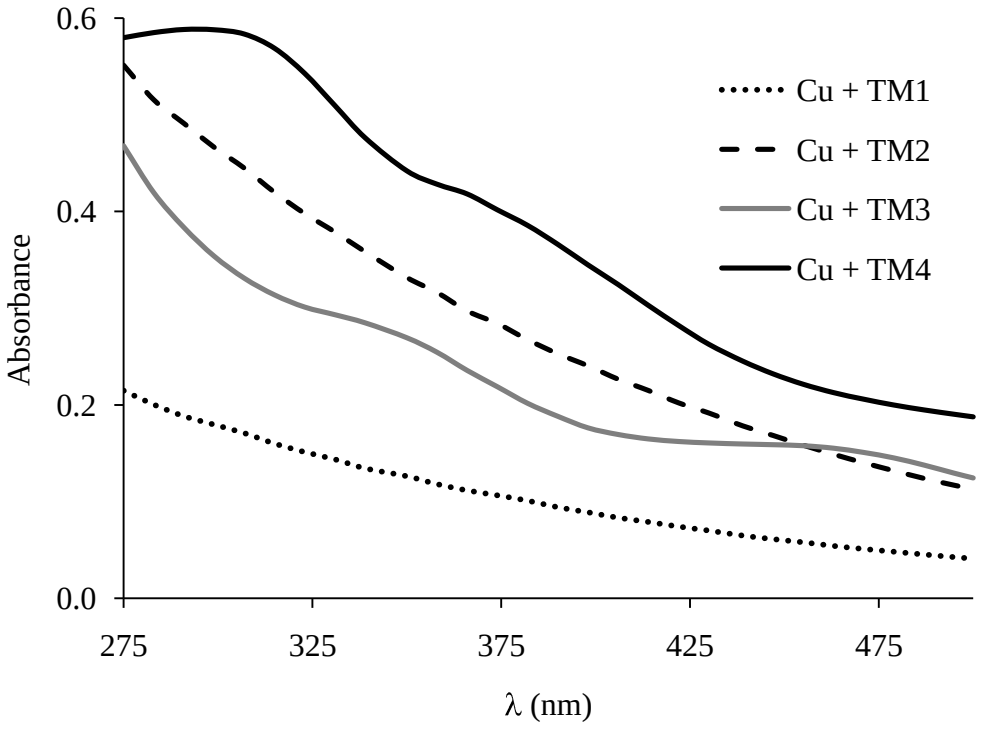

Figure 3.16. UV-visible spectra of the products of Cu(II) mixed with the TMs.

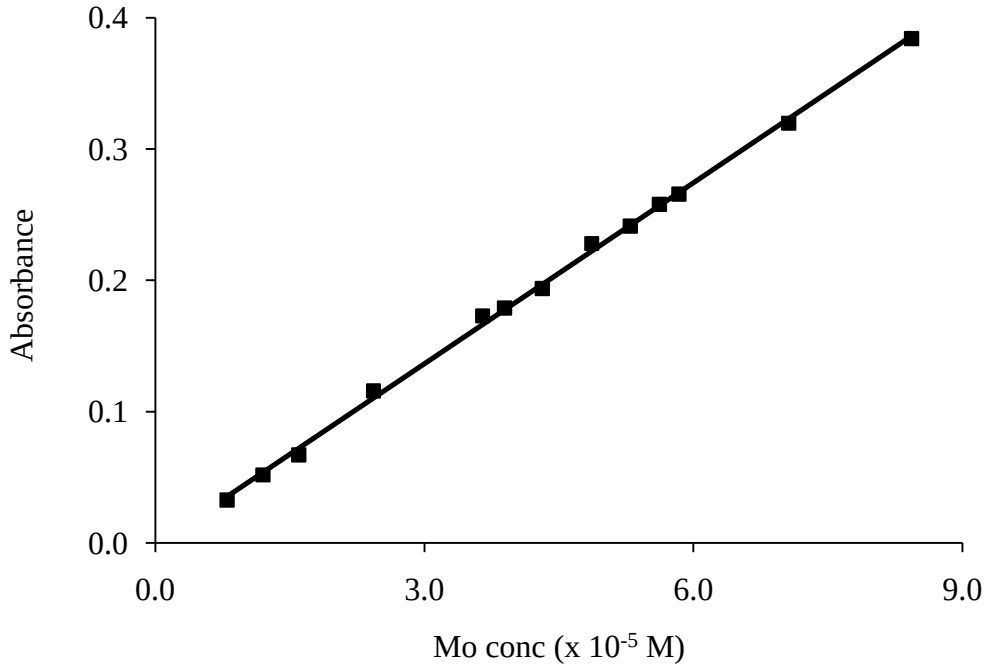

Figure 3.17. Beer's Law curve of Cu-TM4 mixture at 450 nm. Initial reagent Mo concentration is equal to the initial TM4 concentration.

Neither the structure or the Cu:Mo product ratio of the Cu-TM species are known at this point. Therefore, the molar absorptivities (in L mol^{-1} cm^{-1}) cannot be calculated on a basis of moles of Cu-TM molecules, which may in fact be polymeric or large clusters (section 1.5.3). However, if the Mo is completely in the Cu-TM form, the calculated molar absorptivity will be in terms of moles of Mo atoms. Molar absorptivities could then be determined from the Beer's Law curves (see above). The resulting molar absorptivities obtained at the selected wavelengths are shown in Table 3.7.

Complete TM reaction was determined by increasing the initial Cu:Mo ratio above 2:1. When this was done, no changes to the UV-visible spectra were observed indicating that no further reaction was occurring. It can therefore be assumed that the TM was fully reacted. In addition, the usual UV-visible TM features (Figure 3.5) were no longer observed (Figure 3.16).

Table 3.7. Molar absorptivities of the Cu-TMs at selected wavelengths. Numbers in parenthesis are the standard deviation of the slope of the Beer's Law curve.

	Molar Absorptivities * (L mol^{-1} cm^{-1})			
λ (nm)	Cu + TM1	Cu + TM2	Cu + TM3	Cu + TM4
287	4030 (40)	8700 (200)	7900 (300)	11400 (300)
291	3900 (40)	8500 (200)	7800 (300)	11500 (200)
305	3520 (40)	7600 (200)	7100 (200)	11300 (200)
312	3350 (40)	7300 (200)	6800 (200)	11100 (200)
317	3230 (40)	7000 (200)	6600 (200)	10900 (200)
322	3110 (40)	6700 (200)	6500 (200)	10600 (200)
380	2100 (30)	4500 (200)	4620 (90)	7600 (100)
395	1890 (30)	4000 (200)	4120 (90)	6960 (80)
410	1690 (30)	3600 (100)	3800 (80)	6200 (70)
450	1260 (20)	2700 (100)	3490 (60)	4600 (50)
461	1160 (20)	2520 (90)	3430 (70)	4330 (50)
468	1100 (20)	2410 (80)	3370 (70)	4200 (40)
480	1010 (20)	2210 (70)	3210 (60)	4000 (40)

*based on added Mo

3.3.3 Kinetics of Reactions Between Copper(II) and the Thiomolybdates

Although TM4 is the last TM to form and typically the least abundant, it is likely the most efficient copper antagonist of the thiomolybdate series. It has also been the most studied TM in terms of interactions with Cu (section 1.5.3). The use of TM4 to study Cu antagonism provides the simplest possible scenario to work with. A study of the kinetics of the interaction between Cu(II) and TM4 in solution was carried out by Essilfie –Dughan using a Cu^{2+} ISE. This work was discussed briefly in section 1.7.3 and comprehensively in reference [113].

Of note from this work, a reaction scheme for the reaction between Cu(II) and TM4 was deduced. The general reaction scheme in terms of Cu is shown in equation 3.24. The identity of the intermediate could not be ascertained from these

$$Cu^{2+} \underset{k_{-1}}{\overset{k_1}{\rightleftharpoons}} \text{Intermediate} \xrightarrow{k_2} \text{Product} \qquad \textbf{(3.24)}$$

measurements. It was speculated, though, that it may be Cu(I), formed by simple reduction of Cu(II). The mechanism that was proposed is shown in equations 3.25 and 3.26. The final product is nominally shown as $CuMoS_4$ but the actual identity is yet to be determined (see section 1.5.3).

$$2Cu(II) + MoS_4^{2-} + 4H_2O \longrightarrow 2Cu(I) + MoO^{2-} + S_2^{2-} + 2HS^- + 6H^+ \quad \textbf{(3.25)}$$

$$2Cu(I) + MoS_4^{2-} \longrightarrow CuMoS_4 \quad \textbf{(3.26)}$$

In order to corroborate the results obtained by ISE, the kinetics of the reaction between Cu(II) and TM4 were studied by UV-visible spectroscopy. The region studied was 390 – 470 nm. Since TM4 and the product of the Cu(II) + TM4 reaction are known to absorb, the progress of this reaction can be followed. UV-visible spectroscopy can also provide further information about the intermediate. If it is indeed Cu(I), devoid of TM complexation, it would not absorb, leaving only TM4 and the product as absorbing species. On the other hand, if a third absorbing species is detected, then the intermediate is likely a complex that includes the TM.

Initially, the UV-visible spectra were fit to a Beer's Law model including only TM4 and the final Cu(II) + TM4 product. A typical graph of species fraction with respect to percentage of Mo vs. time showing the results of this analysis is shown in Figure 3.18. The oscillation of the species fractions is indicative of an insufficient model.

In general, the quality of the fit for each UV-visible spectrum was poor. However, this did tend to improve over time. This suggests the presence of an intermediate species that absorbs in this region. Early on in the reaction, the intermediate will likely be present in high concentrations. This would explain the poor fit. Later in the reaction, the final product would be favored and the intermediate concentration would be expected to be lower. This would give rise to the improved fit.

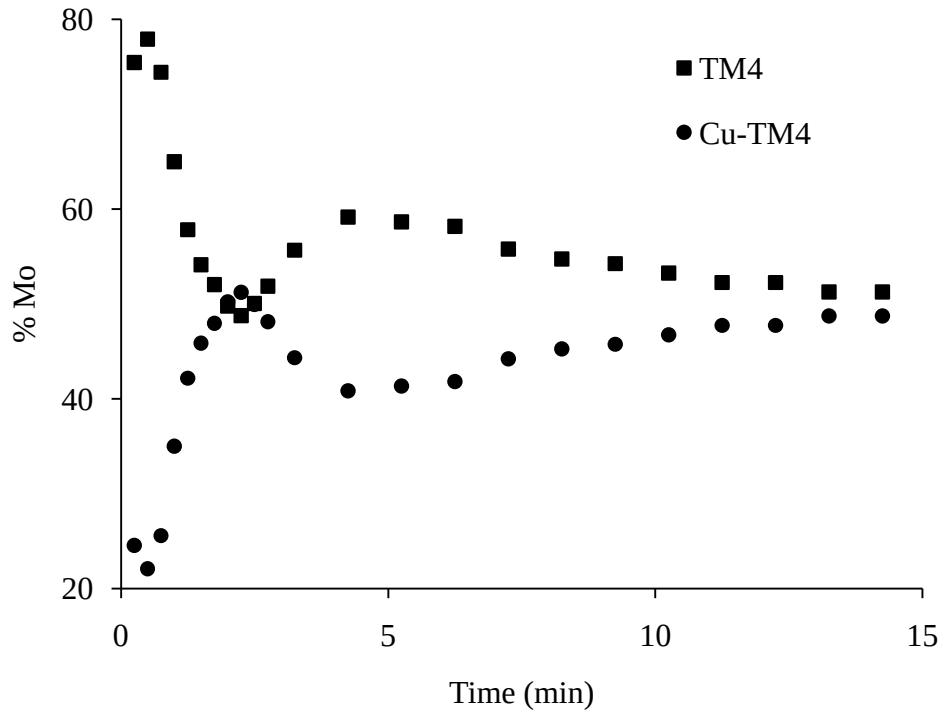

Figure 3.18. Species fraction in terms of % Mo vs. time obtained from fitting Beer's Law model to UV-visible kinetic data. Reaction conditions were: Initial Cu:Mo ratio of 1:1 at 25 °C in unbuffered solution.

Therefore, to effectively analyze the kinetic data, the absorbance due to the intermediate species must be accounted for.

Since the identity of the intermediate has not been isolated, the molar absorptivities could not be obtained from a simple Beer's Law plot. Also, the absorptivities could not be determined using the methods described in section 3.1.4 since a constant composition could not be obtained. Instead, a combination of mathematical simulations and curve fitting were used to try to quantify the UV-visible spectrum of the intermediate.

From the work of Essilfie-Dughan it is known that the reaction between Cu(II) and TM4 proceeds as equation 3.24 [113]. Since the emphasis in this work is on TM4, this can be rewritten as equation 3.27. Essilfie-Dughan was also able to determine

$$Cu^{2+} + TM4 \underset{k_{-1}}{\overset{k_1}{\rightleftharpoons}} \text{Intermediate} \xrightarrow{k_2} \text{Product} \qquad \textbf{(3.27)}$$

observed first order rate constants for this reaction scheme. These values will be shown later along with the results from this work.

Using the integrated rate equations (see section A2.5.2) for this reaction scheme and the rate constants, species concentrations can be simulated as a function of time. Since the absorptivities for TM4 and the product are known, the absorbance, A_{known}, due to these species can be calculated at each wavelength and at each time interval using equation 3.28.

$$A_{known} = c_{TM4}\varepsilon_{TM4} + c_{product}\varepsilon_{product} \qquad \textbf{(3.28)}$$

This absorbance can then be subtracted from the experimental absorbance using equation 3.29. The remaining absorbance is due to the intermediate. From here, the absorptivities of the intermediate can be calculated using equation 3.30. The

$$A_{intermediate} = A_{experiment} - A_{known} \qquad \textbf{(3.29)}$$

$$\varepsilon_{intermediate} = A_{intermediate}\, c_{intermediate} \qquad \textbf{(3.30)}$$

absorptivities were calculated for each wavelength and at each time interval. At each time interval the absorptivities were constant as expected. The actual absorptivities were therefore an average of those determined at each time interval. The average values generally had a standard deviation of less than 10 %.

It should be noted that data from the first three time intervals were excluded since they were not consistent with the rest. This is likely due to errors caused by the speed of the measurement relative to the rate of the reaction. For each measurement it is assumed that the composition of the sample is constant. It is therefore described by a single set of species concentrations. However, because the reaction is proceeding

quickly, the composition may change from the time the scan is initiated until it is concluded. This is especially true for the early scans when the reaction rate is the highest. As a result, the calculated absorbances and absorptivities are invalid.

With the absorptivities for all three species are known, the absorbance spectrum at each time interval can be recalculated. These spectra were slightly different than the experimental spectra. This is especially true for the early spectra which are now being theoretically calculated and are not affected by fast reaction errors. Otherwise, the primary difference is due to the rate constants used in the simulation. Errors in these values propagate into the absorptivities and hence into the recalculated spectra. The rate constants must therefore be further refined. This will be discussed later in this section.

These recalculated spectra can now be fit using a Beer's Law model that includes all three species. As expected, the quality of fit is vastly improved compared to the two species fit performed earlier. By fitting the spectrum at each time interval a new concentration vs. time graph can be obtained which shows the concentrations of all three species. A sample of this graph is shown in Figure 3.19.

Rate constants were then determined using the methods outlined in section 3.2.3. The integrated rate equations used to fit this data were obtained from the reaction scheme shown in equation 3.27. The actual equations used are shown in the A2.5.2. The resulting fit was of very good quality indicating that the kinetic scheme was suitable. A sample of the fit is shown in Figure 3.20.

In this case there are two sets of unknowns; the absorptivities of the intermediate and the rate constants. Therefore, the rate constants that were just determined were used to carry out the procedure again. The goal here was to further optimize the absorptivities and subsequently the rate constants. This procedure was continually carried out in this fashion until the absorptivities and the rate constants no longer changed. Figure 3.21 shows the optimized UV-visible spectrum of the intermediate along with those of TM4 and the product.

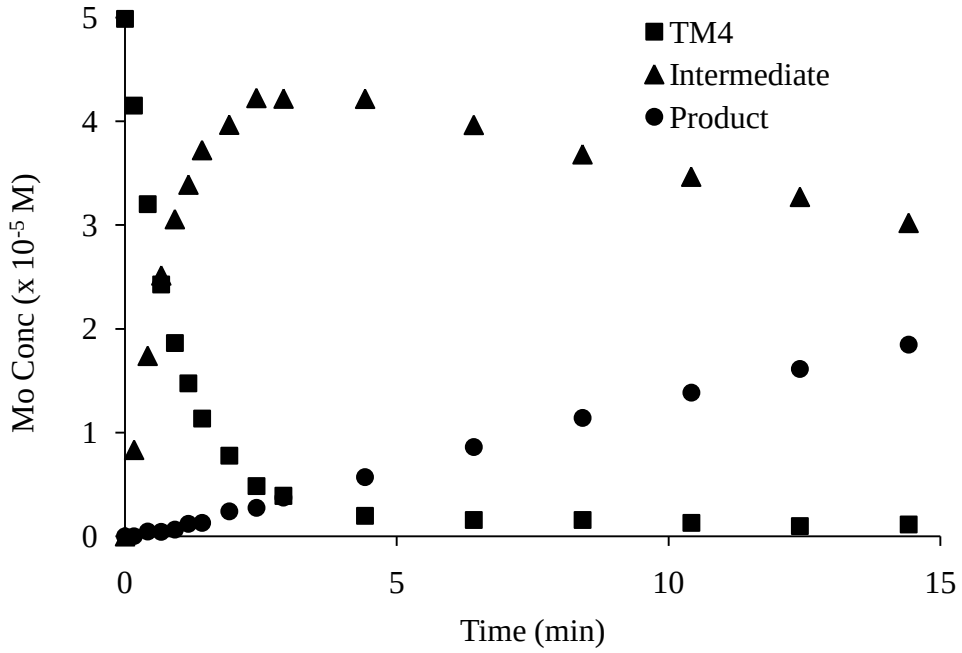

Figure 3.19. Concentration as a function of time results from fitting including all three species.

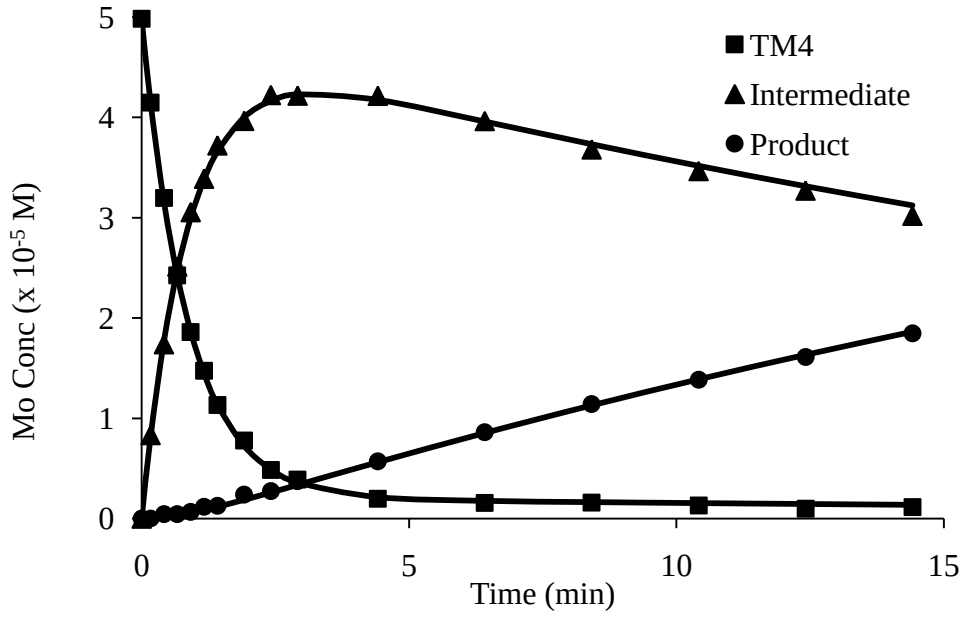

Figure 3.20. Origin7® fit of concentration vs. time data. Data points represent the experimental concentrations. The solid lines are the fit.

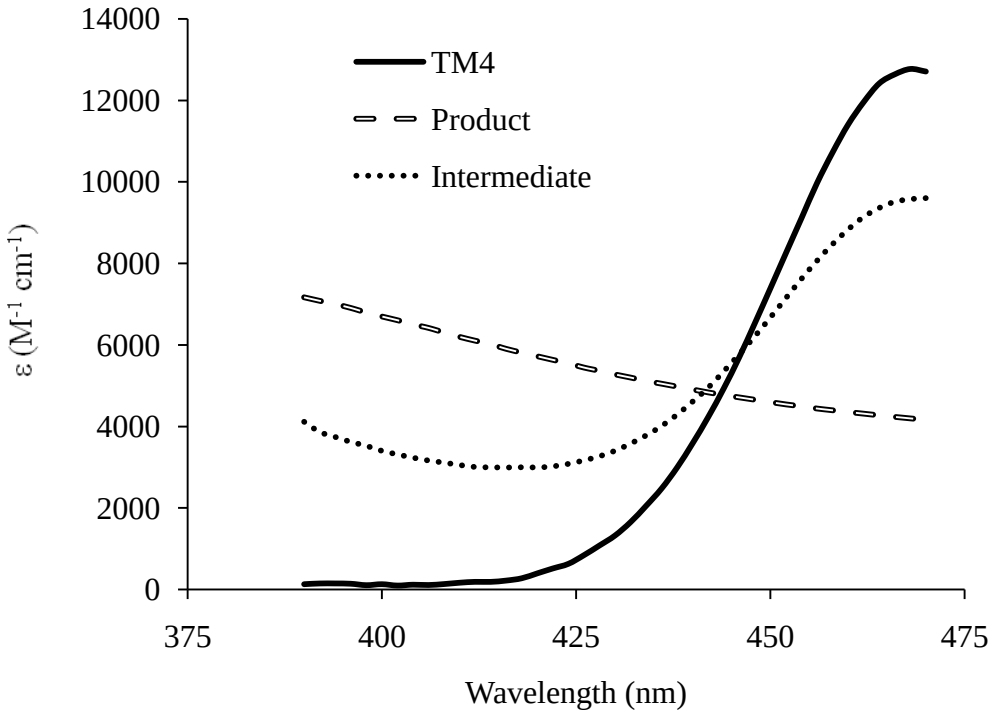

Figure 3.21. UV-visible spectra of TM4, the intermediate and the product of the reaction of Cu(II) with TM4.

This method was then extended to study the kinetics of the reaction of Cu(II) with TM3. The same kinetic scheme was applied as with the TM4 case with the same quality of fit. The absorptivities for this intermediate were determined by taking the average at each time interval with the first three intervals excluded. As with TM4, the standard deviations of the absorptivities were generally around 10 %. The UV-visible spectrum of this intermediate is shown in Figure 3.22 along with those of TM3 and the product.

Rate constants were obtained using a 1:1 Cu:Mo ratio at 25 °C in unbuffered solution as these were the conditions used by Essilfie-Dughan. Table 3.8 shows the rate constants obtained from the reaction of Cu(II) with TM4 from this work as well as from Essilfie-Dughan's work using ISE. Rate constants for the reaction of Cu(II) with TM3 obtained from this work are also included for comparison.

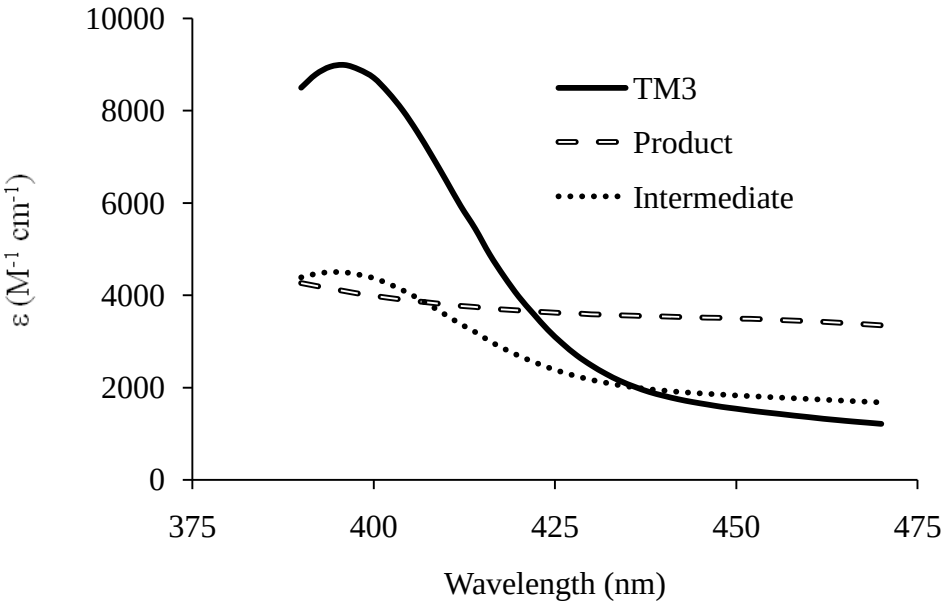

Figure 3.22. UV-visible spectra of TM3, the intermediate and the product of the reaction of Cu(II) with TM3.

The rate constants obtained for the Cu(II) + TM4 reaction using UV-visible spectroscopy are in good agreement with those obtained using ISE. The main difference between the two techniques is with k_1 and k_{-1} in which values from the ISE are slightly higher. One reason for this may be with the techniques themselves. With the ISE, the measurement is affected by complexation with OH^- or S^{2-} (a product of hydrolysis).

Table 3.8. Rate constants for the reaction of Cu(II) + TM4 and Cu(II) + TM3 as determined by UV-visible spectroscopy and Cu^{2+} ISE at 25 ºC in water. The initial Cu:TM ratio was 1:1. All rate constants are in min^{-1}. Errors are in terms of standard deviation of replicate measurements.

	UV-vis		ISE
	Cu(II) + TM4	Cu(II) + TM3	Cu(II) + TM4
k_1	1.09 ± 0.03	1.09 ± 0.03	1.26 ± 0.08
k_{-1}	0.05 ± 0.01	0.071 ± 0.001	0.14 ± 0.01
k_2	0.037 ± 0.001	0.031 ± 0.001	0.034 ± 0.0009

This would lead to a slightly higher k_1. Conversely, by scanning a spectral region, UV-visible spectroscopy is significantly slower than ISE measurements. Since this reaction occurs very quickly, there may be some error incurred for the UV-visible measurements that isn't present with the ISE measurements.

A second reason for these differences may arise from the analysis. The rate constants were obtained from the ISE data by fitting only to the Cu^{2+} concentration. However, using UV-visible spectroscopy, the concentrations of all three species could be determined. The rate constants were then determined by fitting simultaneously to all three concentration profiles. This increases the certainty of the results. Overall, the similarity of the rate constants between the two methods shows that they are complimentary. Even though both methods have their advantages and disadvantages, the results from both appear to be consistent.

The rate constants obtained from UV-visible data from the reactions with TM3 and TM4 are again very similar. Only slight differences appear in k_{-1} and k_2. For the TM3 reaction, k_{-1} (the reverse rate constant) is slightly greater. This can be simply explained if we assume that the intermediate involves Cu-TM complexation. TM3 is expected to have a reduced chelating effect compared to TM4 since it only has three S ligands. Whereas TM4 may form a chelate with two or more Cu atoms, TM3 is likely to only chelate one. Reaction with a second Cu atom would then likely be singly bonded which is more labile. This would lead to a faster "off" rate constant.

The k_2 value for the TM4 reaction is greater than for the TM3 reaction. Again, the reason for this can be speculated if we assume the product forms from further Cu-TM complexation. The increased number of S ligands around TM4 increases the likelihood of reaction with Cu. This would increase the reaction efficiency leading to a greater rate constant compared to k_2 for the TM3 case. Overall, though, due to the time it takes to collect a UV-visible spectrum, further studies should be performed using faster methods to confirm these results (see section 4.3).

Further information on the identities of the intermediates and products are necessary before mechanisms can be thoroughly discussed. However, some new information can be surmised. The intermediates from both the TM4 and TM3 reactions absorb in the UV-visible region. Furthermore, the intermediate spectra appear to have similar features to both the TM and the product. In other words, they have peaks in similar positions to the TMs but they are slightly flattened as with the products. Work done by Slamova in the Reid group shows that the product of the Cu(II) + TM4 reaction contains both Mo and Cu [134]. If this is the case then it appears that the intermediate may also contain Mo and Cu. Therefore, the intermediate would be a bimetallic complex as opposed to simply Cu(I) as suggested from the ISE results.

3.3.4 Thiomolybdate Formation in Presence of Copper(II)

No *in vitro* studies to date have looked at the 3-way interaction involving TM0, S and Cu. The complexity of dealing with this system has been a deterrent but it more closely mimics the true actions of the rumen. Also, there is no worry of initial TM purity and the lack of effect of TM1 and TM2 are not assumed. It is worthwhile given the robust nature of the fitting methods described in this thesis to examine this system.

There were a number of experimental nuances to sort out before these reactions could be performed. First, there is the issue of pH. At the higher concentrations of sulfide (~ 1.5×10^{-2} M), the solution sometimes became cloudy as the pH was lowered toward 6.0. On the other hand, Cu precipitates as $Cu(OH)_2$ at these pH's. The second issue involved the order with which the reagents were combined.

In dealing with the pH issue, it was found that when the sulfide concentration was lowered below 10^{-2} M, the pH of the solution could be lowered to 6.0 without becoming cloudy. The lowering of the sulfide concentration required a reduction in the S:Mo ratio to 150:1 as opposed to 250:1 used in TM kinetics.

When phosphate buffer of any pH used in this study was added directly to $Cu(NO_3)_2$, a precipitate formed. However, if the Cu salt was dissolved first in water, phosphate buffer could then be added without the noticeable formation of precipitate. Cu solutions were therefore made up in water. Only a small amount of this solution was later added to the buffered reaction mixture. These experiments were thus able to be run at pH 6.0, 6.4 and 6.8.

The order of mixing proved to be important in preventing precipitate formation. Mixing the Cu solution with TM0 resulted in a cloudy greenish solution. On the other hand, mixing Cu with sulfide formed the solid CuS. Mixing TM0 and S first, as in the TM formation studies, followed by Cu was successful. TM0 reacts immediately upon addition of S and the resulting TMs do not form a precipitate initially with Cu, especially at low concentrations. There was also no visible indication of CuS formation. The initial TM formation may reduce the concentration of free sulfide in solution to a point where this reaction is negligible, at least by visible inspection.

Absorbance spectra were taken immediately after the addition of Cu solution. Fitting of the spectra was accomplished in the same way as the TM formation spectra. The initial TM0 concentration was a constant value used in the fitting. Since Cu does not absorb in the range studied, the spectra were due strictly to Mo based compounds. The absorbance due to sulfide was determined before the addition of the metal salts and this absorbance was subtracted from all other spectra.

Initially all TMs and all Cu-TMs were included in the fit. Some species could not be detected from the fit and were subsequently removed. These species included TM0, TM3, Cu-TM1 and Cu-TM3. Suspected reasons for the absence of these species will be discussed shortly.

A 3D graph showing the progress of a reaction with an initial Cu:Mo ratio of 1:1 is shown in Figure 3.23. The corresponding fractional speciation of Mo vs. time graph is shown in Figure 3.24. From the 3D graph it is apparent that there are TMs present in

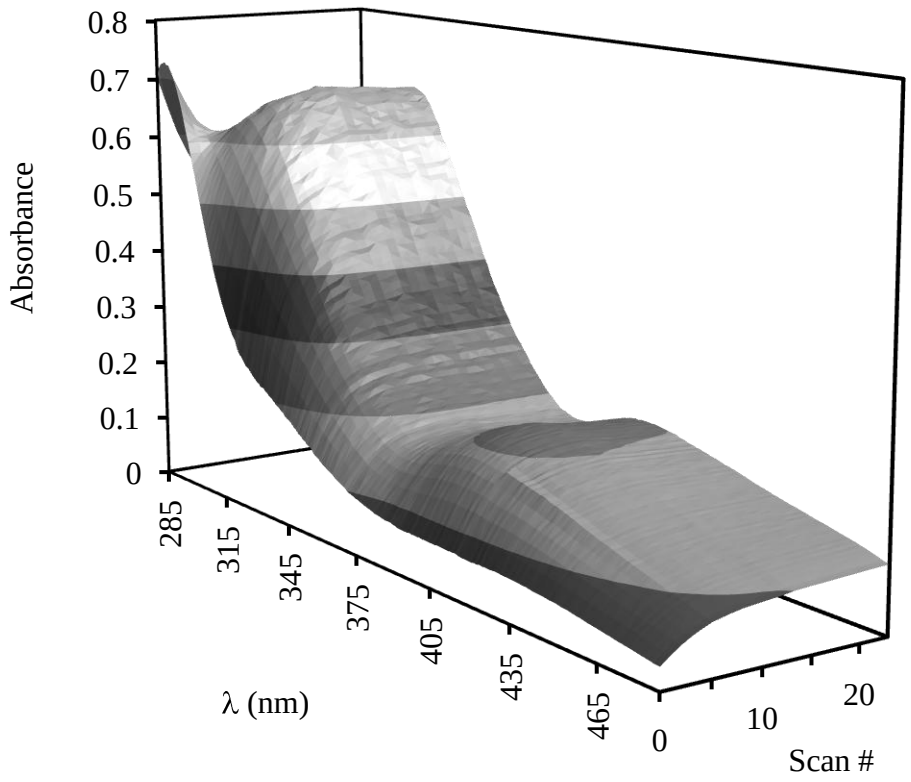

Figure 3.23. UV-visible spectra of progress of TM formation in the presence of copper. Reaction conditions: pH 6.8, 38 ºC, 1:1 Cu:Mo , 150:1 S:Mo.

solution that are likely not complexed to Cu. This is evidenced by the peaks at 310 nm and at 395 nm.

310 nm is close to the 312 nm that is a λ_{max} for TM3. The slight shift is probably due to the absorbances of other species, especially TM2. The peak at 395 nm is indicative of TM2 and TM3. A sharp peak at 290 nm is also seen in the first few spectra, characteristic of TM1. There is no obvious evidence of TM4 in Figure 3.23 as would be indicated by a peak around 468 nm. Overall, the spectra contain less pronounced peaks than seen during TM formation experiments. This is a result of the formation of Cu-TMs and their featureless spectra.

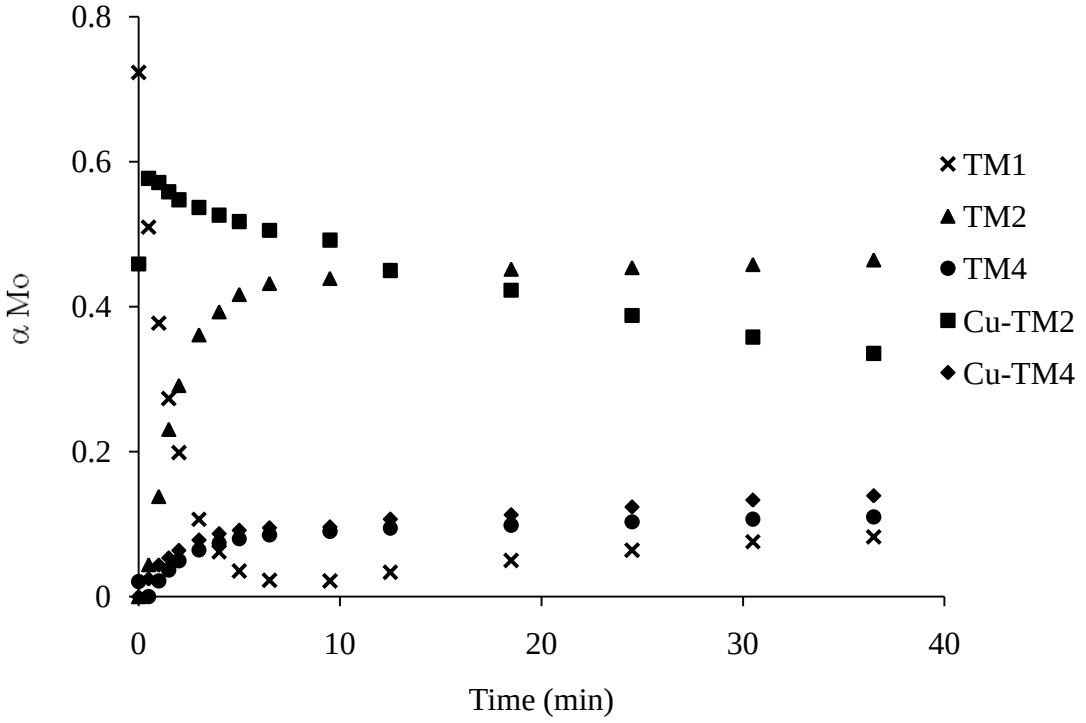

Figure 3.24. Change in concentration over time during TM formation in the presence of Cu. Reaction conditions: pH 6.8, 38 ºC, 1:1 Cu:Mo , 150:1 S:Mo.

By comparing this information to that shown in Figure 3.24 it is possible to identify some of the strengths and shortfalls of the fitting process. The initial presence of TM1 was identified as was its conversion to TM2. However, the fitting shows the major species present throughout to be TM2 and Cu-TM2. It was shown in the previous section that Cu reacts readily with TM3 and so we would expect to see the Cu-TM3 fraction begin to rise. In addition, the TM2 fraction appears to rise and achieve equilibrium at a maximum value. In TM formation experiments TM3 was usually present in large quantities as TM2 declined. This TM2 fraction may include TM3 as well. This aspect will be discussed shortly.

It is apparent by the appearance of Cu-TM4 that copper is available for reaction with TMs beyond TM2 and is not fully sequestered by TM2. Also, since some free TM4 is present, it is logical to assume that there should be free TM3 as well. This is

also expected because of the peak at 310 nm. We also see the expected rise of Cu-TM4 although this and the increase of TM4 are faster than expected. The apparent fraction of TM4 should produce a noticeable peak at 468 nm.

A similar experiment was run using an initial Cu:Mo ratio of 2:1. A 3D graph of this experiment is shown in Figure 3.25 and the corresponding αMo vs time graph is shown in Figure 3.26. These spectra are noticeably flatter than those from the

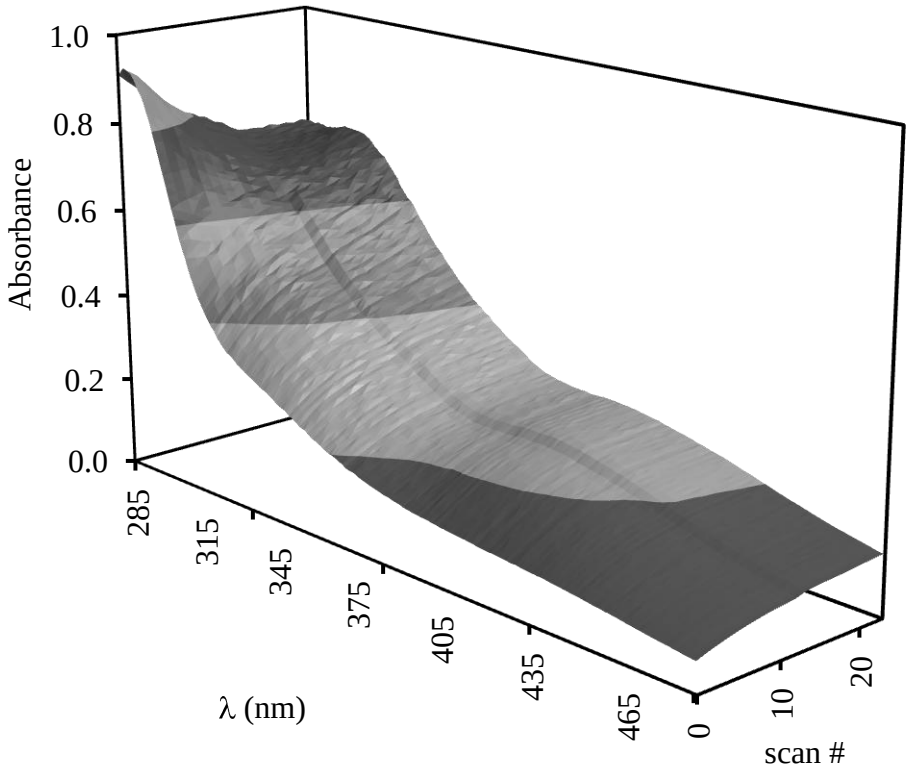

Figure 3.25. UV-visible spectra of progress of TM formation in the presence of copper. Reaction conditions: pH 6.8, 38 ºC, 2:1 Cu:Mo , 150:1 S:Mo.

previously described experiment. Clearly, the Cu-TM species are now more dominant and the contribution from free TMs is very small. The position and intensity of the plateaus around 300 and 390 nm are consistent with the features seen in the Cu-TM4 spectrum (see Figure 3.16) and so are likely not due to small amounts of TMs. There is

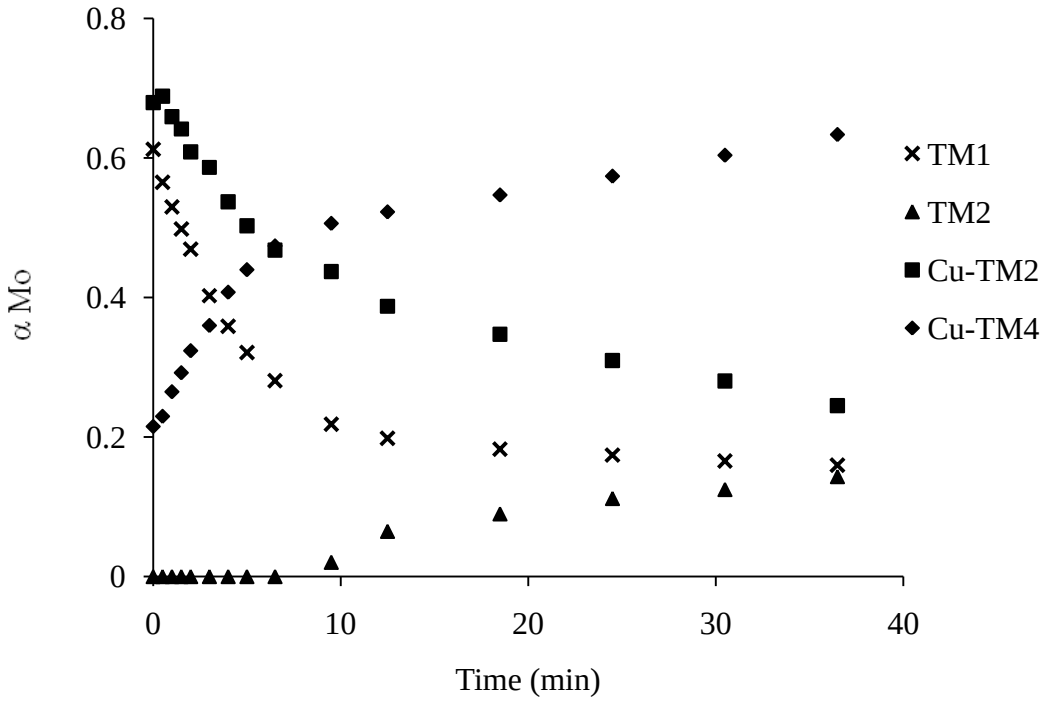

Figure 3.26. Change in concentration over time during TM formation in the presence of Cu. Reaction conditions: pH 6.8, 38 ºC, 2:1 Cu:Mo , 150:1 S:Mo.

again the initial presence of TM1. Since a Cu-TM1 complex is likely to be somewhat labile, Cu would preferentially complex TM2 as it is formed.

The results from fitting shows the decay of TM1 as expected though it is present throughout. TM2 forms after 6.5 minutes. This appears to be anomalous and may be an artifact of the fitting routine. The Cu-TM2 and Cu-TM4 species are dominant throughout the experiment. Unexpectedly, Cu-TM4 is the most abundant and forms much faster than under similar conditions without Cu. Again there is no apparent contribution from Cu-TM3 but this may be hidden within the Cu-TM2 or even the Cu-TM4 fraction.

From the results of both experiments, some important conclusions can be drawn. First of all, TM1 is obviously a minor player in terms of Cu antagonism, as was

suggested by Suttle [37]. Second, a 1:1 Cu:Mo ratio is not sufficient to completely exhaust the free TMs. This is significant because it suggests that, on average, the Cu-TM product ratio is likely to be greater than 1:1. Or at least, one equivalent of Cu is not likely sufficient to allow free copper to exist. Third, the seemingly rapid formation of TM4 and Cu-TM4 species may indicate that Cu increases the rate of TM formation. Further studies must be performed before confidently making this claim.

A major limitation of fitting these spectra was the similarity of the various Cu-TM absorbance spectra. Further to this, is the fact that throughout the spectra, the molar absorptivities parallel one another. In other words, as the absorbance increases for one species, the absorbances of the other species are increasing similarly. This reduces the ability to distinguish between the Cu-TM species in the fit. This is likely the reason that the presence of Cu-TM2, and perhaps the larger than expected level of Cu-TM4, is detected and not Cu-TM3.

This problem is compounded by the fact that molar absorptivities were determined for the final Cu-TM products only. The expected presence of unaccounted for intermediate species with slightly different molar absorptivities reduces the overall quality of fit. The addition of Cu-TM3 does not improve the fit enough to be recognized by the fitting algorithm.

A byproduct of the molar absorptivity limitation is that the sum of all fractions in both experiments was significantly higher than 1 despite constraints being set. In some cases the sum was as high as 1.3. Consistently, the sum decreased with time as did the quality of fit, presumably as the Cu-TM species in solution more closely matched those used to measure the molar absorptivities. This may also be indicative of the presence of intermediate species as suggested in section 3.3.3. This anomaly did not appear to affect the consistency of the results. Replicate trials showed all the same features and in consistent quantities. Also, the αMo curves show very little scatter. Therefore, the absolute concentrations will be slightly inaccurate but the results are sufficient to extract some qualitative lessons.

3.3.5 Mimicking Bovine Feeding Habits

In the previous section, the reactions between Cu and the TMs as they form were examined. Also, the differences between a 1:1 and 2:1 Cu:Mo ratio were observed. In a biological system, there will be a regular cycling of chemical species. As the animal eats and drinks fresh reagents, like MoO_4^{2-}, Cu^{2+} and various forms of S, will be ingested. Conversely, reaction products will be removed during elimination events. To study the long term speciation expected in the rumen, the effects of constant input and output must be accounted for.

A schedule of possible feeding times for a typical bovine was created for a 48 hour period (see Table 2.1 in section 2.35). At the first time interval, a buffered solution of Na_2MoO_4 was added to the Na_2S solution followed immediately by addition of $Cu(NO_3)_2 \cdot 2.5H_2O$. At all further times a volume was removed to simulate elimination of all relevant species from the rumen. The three fresh reagents were immediately added such that the total volume added was equal to the volume removed. This was necessary to continually keep an adequate volume for measurement in the cuvette. S was maintained in an excess of at least 100:1 over Cu and Mo. Cu and Mo were added to achieve desired ratios.

Initially, a 1:1 Cu:Mo molar ratio was used. After some time this ratio was increased in order to create a ratio near 2:1. Later, the ratio was gradually reduced to 1:1. This was meant to examine the long term effects of intake of constant ratios as well as the reversibility of the species concentrations as ratios were changed. Figure 3.27 shows the progress of this experiment. The last spectrum taken for each cycle is shown in this graph.

Cycles one through eight consisted of inputting 1:1 ratios of Cu:Mo. During this time the absorbance around 300 nm quickly reaches a maximum and then declines. Meanwhile, the peak at 395 nm steadily increases and there is a gradual increase of absorbance at 468 nm. This indicates that over these cycles a significant portion of TMs

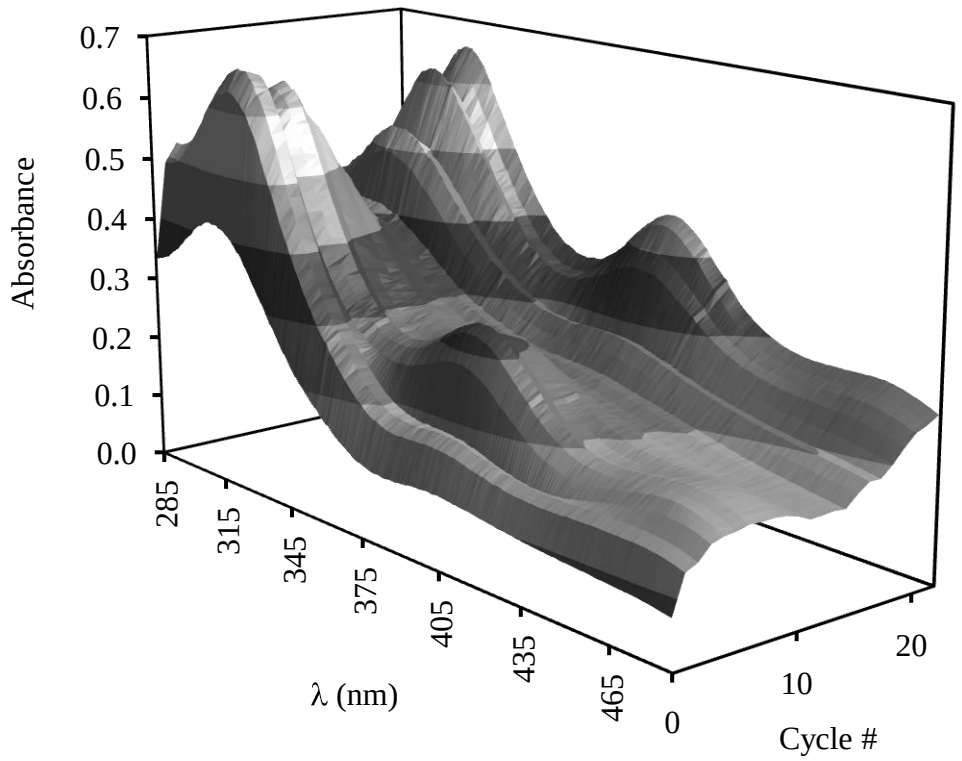

Figure 3.27. Change in UV-visible spectra with cycling events during bovine mimicking experiment.

remain uncomplexed as was seen in the previous section. This also shows the shift in TM speciation to favor TM3 and TM4.

The volume exchanged was typically between 5 and 10 % of the total contents. At this volume, the overall reaction still progressed forward noticeably. Figure 3.28 shows how the absorbance at 395 nm 468 nm (representing TM3 and TM4, respectively) changes over time. After the first five cycles the overall progress of the reaction began to slow such that the absorbance at 395 nm began to level off. The absorbance at 468 nm was still rising, however. In general the absorbance at 468 nm lags behind that of 395 nm during the formation stage. By this time the fractions of TM1 and TM2 would be lower as the fresh MoO_4^{2-} would be the only source for these species and would be quickly converted. As the TM3 fraction increases, there is greater

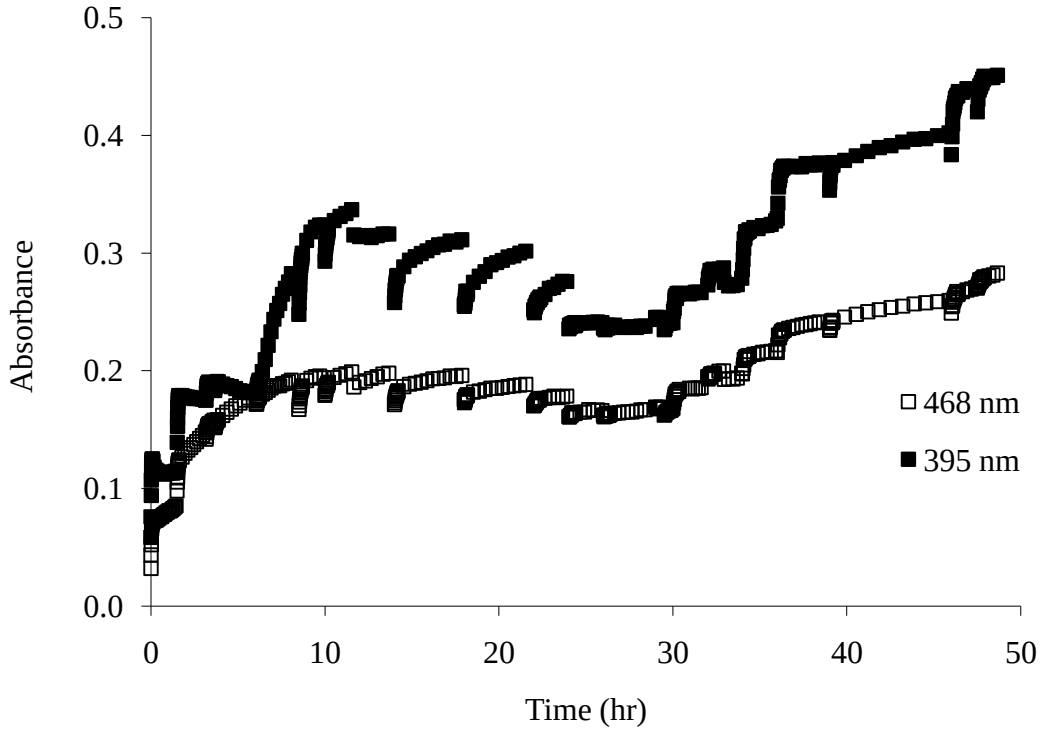

Figure 3.28. Absorbance changes at 468 and 395 nm during bovine mimicking experiment.

capacity for TM4 to form and so we see the continual increase of the absorbance at 468 nm.

The time interval between cycles was varied between 30 minutes and four hours. This did not appear to have any significant effect on the progress of the reaction. Within 30 minutes TM0 is likely to be converted completely to TM3. After this point, conversion to TM4 is slow and so no significant change is seen when longer reaction times are used.

During cycles nine to 15, the Cu:Mo ratio was increased. This resulted in a flattening of the UV-visible spectra, reminiscent of the Cu-TM spectra. This happened quickly, over the course of three to four cycles. By the time the final ratio was 1.5:1, there was no further change in the absorbance at 395 or 468 nm, save for small changes

due to changes in the total Mo concentration. The Cu:Mo ratio was further increased to an overall ratio close to 2:1.

During this period there is no noticeable lag between the absorbances at the two wavelengths. Since TM3 and TM4 both react readily and independently with Cu, the loss of one species does not affect the loss of the other. Instead both peaks decline concomitantly.

Cycles 15 to 23 were used to lower the Cu:Mo ratio back toward 1:1. As the ratio decreased the characteristic TM peaks reappeared in the UV-visible spectra. This shows that the effects of an increased (or decreased) Cu:Mo ratio are reversible.

Even though the TM peaks reappeared in a similar fashion as in the early cycles, there is a noticeably higher absorbance. In the first cycle, all Mo was input as TM0. It took some time before TM3 and TM4 formed in significant quantities. On the other hand, as the Cu:Mo ratio was lowered from 2:1, there was a base absorbance due to Cu-TM species that wasn't present in the early cycles. Absorbances due to TM3 and TM4 are now appearing on top of the absorbance of the Cu-TMs. Eventually these species would be reduced with more cycles at the lower ratio. By this time a significant concentration of TM3 and TM4 would be built up and so a greater absorbance would be maintained. In addition, there was a slight increase in Mo concentration over the course of this experiment.

3.3.6 Simulations of Reactions Between Copper(II) and the Thiomolybdates

Obtaining quantitative information by experiment of a complex set of reactions is difficult. The more steps to the reaction there are, the more difficult it becomes to extract detailed information. This becomes increasingly true if the experimental technique cannot adequately distinguish between certain species. This is the case with the Cu-TMs as shown in section 3.3.4.

An alternative method of gaining quantitative information is to mathematically simulate the reaction of interest. Instead of determining the concentrations of the species present at various times in the experiment, they are calculated based on the reaction scheme and rate constants that were previously determined. If the reaction scheme used in the simulation resembles closely the true reaction scheme, the results should be corroborated by the observations of the experiment.

The reaction scheme used for the simulation is shown in equation 3.31. It was

$$TM1 \underset{k_{-2}}{\overset{k_2}{\rightleftharpoons}} TM2 \xrightarrow{k_3} TM3 \xrightarrow{k_4} TM4 + Cu^{2+} \xrightarrow{k_5} Cu\text{-}TM4 \qquad \textbf{(3.31)}$$

assumed the Cu^{2+} will react exclusively with TM4 upon its formation. The rate constant used for the formation of Cu-TM4 is the rate constant of formation of the intermediate (see section 3.3.3). By using rate constants determined under different conditions, one can simulate changing rumen conditions as well. Accounting for more processes will improve the suitability of the simulation but add to the complexity of the model.

This simulation was conducted by first determining the concentrations of the various TMs after a certain time interval was passed. The initial TM input was assumed to be TM1 (as opposed to TM0) as it was assumed that TM0 would be immediately converted to TM1. After this time interval, TM4 was reacted with copper as per the k_5 rate constant. From this point the process was repeated for a new time interval. This process is similar to that described by Essilfie-Dughan [113] but with the TM kinetic scheme and rate constants determined in this work.

The simulation was then treated as a bovine mimicking experiment. In this case, the reaction was allowed to proceed for a period of time that would simulate the time between feeding and elimination cycles. At the time of feeding, a portion of the reaction mixture was removed and replaced with an equal total volume consisting of TM0 and Cu^{2+}. Sulfide was not specifically included because the rate constants were the observed

rate constants determined under a large excess of sulfide. The reaction was then allowed to proceed for another time interval.

The results for a simulation using continuous 1:1 Cu:Mo inputs were plotted and are shown in Figure 3.29. A total concentration of 1.5×10^{-5} M was used for both Mo and Cu. The time interval between cycles was varied within a reasonable range. Each cycle in the graph is indicated by sharp spikes since the concentration of each species is instantly changed at this time. Initially, the entire reaction consisted of TM0 and unreacted Cu^{2+}. The first few cycles were therefore not what would normally be expected in the rumen. As the time progressed, though, it was possible to see the approximate equilibrium concentrations as well as the effect of varied times between cycles.

As was seen in the bovine mimicking experiment described earlier, the TMs were not completely converted to Cu-TM species. With each new addition there was a brief spike followed by a rapid decrease of these species as they reacted to form the higher TMs. For the first number of hours as the TMs were forming, TM3 was the dominant TM. Later, TM4 tended to be the dominant species.

During experiments with 1:1 Cu:Mo, the UV-visible peak at 395 nm was always significantly larger than the one at 468 nm. This is indicative of TM3 being the dominant species. This may be because the experiment was not continued for as long under these conditions as the simulation represents. It may also suggest an increased role of TMs other than TM4 preventing the formation of TM4. In the simulation, TM4 is always allowed to form before any reaction with Cu.

One advantage of the simulation is that the calculation of free Cu^{2+} is included whereas in the experiment it was not measured. This calculation is based on a 1:1 Cu:Mo product ratio, however, but can easily be adjusted with an updated value. Because of the 1:1 ratio and Cu-TM4 being the only product of Cu, the curves for free Cu and Cu-TM4 mirror each other closely.

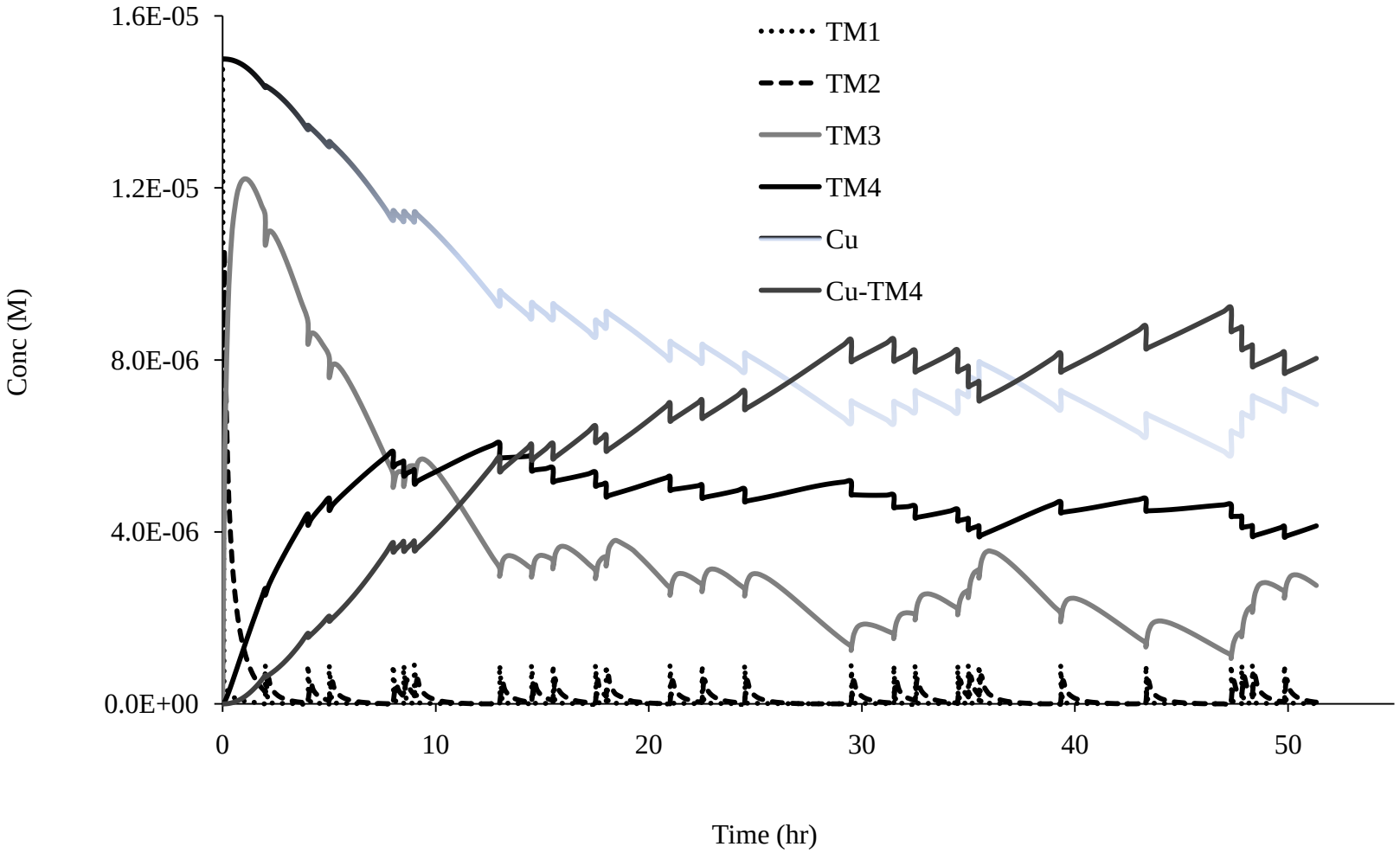

Figure 3.29. Simulation of Cu and TM speciation at 1:1 Cu:Mo ratio.

After about 25 hours all species appear to reach a state of approximate equilibrium. From here the effect of time between cycles becomes apparent. When short intervals are used, there is a positive effect on the free Cu concentration. In this case, there is not sufficient time for significant amounts of TM4 to form before the next cycle. The less TM4 that forms, the less Cu-TM4 and therefore more free Cu. On the other hand, when long intervals were used, there was a drastic decrease in Cu because of the increased reaction time. This effect was not observed in the experiment.

A similar simulation was run using a constant 2:1 Cu:Mo ratio. This is shown in Figure 3.30. The Mo concentration was maintained at 1.5×10^{-5} M but the Cu^{2+} input concentration was 3.0×10^{-5} M. As in the 1:1 simulation TM1 and TM2 quickly reacted and never maintained a significant concentration. There is no apparent difference in concentration of TM3 versus in the 1:1 simulation. The TM4 concentration does, however appear to be lower.

The lower TM4 concentration results in the Cu-TM4 concentration reaching a maximum sooner in the 2:1 simulation. In the 1:1 simulation the higher concentration of free TM4 allowed for continuous reaction with Cu. In the 2:1 simulation, there is a limited supply of TM4 available owing to the excess of Cu and so the Cu-TM4 concentration equilibrates relatively quickly. The free Cu concentration decreases until the point when TM4 reaches a sufficiently low level at which time Cu equilibrates as well.

The bovine mimicking experiment under the same conditions also resulted in a very low free TM concentration as suggested by the lack of peaks in characteristic positions. This loss of TM peaks also happened quite quickly and presumably the Cu concentration increased after this.

Similar to the 1:1 simulation, the length of the time interval between cycles affected the speciation. Short time intervals produced increases in the TM3 concentration. The TM4 concentration showed little change and so the Cu-TM4 fraction

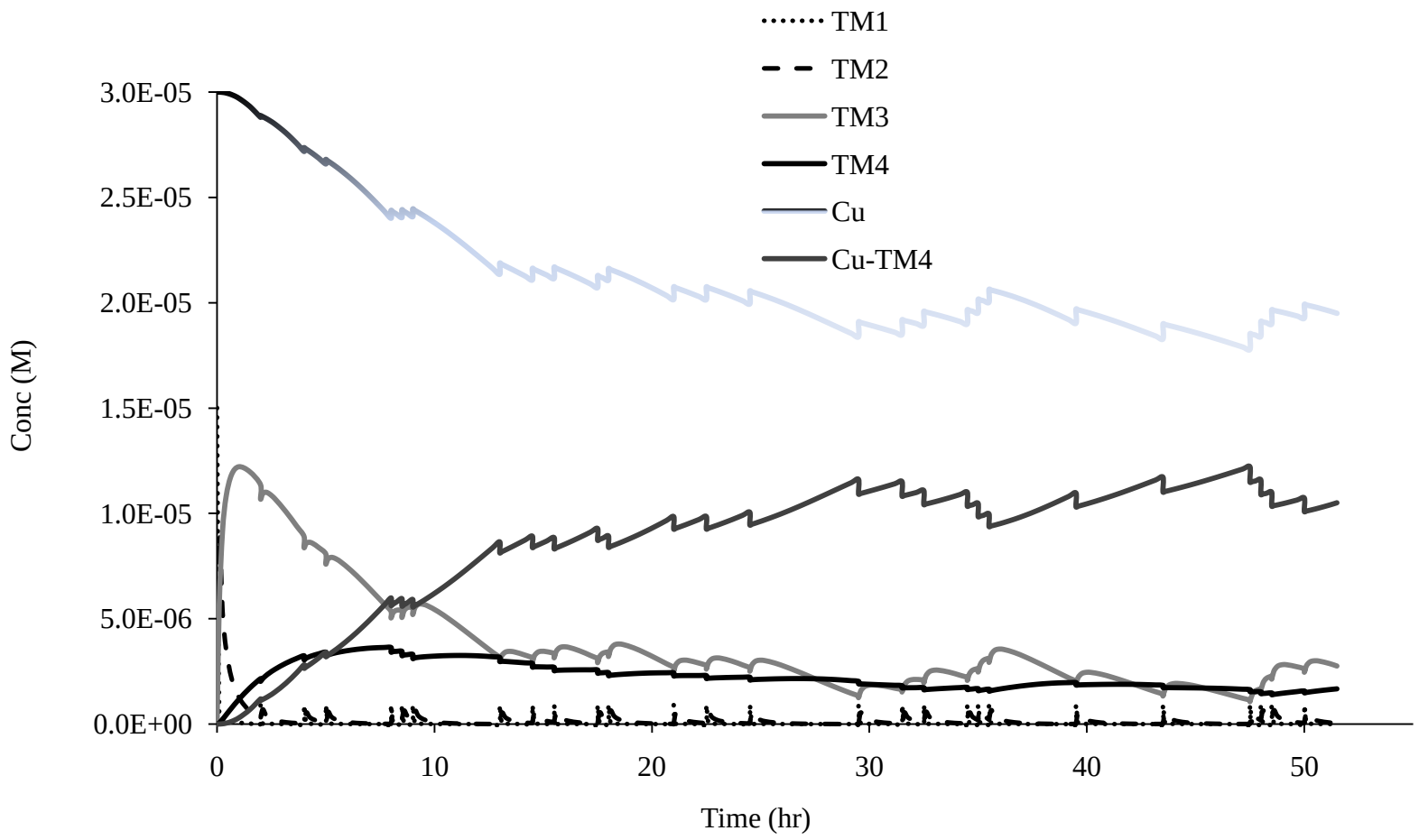

Figure 3.30. Simulation of Cu and TM speciation at 2:1 Cu:Mo ratio.

tended to decrease. This resulted in a concomitant increase in Cu. These trends all reversed when long time intervals were used.

In the bovine mimicking experiment it was evident that changing the Cu:Mo ratio affected the speciation in a reversible manner. The TM peaks that were evident at a 1:1 ratio disappeared when the Cu concentration was increased and returned after the Cu concentration was reduced. This condition was simulated for comparison. Figure 3.31 shows the effects of increasing the Cu:Mo ratio toward 2:1 from 1:1. Figure 3.32 shows the reverse process, the lowering of the Cu:Mo ratio from 2:1 back toward 1:1

As the Cu:Mo ratio is raised above 1:1, the concentrations approach those seen in Figure 3.30, the 2:1 simulation. There is a gradual decrease of TM4 combined with an increase of Cu-TM4. The Cu concentration increases as well but faster than the Cu-TM4 concentration which is limited by the TM4 concentration. There is no significant change in TM1, TM2 or TM3 during this change.

The lowering of the Cu:Mo ratio from 2:1 down to 1:1 produces the opposite changes as the concentrations converge with those shown in Figure 3.29. The TM4 concentration gradually increases while the Cu concentration sharply decreases. The Cu-TM4 concentration stays relatively constant due to the opposing action of TM4 and Cu. Again, there is no notable change in terms of TM1, TM2 or TM3.

These simulations reasonably mirror what was seen in the *in vitro* experiments described earlier. In the process, valuable information was gained that was previously unavailable. In section 3.3.4 the fitting results showed a strong presence of TM2 (and Cu-TM2) while TM3 (and Cu-TM3) did not appear. The simulations seem to enforce the notion that indeed TM3 is more likely to be present than TM2.

There are clearly differences between the simulations and experiment. Undoubtedly there are process occurring that are currently unaccounted for in the simulation scheme. When a 2:1 Cu:Mo ratio was used in the experiments, there were no

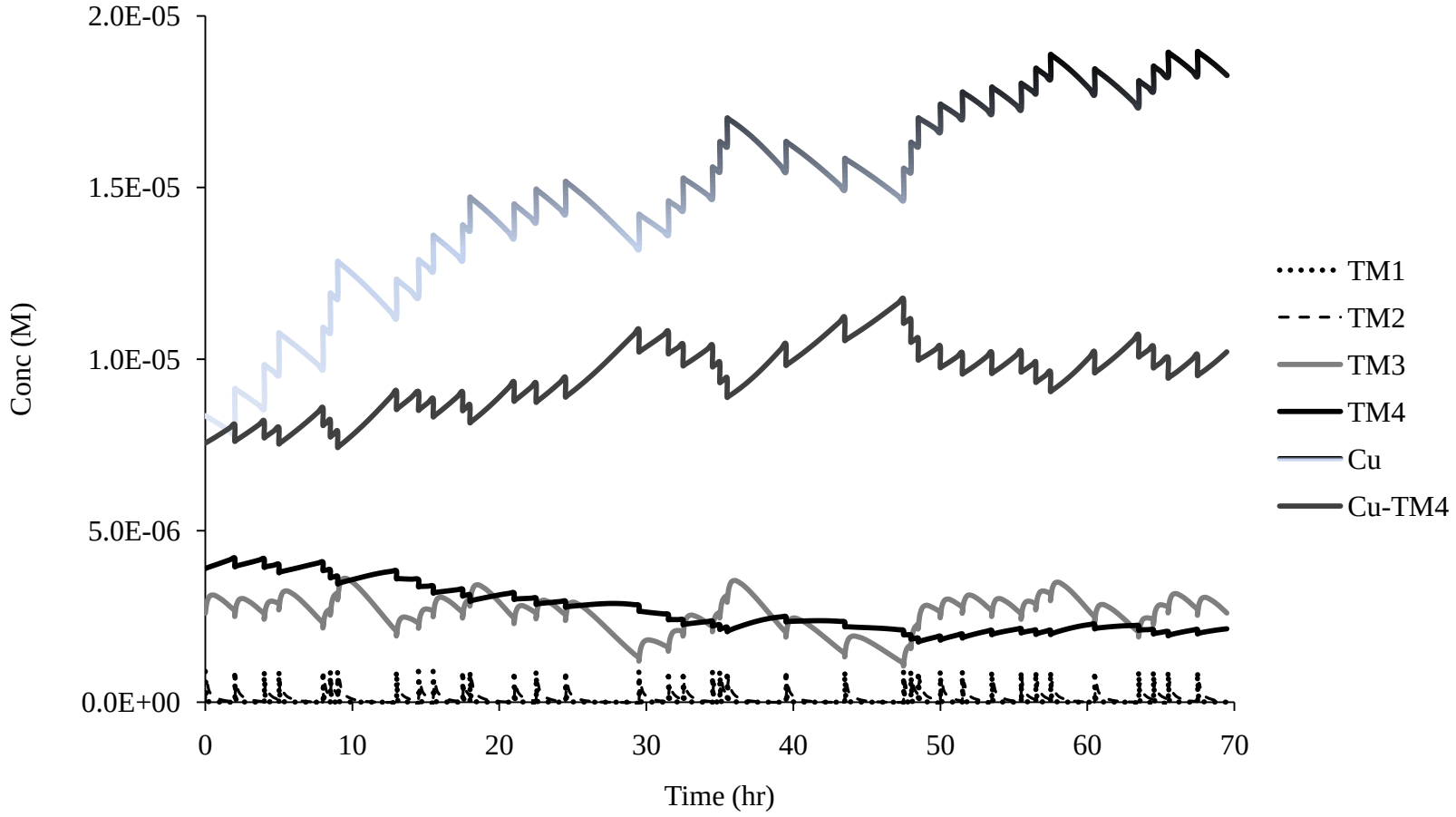

Figure 3.31. Simulation of change of Cu:Mo ratio from 1:1 to 2:1. The conditions at 0 hours are equivalent to the final conditions in Figure 3.29.

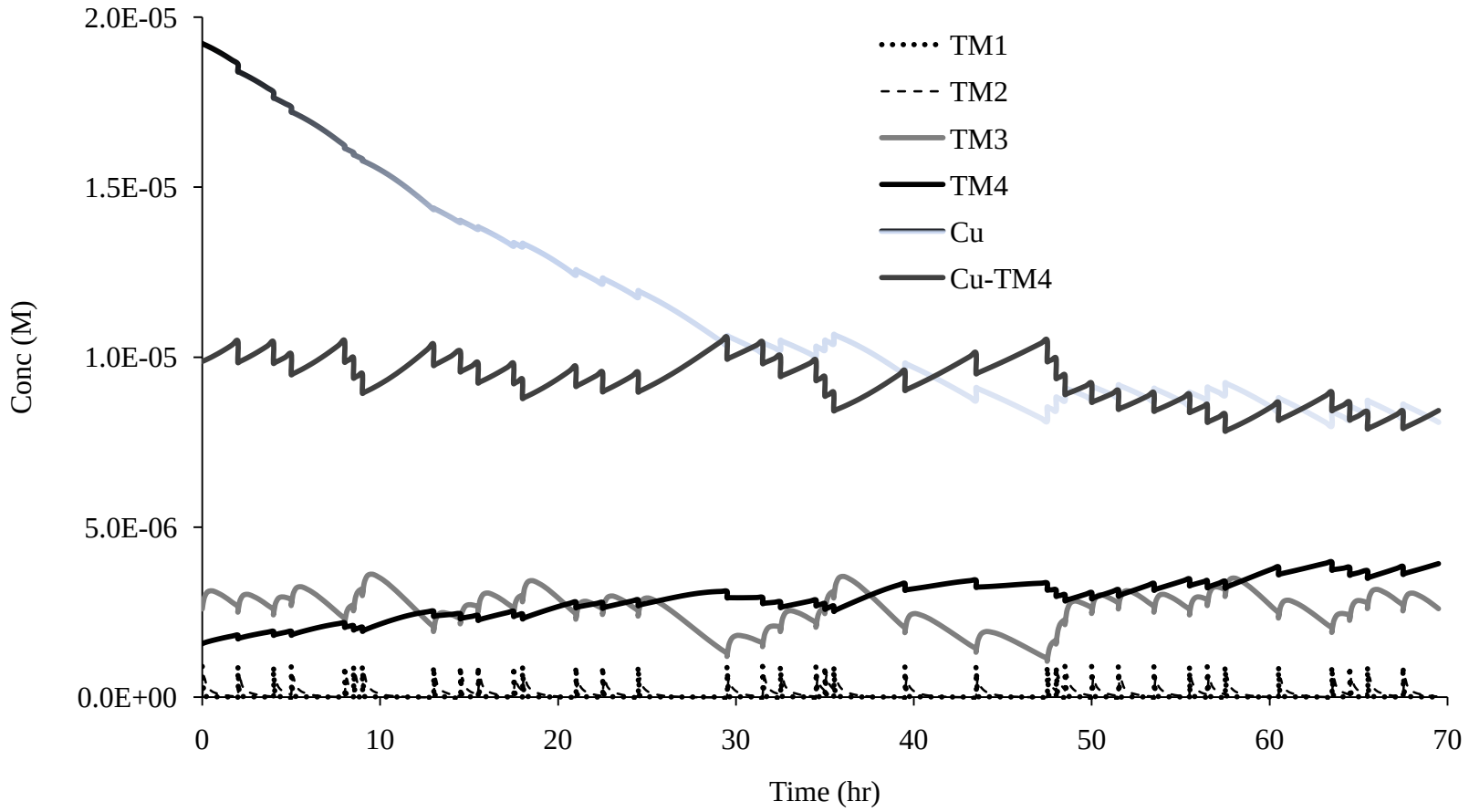

Figure 3.32. Simulation of change of Cu:Mo ratio from 2:1 to 1:1. The conditions at 0 hours are equivalent to the final conditions in Figure 3.30.

noticeable TM peaks present. Simulation of this condition shows a measurable presence of TM3 and TM4. This is perhaps due to interaction between Cu and TM3. If this were the case, the free TM3 concentration would be lowered due to the formation of Cu-TM3. The TM4 concentration, and hence the Cu-TM4 concentration, would be also be lower because of the reduced capacity for TM4 formation.

Overall, the simulations should approach what is expected in the rumen as the complexity of the model increases. This will occur as more information is gained about interactions between Cu and the various TMs. Information from these simulations can in turn be used to advance the Cu-ligand speciation model being developed in the Reid group.

4. SUMMARY, CONCLUSIONS AND FUTURE WORK

4.1 SUMMARY

Cu is an essential trace element in cattle and is found in a variety of enzymes and proteins. Many of these enzymes carry out functions that are crucial to the well-being of the animal. Chronic deficiency of Cu will result in various symptoms including, possibly, death. Testing of Cu levels in the blood of cattle is expensive, time consuming and often an inaccurate indication of the true Cu status. Meanwhile, liver Cu is a more accurate indicator but requires invasive sampling. One goal in the Reid group is to develop a computer based Cu-ligand speciation model that predicts the Cu status of an animal given various input conditions. This will provide a rapid, cheap method of identifying potentially Cu deficient herds.

Secondary copper deficiency results from the presence of an antagonist. Thiomolybdates (MoS_xO_{4-x}, x = 0 – 4), referred to as TMx (where x refers to the number of S ligands) are potent antagonists in ruminants. TMs form in the rumen from MoO_4^{2-} acquired in the feed and H_2S produced by the reduction of various forms of S by rumen microbes. TM formation occurs by successive substitution of O with S ligands at a decreasing rate to the final product, TM4. This formation is relatively slow but the long residence time in the rumen allows the reaction to occur to a significant extent. Each thiomolybdate reacts differently with Cu. TM1 and TM2 are not expected to be major antagonists. On the other hand, TM3 and TM4 result in the irreversible formation of adduct structures that sequester Cu and prevent it from being absorbed. In order to account for TMs in the rumen model, accurate rate constants for their formation are needed.

The goal of the work presented in this thesis was to establish the kinetics of thiomolybdate formation in conditions relevant to the bovine rumen. These rate constants can then be incorporated into the computer model. This first required the development of a method to establish the purity of the TMs in solution and hence a means of determining species concentrations in a mixture. Finally, the interactions of the TMs with Cu were examined in order to gain kinetic information on Cu-TM adduct formation. Simulations of TM and Cu-TM formation were then performed.

4.1.1 Thiomolybdate Characterization

The TMs are best studied using UV-visible spectroscopy. However, there is a great deal of overlap amongst the species in the region of interest. The consecutive nature with which TMs form makes synthesis of a single species free from contamination difficult, even unlikely. The simple UV-visible measurement of a synthesized TM is thus an inadequate method for characterizing the spectrum of a pure species. Similarly, the accurate composition of a TM sample cannot be determined from a mixture.

TM0 and TM4 could be obtained in pure form. The molar absorptivities of these species could therefore be obtained from Beer's Law curves. TM1, TM2 and TM3 molar absorptivities, however, were determined simultaneously with sample composition using curve fitting methods. This was done using the curve fitting algorithms that are part of the Origin7® software.

TM1 and TM3 were synthesized to contain only TM0 or TM4, respectively, so that there was only one uncharacterized TM in each sample. UV-visible spectra were then taken at varying concentrations for each sample. This data was fit in two separate steps. The equations used for fitting resemble Beer's Law such that the total absorbance is equal to the sum of the absorbances of each species present. However, since the molar concentration could not be known, the g/L concentration and an average formula mass were used instead.

In the first fitting step, the absorptivities at selected wavelengths were determined. The TM proportions were set to reasonable values and the average formula mass was calculated accordingly. The absorptivities were then found by iteration. In the second fitting step, the absorptivities (just determined), were fixed and the composition was found by iteration. These two steps were repeated until no further improvement was seen. This process was performed for the TM0/TM1 and TM3/TM4 samples to find the absorptivities of the TM1 and TM3 spectra, respectively. Finally, TM2 could be synthesized and characterized using the same method.

TM formation experiments were then performed by mixing TM with excess sulfide and measuring the UV-visible spectra over time. With the UV-visible spectra of the pure TMs now known, the composition could be determined from each spectrum. In this case, all TM absorptivities were fixed and, knowing the initial TM concentration, the composition (and hence concentrations) at each time interval was found by iteration. The concentration vs. time data was then used for kinetic analysis. TM characterization was presented in detail in section 3.1.

4.1.2 Thiomolybdate Interconversion Kinetics

The kinetics of TM interconversions are important for the modeling of Cu-ligand speciation in the rumen. However, the complete reaction scheme for TM interconversions includes stepwise formation from TM0 to TM4 as well as stepwise hydrolysis from TM4 to TM0. Past studies of TM kinetics have looked at simplifying this scheme by isolating individual reactions to measure the rate constants. The quality of this work is limited by the assumptions that consecutive and reverse reactions are not occurring. Also, there is no direct correlation to TM formation in the rumen which propels forward from a TM0 starting point. A method for simultaneously determining all relevant rate constants is necessary.

Reaction order with respect to the TMs was determined from the concentration vs. time data that was obtained from the formation experiments. In all cases this was

found to be a first order relationship. Since a large excess of sulfide and buffered solutions were used in the experiments, these reactions were pseudo-first order. Further studies showed that the forward reactions were also first order with respect to sulfide and the reverse process, k_{-2}, was first order with respect to H^+.

Since the reactions were being carried out under pseudo-first order conditions, the Laplace Transform method could be used to solve the integrated rate equations. This method allowed this complex reaction scheme to be handled without the use of advanced calculus. The resulting integrated rate equations were then used to fit the concentration vs. time data and obtain, simultaneously, all relevant rate constants. Also, by adjusting the reaction scheme until a good fit was achieved, it was possible to determine which TM interconversion processes occur under the conditions studied.

The rate constants of TM interconversions were determined under a variety of biologically relevant conditions. These could then be used in the Cu-ligand speciation model. In addition, information could be gained in order to propose a plausible mechanism. By changing the ionic strength and then plotting log k vs. $\sqrt{I}$, the identities of the reacting species could be deduced. The slope of this curve is equal to $1.02z_Az_B$, where z_A and z_B are the charges of reacting species A and B, respectively. The slope of this curve for all processes was zero indicating H_2S was involved in TM formation while H_2O was the reacting species for the hydrolysis.

Decreasing the pH caused an increase in each of the rate constants. This is logical since this would cause an increase in the proportion of H_2S that is present. In the case of k_{-2} a first order dependence on H^+ was observed. An additional effect of H^+ was also observed, though, and this is likely due to pre-protonation of the TM species. Increases in the temperature caused increases in the rate constants, except for k_4, for which no effect was observed over the range studied. The calculated activation energies showed were similar for k_2 and k_3. The greater magnitude of k_2, though, leads to a greater pre-exponential factor indicating a greater reaction efficiency. The activation energy for k_{-2} was greater than for k_2 and k_3 indicating that it is a less favorable process.

From the information that was acquired, plausible mechanisms were proposed. For both the forward and reverse reactions, the overall second order result indicates associative mechanisms. Pre-protonation of the TM must occur for k_{-2} and also appears to enhance the forward reactions. A discussion of TM kinetics was given in section 3.2

4.1.3 Interactions Between Copper(II) and the Thiomolybdates

Interactions between the TMs and Cu do not form simple, well characterized solid products. What happens in solution is even less certain. This makes the study of these reactions difficult. Nonetheless, some information can be gained from solution studies. The first order of business was to develop a method by which the products of the reactions of Cu with the TMs could be analyzed. Each synthesized TM was mixed with excess Cu to ensure complete reaction of TM while making sure that precipitation did not occur. Measuring the UV-visible spectra of these solutions at varying concentrations allows a nominal molar absorptivity to be calculated for each "Cu-TM" product. Since the identity of these products are not known, the absorptivities are calculated on a per mole of Mo basis.

The kinetics of the reactions between Cu(II) and TM4 and Cu(II) and TM3 were studied by UV-visible spectroscopy. Previous work by Essilfie-Dughan showed that this reaction proceeded via an intermediate. It was determined that there were indeed three absorbing species present: the TM, the reaction product and the intermediate. To properly extract species concentrations from the spectra, the absorptivities of the intermediate had to be determined. This was done by first simulating species concentrations using the rate constants from Essilfie-Dughan's work and then establishing what fraction of the experimental absorbance was due to known (TM and product) species and what was due to the intermediate. From here, absorptivities could be calculated and the absorbance data was recalculated. Species concentrations and then rate constants were then determined by curve fitting as with the TM kinetics. This procedure was reiterated until the rate constants and intermediate absorptivities converged.

The rate constants of TM formation and the reaction between Cu(II) and TM4 were then used in computer based simulations. This helps to provide insight into the effects of the TMs on Cu in the rumen. This simulation was set up to include the complete TM formation scheme followed by the reaction of TM4 with Cu(II). The simulation provided species concentrations as a function of time. It showed that as TM4 forms it immediately reacts with Cu(II). Further simulations involved mimicking the cycling of rumen contents with fresh reagents (TM0, sulfide and Cu(II)).

TM formation was monitored by UV-visible spectroscopy in the presence of Cu(II). This was then extended to mimic bovine feeding habits. In this case, some of the reaction mixture was removed at various time intervals and replaced with fresh reagents (TM0, sulfide and Cu(II)). Although quantitative analysis of the spectra was not achieved, qualitative inspection provided some insight. Section 3.3 outlined the studies involving reactions between Cu(II) and the TMs.

4.2 CONCLUSIONS

The three goals of this project as outlined in section 1.2 have been achieved.

1. Thiomolybdates play a crucial role in the speciation of Cu in the bovine rumen. The successive nature of TM formation, however, complicates analysis of mixtures. In this work, curve fitting methods were used to accurately establish the UV-visible spectra of the individual, pure TMs. This method did not require the synthesis of pure samples nor was the assumption of initial purity necessary. The molar absorptivities determined here were typically greater than comparable values in the literature. These discrepancies are likely due to presence of contaminating TMs which would cause the lowering of the absorptivities. Using the information obtained here, any TM mixture in solution can be analyzed for its composition.

2. The rate constants of TM interconversions are crucial to the Cu-ligand speciation model being developed in the Reid group. TM kinetics are difficult to measure because of the complexity of their interconversions. Monitoring isolated reactions leads to limiting assumptions of initial TM purity and the absence of other reactions occurring. These assumptions were bypassed by performing TM formation reactions from a TM0 starting point, analyzing the UV-visible spectra for TM concentrations and then using curve fitting methods to determine all relevant rate constants simultaneously. Further kinetic analyses performed under varying conditions showed that forward and reverse processes proceed via associative mechanisms. In addition, the reacting nucleophiles are H_2S and H_2O for the forward and reverse processes, respectively.

3. The kinetics of the reaction between Cu(II) and either TM4 or TM3 were studied by UV-visible spectroscopy. These results were then compared to those obtained by Essilfie-Dughan using ISE. Favorable agreement was obtained which corroborated the validity of each method and confirmed the reaction scheme proposed by Essilfie-Dughan. The rate constants were then used in simulations to show the effects of the TMs on Cu(II). These results were then compared qualitatively to experiment. These experiments involved TM formation from a TM0 starting point in the presence of Cu. In both cases it was seen that when Cu levels are low, the TMs predominate and the available Cu is nullified. Experiments that mimic bovine feeding habits were also performed and compared to simulations. It was seen that the effects of TM antagonism are reversible in that available Cu levels recuperate when the input concentration is increased.

4.3 FUTURE WORK

Future work in this area should focus on Cu related studies. Although the kinetics of the reaction between Cu(II) and TM4 were determined, the conditions used were not biologically relevant. Increasing the temperature to 38 °C and using slightly acidic buffered solutions increased the rate of this reaction. This made it very difficult to monitor using standard UV-visible techniques. Improved results may be achieved using stop-flow techniques. UV-visible spectroscopy is preferred over ISE, however, because information can be gained on multiple species. Reactions should then be performed involving each of the TMs to establish the appropriate kinetics.

TM formation reactions in the presence of Cu were performed in this work. These could not be quantitatively analyzed, likely because there were unaccounted for absorbing species. Throughout the kinetic studies, it would be beneficial to identify other intermediates and characterize their UV-visible spectra under various conditions. This information could then be used to analyze the experimental data. In turn, a better understanding of the effects of TM formation on Cu speciation could be gained.

With a more complete kinetic picture, the computer simulations can be enhanced. In this work the reactions of Cu(II) with TM4 and TM3 were considered. Analysis of these reactions may be enhanced by the results of Slamova's work regarding Cu-TM adduct structures and stoichiometry. Knowledge of the reaction products and stoichiometry may provide clues about the mechanism. This information may also help to optimize the current model for reactions between Cu and the TMs. Information regarding reactions with other TMs may also be incorporated to give a fuller picture.

REFERENCES

[1] J.R. De Laeter, J.K. Bohlke, P. De Bievre, H. Hidaka, H.S. Peiser, K.J.R. Rosman, P.D.P. Taylor, Pure Appl. Chem., 75 (2003) 683.

[2] B.J. Hathaway, in: G. Wilkinson, R.D. Gillard, J. McCleverty (Eds.), Comprehensive Coordination Chemistry, Permagon Press, Oxford, 1987, p. 533.

[3] R.F. Jameson, in: H. Sigel (Ed.), Metal Ions in Biological Systems, Marcel Dekker, Inc., New York, 1981, p. 1.

[4] F.A. Cotton, G. Wilkinson, C.A. Murillo, M. Bochmann, Advanced Inorganic Chemistry, 6th Ed., John Wiley & Sons, Inc., Toronto, 1999.

[5] F.A. Cotton, G. Wilkinson, P.L. Gaus, Basic Inorganic Chemistry, 3rd Ed., John Wiley & Sons, Inc., Toronto, 1995.

[6] J.E. Brule, Y.T. Hayden, K.P. Callahan, J.O. Edwards, Gazetta Chimica Italiana, 118 (1988) 93.

[7] M.A. Harmer, A.G. Sykes, Inorg. Chem., 19 (1980) 2881.

[8] J.W. Akitt, NMR and Chemistry, Chapman and Hall, London, 1983.

[9] A. Muller, E. Diemann, R. Jostes, H. Bogge, Angew. Chem. Int. Ed., 20 (1981) 934.

[10] D.M. Thome, X-Ray Crystallography Studies of Thiomolybdates and Bovine Serum Albumin, Chemistry, University of Saskatchewan, Saskatoon, 2001.

[11] S.H. Laurie, Eur. J. Inorg. Chem. (2000) 2443.

[12] A. Muller, E. Diemann, in: G. Wilkinson, R. D. Gillard, J. A. McCleverty (Eds.), Comprehensive Coordordination Chemistry, Vol. 2, Pergamon, Oxford, 1987.

[13] R.S. Saxena, M.S. Jain, M.L. Mittal, Aust. J. Chem., 21 (1968) 91.

[14] W.B. Simpson, C.F. Mills, J. Inorg. Biochem., 17 (1982) 155.

[15] W.-H. Pan, M.A. Harmer, T.R. Halbert, E.I. Stiefel, J. Am. Chem. Soc., 106 (1984) 459.

[16] W.-H. Pan, T.R. Halbert, L.L. Hutchings, E.I. Stiefel, J. Chem. Soc. Chem. Commun. (1985) 927.

[17] C.L. Coyle, M.A. Harmer, G.N. George, M. Daage, E.I. Stiefel, Inorg. Chem., 29 (1990).

[18] J. Chandrasekaran, M.A. Ansari, S. Sarkar, Inorg. Chem., 27 (1988) 3663.

[19] D. Coucouvanis, Adv. Inorg. Chem., 45 (1998) 1.

[20] J.W. McDonald, G.D. Friesen, L.D. Rosenhein, W.E. Newton, Inorg. Chim. Acta, 72 (1983) 205.

[21] G. Jin, X. Xin, H. Chen, X. Zheng, A. Dai, Wuji Huaxue, 3 (1987) 106.

[22] G.A. Zank, T.B. Rauchfuss, S.R. Wilson, A.L. Rheingold, J. Am. Chem. Soc., 106 (1984) 7621.

[23] J. Mason, M. Lamand, M. Hynes, J. Inorg. Biochem., 19 (1983) 153.

[24] E.K. Quagraine, Competitive Interactions Between Copper(II) Ions, Thiomolybdates, and some Biological Ligands, Department of Chemistry, University of Saskatchewan, Saskatoon, 2002.

[25] N.J. Clarke, S.H. Laurie, J. Inorg. Biochem., 12 (1980) 37.

[26] N.J. Clarke, S.H. Laurie, M.J. Blandamer, J. Burgess, A. Hakin, Inorg. Chim. Acta, 130 (1987) 79.

[27] P. Kroneck, O. Lutz, A. Nolle, Z. Naturforsch., 35a (1980) 226.

[28] S. Yue-ming, Z. Long-geng, Y. Xiao-zeng, J. Yuang-sheng, Theor. Chim. Acta, 82 (1992) 213.

[29] M. Minelli, J.E. Enemark, R.T.C. Brownlee, M.J. O'Connor, A.G. Wedd, Coord. Chem. Rev., 68 (1985) 169.

[30] B.E. Erickson, G.R. Helz, Geochim. Cosmochim. Acta, 64 (2000) 1149.

[31] J.C. Bernard, G. Tridot, Bull. Soc. Chim. France (1961) 810.

[32] J.C. Bernard, G. Tridot, Bull. Soc. Chim. France (1961) 818.

[33] A. Muller, E. Diemann, Z. Naturforsch. B, 23 (1968) 1607.

[34] P.J. Aymonino, A.C. Ranade, E. Diemann, A. Muller, Z. Anorg. Allg. Chem., 371 (1969) 300.

[35] A. Muller, E. Diemann, A.C. Renade, P.J. Aymonino, Z. Naturforsch. B, 24 (1969) 1247.

[36] B.E. Erickson, The Speciation of Molybdenum in Sulfidic Natural Waters, Dept. of Chemistry and Biochemistry, University of Maryland, 1998, p. 259.

[37] N.F. Suttle, Annu. Rev. Nutr., 11 (1991) 121.

[38] J. Mason, M. Lamand, C.A. Kelleher, J. Comp. Path., 92 (1982) 509.

[39] J. Mason, M. Lamand, C.A. Kelleher, Br. J. Nutr., 43 (1980) 515.

[40] N.F. Suttle, A.C. Field, J. Comp. Path., 93 (1983) 379.

[41] A. Muller, O. Glemser, E. Diemann, H. Hofmeister, Z. anorg. allg. Chem., 371 (1969) 74.

[42] J.A. Tossell, Geochim. Cosmochim. Acta, 69 (2005) 2497.

[43] A.T. Dick, D.W. Dewey, J.M. Gawthorne, J. Agric. Sci., 85 (1975) 567.

[44] W.G. Zumft, Eur. J. Biochem., 91 (1978) 345.

[45] V.C. Culotta, J.D. Gitlin, in: C.R. Scrive, A.L. Beaudet, W.S. Sly, D. Valle (Eds.), The Metabolic & Molecular Bases of Inherited Disease, McGraw-Hill, New York, 2001.

[46] S. Sarkar, S.B.S. Mishra, Coord. Chem. Rev., 59 (1984) 239.

[47] N.J. Clarke, S.H. Laurie, Inorg. Chim. Acta, 66 (1982) L35.

[48] S.H. Laurie, D.E. Pratt, J.B. Raynor, Inorg. Chim. Acta, 123 (1986) 193.

[49] N.J. Clarke, S.H. Laurie, D.E. Pratt, Inorg. Chim. Acta, 138 (1987) 103.

[50] S. Sarkar, S.B.S. Mishra, J. Indian Chem. Soc., 62 (1985) 821.

[51] T. Ecclestone, I. Harvey, S.H. Laurie, M.C.R. Symons, F.A. Taiwo, Inorg. Chem. Comm., 1 (1998) 460.

[52] Y. Komatsu, I. Sadakata, Y. Ogra, K.T. Suzuki, Chemico-Biological Interactions, 124 (2000) 217.

[53] Y. Ogra, Y. Komada, K.T. Suzuki, J. Inorg. Biochem., 75 (1999) 199.

[54] Y. Ogra, M. Ohmichi, K.T. Suzuki, Toxicology, 106 (1996) 75.

[55] G.N. George, I.J. Pickering, H.H. Harris, J. Gailer, D. Klein, J. Lichtmannegger, K.H. Summer, J. Am. Chem. Soc., 125 (2003) 1704.

[56] A. Muller, H. Bogge, H.G. Tolle, R. Jostes, U. Schimanski, M. Dartmann, Angew. Chem. Int. Ed. Engl., 19 (1980) 654.

[57] S.F. Gheller, T.W. Hambley, J.R. Rodgers, R.T.C. Brownlee, M.J. Oconnor, M.R. Snow, A.G. Wedd, Inorg. Chem., 23 (1984) 2519.

[58] Q. Huang, X.T. Wu, Q.M. Wang, T.L. Sheng, J.X. Lu, Inorg. Chem., 35 (1996) 893.

[59] C. Zhang, Y.L. Song, Y. Xu, H. Fun, G.Y. Fang, Y.X. Wang, X.Q. Xin, J. Chem. Soc. Dalton Trans. (2000) 2823.

[60] C. Zhang, Y.L. Song, Y. Xu, G.C. Jin, G.Y. Fang, Y.X. Wang, H. Fun, X. Xin, Inorg. Chim. Acta, 311 (2000) 25.

[61] M.H. Sadr, W. Clegg, H.R. Bijhanzade, Polyhedron, 23 (2004) 637.

[62] Z.H. Li, S.W. Du, X.T. Wu, J. Chem. Soc. Dalton Trans. (2004) 2438.

[63] J. Guo, T.L. Sheng, W.J. Zhang, X.T. Wu, P. Lin, Q.M. Wang, J.X. Lu, Inorg. Chem., 37 (1998) 3689.

[64] H.W. Hou, H.G. Zheng, H.G. Ang, Y.T. Fan, M.K.M. Low, Y. Zhu, W.L. Wang, X.Q. Xin, W. Ji, W.T. Wong, J. Chem. Soc. Dalton Trans. (1999) 2953.

[65] D.X. Wu, M.C. Hong, R. Cao, H.Q. Liu, Inorg. Chem., 35 (1996) 1080.

[66] E. Brouwer, A.M. Frens, P. Reitsma, C. Kalisvaart, Rijkslandbouwproefstation, Hoorn Verslagen van landbouwkundige Onderzoekingen, 44 (1938) C.

[67] W.S. Ferguson, A.H. Lewis, S.J. Watson, J. Agric. Sci., 33 (1943) 44.

[68] A.T. Dick, Aust. Vet. J., 28 (1952) 30.

[69] A.T. Dick, Aust. Vet. J., 29 (1953) 18.

[70] G.N. Havre, O. Dynna, Acta Vet. Scand., 2 (1961) 375.

[71] I. Thornton, G.F. Kershaw, M.K. Davies, J. Agric. Sci., 78 (1972) 157.

[72] B.J. Alloway, J. Agric. Sci., 80 (1973) 521.

[73] S. Jamieson, R. Allcroft, Br. J. Nutr., 4 (1950) 16.

[74] R. Allcroft, G. Lewis, Landbouwkundig Tijdschrift, 68 (1956) 711.

[75] H.I. Field, Vet. Rec., 69 (1957) 788.

[76] I. Thornton, G.F. Kershaw, M.G. Davies, Vet. Rec., 90 (1972) 11.

[77] N.F. Suttle, A.C. Field, J. Comp. Path., 78 (1968) 351.

[78] N.F. Suttle, A.C. Field, J. Comp. Path., 78 (1968) 363.

[79] B.S.W. Smith, A.C. Field, N.F. Suttle, J. Comp. Path., 78 (1968) 449.

[80] N.F. Suttle, A.C. Field, J. Comp. Path., 79 (1969) 453.

[81] R.F. Miller, N.O. Price, R.W. Engel, J. Nutr., 60 (1956) 539.

[82] L.F. Gray, L.J. Daniel, J. Nutr., 84 (1964) 31.

[83] S. Gaballah, L.G. Abood, A. Kapsalis, Sturdiva.D, Proc. Soc. Exp. Biol. Med., 119 (1965) 625.

[84] D. Arthur, J. Nutr., 87 (1965) 69.

[85] R.P. Dowdy, G. Matrone, J. Nutr., 95 (1968) 191.

[86] R.P. Dowdy, G. Matrone, J. Nutr., 95 (1968) 197.

[87] P.R. Bird, Proc. Aust. Soc. Anim. Prod., 8 (1970) 212.

[88] J. Huisingh, G. Matrone, Proc. Soc. Exp. Biol. Med., 139 (1972) 518.

[89] J. Huisingh, D.C. Milholland, G. Matrone, J. Nutr., 105 (1975) 1199.

[90] J.M. Gawthorne, C.J. Nader, Br. J. Nutr., 35 (1976) 11.

[91] N.F. Suttle, Br. J. Nutr., 32 (1974) 559.

[92] N.F. Suttle, A.C. Field, Vet. Rec., 95 (1974) 165.

[93] N.F. Suttle, Proc. Nutr. Soc., 33 (1974) 299.

[94] N.F. Suttle, Ann. N. Y. Acad. Sci., 355 (1980) 195.

[95] J. Mason, Irish Vet. J., 35 (1981) 221.

[96] J.D. Allen, J.M. Gawthorne, J. Inorg. Biochem., 31 (1987) 161.

[97] N.D. Grace, N.F. Suttle, Br. J. Nutr., 41 (1979) 125.

[98] C.F. Mills, I. Bremner, T.T. El-Gallad, A.C. Dalgarno, B.W. Young, Proceedings, Third International Symposium on Trace Element Metabolism in Man and Animals, Arbeitskreis Tierernahrung, Weihenstephan, Federal Republic of Germany, 1978.

[99] A.C. Bray, N.F. Suttle, A.C. Field, Proc. Nutr. Soc., 41 (1982) 67A.

[100] J. Mason, Irish Vet. J., 36 (1982) 164.

[101] J. Mason, C.A. Kelleher, J. Letters, Br. J. Nutr., 48 (1982) 391.

[102] C.F. Mills, T.T. El-Gallad, I. Bremner, J. Inorg. Biochem., 14 (1981) 189.

[103] I. Bremner, C.F. Mills, B.W. Young, J. Inorg. Biochem., 16 (1982) 109.

[104] T.T. El-Gallad, C.F. Mills, I. Bremner, R. Summers, J. Inorg. Biochem., 18 (1983) 323.

[105] A.C. Bray, N.F. Suttle, A.C. Field, Proc. Nutr. Soc., 41 (1982) 66A.

[106] M. Hynes, M. Woods, D. Poole, P. Rogers, J. Mason, J. Inorg. Biochem., 24 (1985) 279.

[107] M. Hynes, M. Lamand, G. Montel, J. Mason, Br. J. Nutr., 52 (1984) 149.

[108] M. Woods, J. Mason, J. Inorg. Biochem., 30 (1987) 261.

[109] J.D. Allen, J.M. Gawthorne, Br. J. Nutr., 58 (1987) 265.

[110] J. Mason, M. Lamand, J.C. Tressol, G. Mulryan, Br. J. Nutr., 59 (1988) 289.

[111] E.J. Underwood, N.F. Suttle, The Mineral Nutrition of Livestock, CABI Publishing, New York, 1999.

[112] D.C. Church, The Ruminant Animal, Digestive Physiology and Nutrition, Prentice Hall, New Jersey, 1988.

[113] J. Essilfie-Dughan, Speciation Modelling of Copper(II) in the Thiomolybdate-Contaminated Rumen, Department of Chemistry, University of Saskatchewan, Saskatoon, 2007.

[114] S. Smith, The Microbiology and Biochemistry of the Rumen, Munton and Fisson, Ltd., England, 1973.

[115] J.W. Czerkawski, An Introduction to Rumen Studies, Permagon Press, Toronto, 1986.

[116] B.L. O'Dell, in: R.E. Olson (Ed.), Present Knowledge in Nutrition, The Nutrition Foundation, Inc., Washington DC, 1984, p. 506.

[117] R.J. Cousins, Physiol. Rev., 65 (1985) 238.

[118] H.L. Davies, Aust. J. Exp. Agric. Anim. Hus., 17 (1977) 905.

[119] S.E. Wikse, D. Herd, R. Field, P. Holland, J. Amer. Vet. Med. Assoc., 200 (1992) 1625.

[120] L.R. Legleiter, J.W. Spears, J. Anim. Sci., 85 (2007) 2198.

[121] N.F. Suttle, Vet. Rec., 119 (1986) 519.

[122] D.A. Dargatz, F.B. Garry, G.B. Clark, P.F. Ross, J. Am. Vet. Med. Assoc., 215 (1999) 1828.

[123] R.K. Tessman, J. Lakritz, J.W. Tyler, S.W. Casteel, J.E. Williams, R.K. Dew, J. Am. Vet. Med. Assoc., 218 (2001) 756.

[124] N.F. Suttle, S. Afr. J. Anim. Sci., 18 (1988) 15.

[125] J.L. Albright, J. Dairy Sci., 76 (1993) 485.

[126] B.J. Tolkamp, D.P.N. Schweitzer, I. Kyriazakis, J. Dairy Sci., 83 (2000) 2057.

[127] M. Melin, H. Wiktorsson, L. Norell, J. Dairy Sci., 88 (2005) 71.

[128] M.A. Attaelmannan, 1H NMR and Potentiometric Studies of Copper (II) Speciation in Ruminants, Department of Chemistry, University of Saskatchewan, Saskatoon, 1999.

[129] M.A. Attaelmannan, R.S. Reid, J. Inorg. Biochem., 64 (1996) 215.

[130] R.S. Reid, M.A. Attaelmannan, J. Inorg. Biochem., 69 (1998) 59.

[131] E.K. Quagraine, R.S. Reid, J. Inorg. Biochem., 85 (2001) 53.

[132] E.K. Quagraine, H.-B. Kraatz, R.S. Reid, J. Inorg. Biochem., 85 (2001) 23.

[133] M.A. Koranteng, 1H NMR and Potentiometric Studies of Mixed-Ligand Complexes of Copper(II) with some Amino Acids, Department of Chemistry, University of Saskatchewan, Saskatoon, 2004.

[134] D. Slamova, in preparation, Department of Chemistry, University of Saskatchewan, Saskatoon, 2008.

[135] R.S. Reid, R.J. Clark, E.K. Quagraine, Can. J. Chem., 85 (2007) 1083.

[136] A. Muller, E. Diemann, U. Heidborn, Z. Anorg. Allg. Chem., 371 (1969) 136.

[137] P.J. Aymonino, A.C. Ranade, A. Muller, Z. Anorg. Allg. Chem., 371 (1969) 295.

[138] J. Andraos, J. Chem. Ed., 76 (1999) 1578.

[139] G.E. Roberts, H. Kaufman, Table of Laplace Transforms, Saunders, Philadelphia, 1966.

[140] Y. Zhao, G. Wang, W. Li, Z.-L. Zhu, Chemom. Intell. Lab. Syst., 82 (2006) 193.

[141] S. Licht, F. Forouzan, K. Longo, Anal. Chem., 62 (1990) 1356.

[142] K.J. Laidler, J.H. Meiser, Physical Chemistry, Houghton Mifflin Company, Toronto, 1995.

[143] M. Li, Z. Twardowski, F. Mok, N. Tam, J. Appl. Electrochem, 37 (2007) 499.

[144] N. Gershenfeld, The Nature of Mathematical Modeling, Cambridge University Press, Cambridge, 1999.

[145] M. Maeder, A.D. Zuberbuhler, Anal. Chem., 62 (1990) 2220.

[146] J. Andraos, J. Phys. Chem. A, 107 (2003) 2374.

APPENDIX

A1 CURVE FITTING

A1.1 Theory

In most cases, unknown values can be determined via simple calculation. For example, from the slope of a Beer's Law plot ($A = \varepsilon cl$), the molar absorptivity, ε, can be calculated from equation A.1, where l is the path length. In this case, the slope and path length are known and ε is the only unknown. The calculation is therefore trivial and the result is exact.

$$\text{Slope} = \varepsilon l \qquad \textbf{(A.1)}$$

A more complicated case might include two unknown values. An example is shown in equation A.2. Here, A is the absorbance and c is the concentration. If we

$$A = (\alpha_1\varepsilon_1 + \alpha_2\varepsilon_2)c \qquad \textbf{(A.2)}$$

assume that ε_1 and ε_2, the absorptivities of species 1 and 2, are known, then there are two unknown values, α_1 and α_2, the molar fractions of species 1 and 2. Therefore a second equation is needed to be able to calculate the two unknowns. However, assuming there are only two species, and using the relationship $\alpha_1 + \alpha_2 = 1$, the calculation can still be performed with relative ease giving exact results.

Often, when there are two unknowns, though, a quadratic equation may be required to find the solution. This provides two possible answers for one of the unknowns. Although intuition may make it obvious which result is the correct one, this demonstrates the increasing uncertainty that arises with an increasing number of unknowns. If the number of unknowns is increased further, the calculations become laborious and eventually unsolvable. Meanwhile, the number of possible solutions

increases as well. It is therefore necessary to find a new method for solving for multiple unknowns.

Curve fitting can be used to obtain values for large numbers of unknowns (herein referred to as parameters) simultaneously. Curve fitting refers to the matching, or fitting, of theoretically calculated data to the experimental curve. Theoretically, this occurs when the correct parameter values are implemented. The parameter values are constantly improved by iteration (trial and error) until a best fit is obtained.

There are three main parts to a curve fitting problem. The first is the function itself, the second is the measured data and the third are the unknown parameters [144]. The measured data is simply the data obtained from some experiment. The source of the data is not important as long as a meaningful relationship (function) can be found to describe it. For example, absorbance data can be described by Beer's Law. The function must contain variables for the experimental data and the parameters.

The iteration process is carried out by software that contains algorithms to guide the fitting. The iteration process is begun by making an initial guess as to the values of the parameters. The theoretical datum is then calculated and compared to its experimental counterpart. The difference between the two values (the residual) and its square is then calculated. If there are multiple data points, a residual is determined for each and the sum of the squares of these is calculated. From here, a correction factor is applied to the initial guess and a new set of residuals are calculated. The new residuals are then compared to that of the previous iteration to see if convergence is occurring. If so, iterations are continued until the best fit is achieved. Convergence is commonly measured by the reduced χ^2 value which is defined by equation A.3. If χ^2 is decreasing, convergence is occurring. Iterations will continue until χ^2 reaches some threshold value.

$$\chi^2 = \sum \frac{res^2}{\sigma^2} \qquad \textbf{(A.3)}$$

The term res refers to the residual value between the calculated parameter and the corresponding datum. σ is a weighting factor and is equal to one for equal weighting.

If divergence occurs (increasing χ^2), the fit might be expected to fail. In this case, improved initial guesses would have to be made and the fit attempted again. This can be very cumbersome if no reasonable estimate is available. The Levenberg-Marquardt adaptation increases the chance of a successful fit even when the initial guesses are poor. If there is divergence between iterations, a Levenberg-Marquardt parameter is calculated which is used to redirect the fit toward convergence. Otherwise, the fit would proceed toward some local minimum instead of the true global minimum. The Levenberg-Marquardt algorithm is described in detail elsewhere [145]. Regardless, the likelihood of a sensible fit is enhanced by a quality initial guess and meaningful constraints.

A1.2 Multivariate Analysis

A basic spectroscopic experiment may involve the collection of data at a single wavelength. This is known as a univariate, or single variable, measurement. In many simple cases, this will be adequate. If there is one absorbing species and the absorptivity is known, the concentration can be calculated. Even if there are two absorbing species, the molar fraction of each can often be determined if the absorptivities are known and different. If the absorptivities are the same (isosbestic point), any combination of molar fractions will give the same absorbance.

If there are three absorbing species, there may be multiple molar fraction combinations that apply. For example, three species, α_1, α_2 and α_3 have molar absorptivities of 1000, 2000 and 3000 M^{-1} cm^{-1}, respectively. The calculated absorbance would be the same if each species was present in equal thirds or if species 2 was the sole species present. In this case, there are too many parameters for the number of variables and this leads to uncertainty in the results.

The use of multivariate data is more reliable. Data would be collected at a number of different variables, in this case, wavelengths. If the absorptivities of all absorbing species are known for each wavelength, there will be a unique set of molar fractions that allows the absorbance to be calculated at each wavelength. To demonstrate, assume that α_1, α_2 and α_3 (from above) have absorptivities at a second wavelength of 500, 1000 and 4000 M^{-1} cm^{-1}. Now, there is a difference in the calculated absorbance if each is present in thirds versus only species 2 being present. Already the possible α_1, α_2 and α_3 values have been narrowed down. Increasing the number of variables further increases this certainty.

Multivariate analysis is effective because it removes linearity. In the univariate example, the α's could be adjusted in a linear fashion in order to achieve the same result. However, this simple linearity is destroyed when other wavelengths are incorporated. At the wavelength described in the univariate example, α_1 and α_3 could be adjusted inversely proportional to each other. In the second wavelength example, α_1 must be increased by a factor of eight as α_3 is decreased to achieve the same result. Therefore, α_1 and α_3 (and hence α_2) are no longer linearly proportional to each other. Multivariate analysis is therefore a non-linear method and analysis can be carried out using non-linear least squares fitting.

There are a number of advantages to using multivariate analysis. First, information on the pure spectra of all reacting species can be determined. This is possible even if pure compounds are not available and the spectra overlap. This was demonstrated in section 3.1. Second, the need to find a suitable data point to monitor is eliminated. Third, multivariate analysis is very robust. A unique set of results can be found even if reasonable initial estimates are unknown.

There are a couple of disadvantages to using multivariate analysis. These involve the collecting of much larger amounts of data in a short period of time and the large number of parameters that need to be fit. These limitations have been minimized by the availability and effectiveness of modern computers.

A1.3 Using Origin® Software

The curve fitting for the work presented in this thesis was done using Origin7® software. Origin® is data analysis software that is designed for use by scientists and engineers. It provides spreadsheets for data handling and a wide variety of graphing features. Most notably for this work, though, it contains a number of curve fitting features under the "Analysis" tab. For example, data can be fit to linear, Gaussian or exponential models. If the standard functions are inadequate, user defined functions can be created to accomplish the fitting task. For advanced users custom programming can be added for increased functionality.

A single UV-visible peak could be reasonably fit as a simple Gaussian curve. However, a more complex function is required when there are overlapping peaks across the spectrum. Also, using the pre-defined functions, there is no capacity for adjusting the number or type of parameters to be determined from the fit. In this case, user defined functions are required to extract the necessary information.

Upon opening the non-linear curve fitter, the user is provided with fields to input the desired parameters and variables as shown in Figure A.1. This is found by selecting "Function" and then "New" (or "Select" to find a saved function). The variables that are to be iterated to obtain values for are input into the "Parameter Names" field. There are also fields for the independent and dependent variables. For fitting to UV-visible spectra the independent variables will be the absorptivities (if the α's are sought) or the input concentrations (if the ε's are sought). The dependent variables will be absorbance values. The textbox below these fields is where the function(s) are included. These can also be added in "Code Builder".

The data corresponding to the independent and dependent variables listed appears in the worksheet in vertical columns. The independent variable columns must be declared as "X" at the top of the column and the dependent variables, "Y" (see Figure A.1). The columns in the worksheet must then be linked to the fitting routine. This is

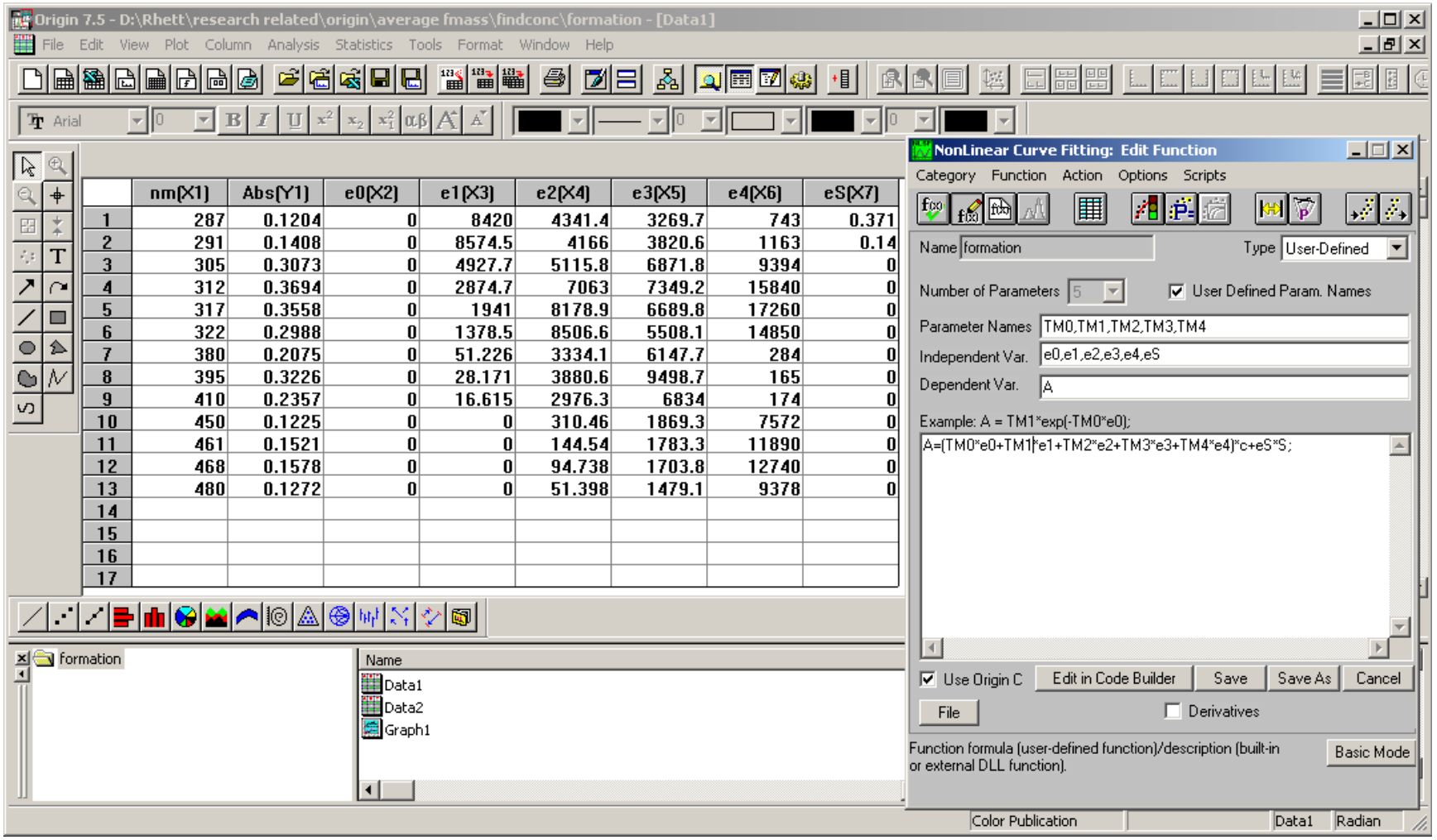

	nm(X1)	Abs(Y1)	e0(X2)	e1(X3)	e2(X4)	e3(X5)	e4(X6)	eS(X7)
1	287	0.1204	0	8420	4341.4	3269.7	743	0.371
2	291	0.1408	0	8574.5	4166	3820.6	1163	0.14
3	305	0.3073	0	4927.7	5115.8	6871.8	9394	0
4	312	0.3694	0	2874.7	7063	7349.2	15840	0
5	317	0.3558	0	1941	8178.9	6689.8	17260	0
6	322	0.2988	0	1378.5	8506.6	5508.1	14850	0
7	380	0.2075	0	51.226	3334.1	6147.7	284	0
8	395	0.3226	0	28.171	3880.6	9498.7	165	0
9	410	0.2357	0	16.615	2976.3	6834	174	0
10	450	0.1225	0	0	310.46	1869.3	7572	0
11	461	0.1521	0	0	144.54	1783.3	11890	0
12	468	0.1578	0	0	94.738	1703.8	12740	0
13	480	0.1272	0	0	51.398	1479.1	9378	0
14								
15								
16								
17								

Figure A.1. Origin7® screen shot of nonlinear curve fitting function editor and the corresponding worksheet.

done by declaring the datasets. Under the "Action" tab, the "Datasets" option is selected for this purpose. Here, the appropriate dataset from the worksheet is selected from the available datasets list and assigned to the corresponding variable.

If there are any known constants, these must be identified under "Parameter Initialization" in the "Scripts" tab. In this window, initial guesses of the fitting parameters can be made. Constraints can also be imposed on the fitting parameters. This can be done either by setting a range of possible values or by setting user defined linear constraints. This can be done under "Options" and then "Constraints". Also, under "Options", the "Control" window provides the ability to control the tolerance of the fit, the maximum number of iterations to be performed as well as various weighting methods.

Before the fit can be accomplished, a graph must be produced. If one has not been created manually, a default graph will be produced. It should be noted that the independent variables declared may not be the independent variable expected on an appropriate graph. For example, when dealing with UV-visible data, the x-axis is the wavelength. However, the wavelength is not part of the absorbance calculation and so the absorptivities may be considered the independent variables for the purpose of the fitting.

The fit can now be performed by selecting "Action" and then "Fit". At this point, if initial guesses have not been made as described previously, they can be made here. One can also select to vary only certain parameters and set others as constant. The fit is initiated by clicking the "100 iterations" button. Origin® will first compile the function that has been entered (if not already done in "Code Builder") and then begin running up to 100 Levenberg-Marquardt iterations until the desired tolerance is achieved. When finished, the parameter values will be displayed at the top of the window and in the texbox, the χ^2 value will appear. If the results are inadequate, any of the previously mentioned options can be readjusted and the fit attempted again.

After each fit, Origin® also produces an estimate of the standard error of each parameter. This is calculated directly from the Levenberg-Marquardt algorithm. Also, a measure of the dependency of each parameter is given. This number will be between zero and one. The closer it is to one, the more dependent that value is on the value of the other parameters. This is an indication of overparameterization. In this case a reduction in the number of parameters may be necessary to improve results.

A2 KINETIC ANALYSIS

A2.1 General Considerations

Previous studies of thiomolybdate kinetics were described in section 1.5.2. In those studies, assumptions were made to simplify the reaction scheme being studied and the rate constants were solved separately from each other. However, due to the sequential nature of the TM interconversion reactions, such assumptions are of dubious validity.

In this work, all relevant rate constants were solved simultaneously under conditions that mimic formation in the bovine rumen. This improves the accuracy of the rate constants but increases the complexity of the analysis. As such there are a number of requisite considerations to address before performing experiments.

Integrated rate equations for all species concerned were solved using the Laplace Transform method. The details of this method will be described in section A2.3. The limitation of this method is that all processes in the reaction scheme studied must be first or pseudo-first order. Reaction conditions must be such that this criterion is observed.

It is also important to note that the inclusion of other reaction processes in the kinetic scheme will affect the magnitude of the rate constants. For example, the observed rate constant for the formation of TM3 from TM2 will be affected by further

formation of TM4. However, once the rate constant is established, it governs that particular single step even though it was determined from a complex scheme. It is therefore important to establish the single step kinetics before the complex reaction scheme can be considered.

An example of a single step TM formation reaction is shown in equation A.4. The corresponding reverse reaction is shown in equation A.5. Reaction byproducts are

$$TM1 + HS^- \rightarrow TM2 \quad \textbf{(A.4)}$$

$$TM2 + OH^- \rightarrow TM1 \quad \textbf{(A.5)}$$

not shown. The nucelophiles shown are the assumed forms of these reactions based on previous literature. The actual identities of these, as determined by our experiments, will be described in section 3.2.

The rate equations for these reactions are shown in equation A.6 and equation A.7, respectively.

$$rate_{TM1} = k_2[TM1]^n\,[HS^-]^m \quad \textbf{(A.6)}$$

$$rate_{TM2} = k_{-2}[TM2]^n\,[OH^-]^m \quad \textbf{(A.7)}$$

The rate of change of the TM concentration is defined as $rate_{TM}$, k is the rate constant and n and m are the orders of reaction with respect to their corresponding species.

By mimicking the conditions normally found in the rumen, the pseudo-first order rate constants with respect to the TM are naturally observed (see section 1.6.2 for rumen conditions). Because the solution is buffered, the OH^- concentration is held constant. Also, the HS^- concentration is expected to be in large excess and so as the reaction proceeds this concentration will remain essentially constant. Equations A.6

and A.7 can now be expressed as in equations A.8 and A.9, where k_2' and k_{-2}' are the observed pseudo-first order rate constants and are defined as in equations A.10 and A.11.

$$\text{rate}_{TM1} = k_2'[TM1]^n \quad \textbf{(A.8)}$$

$$\text{rate}_{TM2} = k_{-2}'[TM2]^n \quad \textbf{(A.9)}$$

$$k_2' = k_2[HS^-]^m \quad \textbf{(A.10)}$$

$$k_{-2}' = k_{-2}[OH^-]^m \quad \textbf{(A.11)}$$

By assuming that the OH^- and HS^- concentrations are constants, the rate as shown in equation A.8 and A.9 is only dependent on the TM concentration. Equations A.8 and A.9 and A.10 and A.11 can be made linear and then exploited to obtain the respective orders of reaction. The logarithm of equations A.8 and A.10, for example, can be taken to give equations A.12 and A.13, respectively.

$$\log \text{rate}_{TM1} = \log k_2' + n \log [TM1] \quad \textbf{(A.12)}$$

$$\log k_2' = \log k_2 + m \log [HS^-] \quad \textbf{(A.13)}$$

The order, n, with respect to the TM can be obtained from the slope of a plot of $\log \text{rate}_{TM1}$ vs. $\log [TM1]$. The rate can be determined simply by calculating the change in concentration per given time interval. The best results will be obtained if the time interval is small and the change in concentration is due to a single, elementary reaction. This is typically the case when the initial rate is determined. The slope will usually be, or very nearly be, a whole number and should be taken as such.

Similarly, the order, m, can be found from experiments in which k' is determined at varying concentrations of the corresponding species; [HS^-] in this case. A plot of log k_2' vs. log [HS^-] will ideally produce a whole number slope for the value of m.

The true rate constant can now be found in one of two ways. First, from the log k_2' vs. [HS^-] plot, k_2 can be extracted from the y-intercept by taking the inverse log of the value read from the graph. Second, k_2 can be calculated directly from equation A.13 for each trial and then averaged. From the second method, the calculated k_2 from each trial should give a constant value. If, however, there is a systematic drift of k_2 with the concentration of HS^- this may be an indication that there is another species affecting the rate constant. Therefore, in order to find the true rate constant, it must be accounted for in the same manner as described for HS^-.

With the orders and rate constants known the rate law can be written. The rate law is the equation that equates the rate of change of a particular species to the concentrations of the species that affect it. The rate law will take on the form of equations A.6 and A.7 with the rate constant (with proper units) and order values included.

A2.2 Using Rate Constants to Determine Mechanism

From the results of kinetic analysis it is often possible to propose a plausible mechanism. How the rate constant changes with varying conditions provides information that can be pieced together to help explain details of the reaction in the form of a mechanism. Some commonly varied parameters are pH, ionic strength and temperature. More information on the effects of these parameters can be found elsewhere [142].

Adjusting the pH is necessary for evaluating the role of H^+ in the reaction. H^+ (or OH^-) may be involved in a reaction in a number of ways. First and foremost, the pH affects the acid-base speciation. This is especially true when the pH is at or near the

pKa of a particular compound. For example, the pKa of H_2S is 7. At pH 7, 50 % each of H_2S and HS^- will be present. At pH 6, there will be 91 % H_2S. If one species or the other is involved in the rate law, it will have a profound role on the rate constant. H^+ may also be part of the rate law itself. For example, it may be involved in a fast pre-equilibrium step that is required for the reaction to proceed. Finally, H^+ may play a catalytic role in which pre-protonation of a reacting species may facilitate the reaction. The relationship between the rate constant and the pH will help to determine the role of H^+ in the mechanism.

Studying changes in the ionic strength provides information about the magnitude and sign of the charges of reacting species. This relationship is defined in equation A.14 [142].

$$\log k = \log k^0 + 1.02\, z_A z_B\, I^{1/2} \qquad \textbf{(A.14)}$$

The charges of two reacting species are z_A and z_B, k^0 is the rate constant at infinite dilution and I is the ionic strength. The slope of a graph of log k vs. $I^{1/2}$ will give the $z_A z_B$ product. This can be used to gain information about the identity of the reacting species.

The effects of temperature on the rate constant can be related by the Arrhenius equation (equation A.15). E_a is the activation energy in J mol^{-1} K^{-1}, R is the universal gas

$$k = Ae^{-E_a/RT} \qquad \textbf{(A.15)}$$

constant and A is the pre-exponential factor and is a measure of reaction efficiency. A plot of log k vs. 1/T gives a slope of $-E_a/R$ from which the activation energy can be derived. Activation energies can be used to identify changes in the mechanism. For example, if a reaction proceeds via a particular mechanism it will have a certain activation energy. If under different conditions the activation energy is different, this

indicates a change in the mechanism. Similarly, if two similar reactions have the same activation energy, this suggests that they likely proceed via the same mechanism.

A2.3 Laplace Transform Method of Integration

Conventional graphical methods of kinetic analysis, as detailed above, are effective for simple kinetic schemes. As the complexity of the system being studied increases, limiting assumptions are often made. These assumptions may be in the form of simplifying the reaction studied. This has typically been the case with TM studies in the past where TM formation was studied in parts (see section 1.5.2). Other assumptions may include approximating the concentration curves by using, for example, Euler's method or the Runge-Kutta method [144].

Euler's method is based on the use of first-order linear differential equations over a defined time range. This method improves as the time step size is reduced. This however, can lead to long computation times and round-off errors can accumulate with each step.

The Runge-Kutta method is an improvement on Euler's method. It includes the use of the midpoint of the interval to cancel out lower-order error terms. Essilfie-Dughan used the classical fourth-order Runge-Kutta method to evaluate TM formation. However, a significant error developed and this method was thus deemed unsuitable for this analysis [113].

Integration of differential rate equations provides an exact analytical solution for kinetic data. This is ideal for accurate quantitative analysis. However, integration becomes very cumbersome as the complexity of the reaction scheme grows. In addition, advanced training in calculus may be required to effectively solve this problem.

The Laplace transform method is a means of solving simultaneous ordinary linear differential equations [138]. These differential equations are functions of time.

This method creates a set of polynomial expressions that are then solved using matrix methods. The polynomials are a function of frequency (denoted as ν). Conversion back to the time domain is simply done using widely available Laplace Transform pair tables [139]. The result is integrated rate equations without the user performing the task of integration. The main advantage is that even complex reaction schemes can be handled almost as easily as simple ones.

The one limitation with using this method for integrating differential rate equations is that all processes must be either overall first or pseudo-first order reactions. This is because this method is only applicable to linear differential equations.

The Laplace transform method is shown for the following example, a single reversible reaction between two species where k_1 and k_{-1} are the first order rate constants for the forward and reverse reactions, respectively (equation A.16). Initial conditions are $[A]_0 = a$ and $[B]_0 = 0$.

$$A \underset{k_{-1}}{\overset{k_1}{\rightleftharpoons}} B \qquad \textbf{(A.16)}$$

The differential rate equations (equations A.17 and A.18) for this scheme are

$$\frac{d[A]}{dt} = -k_1[A] + k_{-1}[B] \qquad \textbf{(A.17)}$$

$$\frac{d[B]}{dt} = k_1[A] - k_{-1}[B] \qquad \textbf{(A.18)}$$

Let [A] = x and [B] = y and rearrange to get equations A.19 and A.20.

$$x'(t) + k_1x(t) - k_{-1}y(t) = 0 \qquad \textbf{(A.19)}$$

$$y'(t) - k_1 x(t) + k_{-1} y(t) = 0 \quad \textbf{(A.20)}$$

The Laplace transform can now be applied to convert these time domain functions into functions of frequency. The Laplace transform is defined by equation A.21. The right hand side of the equation consists of ordinary differential equations

$$F(\nu) = \int_0^{\infty} \exp(-\nu t)\, f(t)dt \quad \textbf{(A.21)}$$

which are a function of time. These are then integrated to form polynomial equations as a function of frequency. Initial conditions can then be applied to the polynomials and solved to obtain a function describing each chemical species. The solution for these equations can be obtained using Cramer's method [138]. Finally, time domain functions can be returned by taking the inverse Laplace transform. This is simply done by using the wide array of Laplace transform pairs that have been tabulated in the literature [139].

Taking the Laplace Transform, therefore, gives equations A.22 and A.23, the frequency domain equations.

$$\nu x(\nu) - x(0) + k_1 x(\nu) - k_{-1} y(\nu) = 0 \quad \textbf{(A.22)}$$

$$\nu y(\nu) - y(0) - k_1 x(\nu) + k_{-1} y(\nu) = 0 \quad \textbf{(A.23)}$$

Applying the initial conditions and simplifying thus gives equations A.24 and A.25.

$$[\nu + k_1]\, x(\nu) - k_{-1} y(\nu) = a \quad \textbf{(A.24)}$$

$$-k_1 x(\nu) + [\nu + k_2]\, y(\nu) = 0 \quad \textbf{(A.25)}$$

These equations can now be solved simultaneously using the method of determinants, also known as Cramer's method. Arranging into matrices gives equation A.26.

$$\begin{bmatrix} \nu + k_1 & -k_{-1} \\ -k_1 & \nu + k_{-1} \end{bmatrix} \begin{bmatrix} x(\nu) \\ y(\nu) \end{bmatrix} = \begin{bmatrix} a \\ 0 \end{bmatrix} \quad \textbf{(A.26)}$$

The determinant is defined as equation A.27. The matrix can be solved to give equation A.28.

$$D = \begin{bmatrix} \nu + k_1 & -k_{-1} \\ -k_1 & \nu + k_{-1} \end{bmatrix} \quad \textbf{(A.27)}$$

$$D = \nu^2 + \nu k_{-1} + \nu k_1 = \nu(\nu + \alpha) \quad \textbf{(A.28)}$$

Where $\alpha = k_1 + k_{-1}$. x(s) and y(s) can then be solved as in equations A.29 and A.30 where $\alpha = k_1 + k_2$

$$x(\nu) = \frac{1}{D} \begin{bmatrix} a & -k_{-1} \\ 0 & \nu + k_{-1} \end{bmatrix} = \frac{a(k_{-1} + \nu)}{\nu(\nu + \alpha)} \quad \textbf{(A.29)}$$

$$y(\nu) = \frac{1}{D} \begin{bmatrix} \nu + k_1 & a \\ -k_1 & 0 \end{bmatrix} = \frac{ak_1}{\nu(\nu + \alpha)} \quad \textbf{(A.30)}$$

The inverse Laplace transform can then be obtained from published transform pairs. Substituting for α gives the final results (equations A.31 and A.32) as a function of time.

$$x(t) = \frac{a}{k_1 + k_{-1}} [k_{-1} + k_1 e^{-(k_1 + k_{-1})t}] \quad \textbf{(A.31)}$$

$$y(t) = \frac{a}{k_1 + k_{-1}} [k_1 - k_1 e^{-(k_1 + k_{-1})t}] \quad \textbf{(A.32)}$$

This is the desired form of the kinetic equations. This method can be expanded to include a greater number of species and all sorts of reaction schemes. The results of a variety of schemes have been demonstrated by Andraos [138, 146]. The derivations for the specific reaction schemes used in this thesis are outlined in detail in A2.5.

A2.4 Using Curve Fitting for Finding Rate Constants

Improvements in computers allow us to solve and deal with large, difficult equations without limiting approximations. Also, curve fitting algorithms remove the need to assume smaller reaction schemes as large numbers of parameters can now be solved simultaneously with relative ease.

In the previous section, the Laplace Transform method of integration was described. From an appropriate reaction scheme, integrated rate equations can be calculated. Rate constants can then be extracted from these equations using the Origin7® curve fitting feature (see section A1.3 for details of its use).

Each species accounted for in the kinetic scheme will be described by an equation. This equation will be in terms of the species concentration as a function of time. Concentrations are included as the dependent variables and time as the independent variable. The concentration and time variables are then related by the various rate constants which are the parameters that will be determined in the fit. The initial concentrations are input as constants.

A potential shortfall of this method is overparameterization. This was discussed in some detail in section A1.2 in terms of univariate analysis. In this case, overparameterization would be the inclusion of too many rate constants in the fitting routine. In other words, too many processes are being accounted for in the reaction

scheme. To avoid overparameterization, the minimum number of rate constants that effectively fit the data should be included. Beyond this, the results will be meaningless even though the fit appears to be good.

The complexity of the integrated rate equations leads to a complicating factor. With each new species present in the kinetic scheme, the polynomial order grows. In order to take the inverse Laplace transform, these equations must be in the appropriate form. With more complex schemes, this requires non-linear substitutions to be made. In the example presented in the A2.5.1, this leaves equations A.32 – A.34 for which f, g and h need to be solved.

$$f + g + h = k_2 + k_{-2} + k_3 + k_4 \quad \textbf{(A.32)}$$

$$fg + fh + gh = k_2k_4 + k_{-2}k_4 + k_3k_4 \quad \textbf{(A.33)}$$

$$fgh = k_2k_3k_4 \quad \textbf{(A.34)}$$

These cannot be solved for by simple math. Instead, f, g and h were solved by iteration. This could not be accomplished in Origin7®. The Origin7® curve fitter requires dependent and independent variables to be input (see Figure A1.1). In other words, a graph must be created. In this case, the expressions contain only constants. The "Goal Seek" function within Microsoft Excel® was therefore used to find values for f, g, and h. These values were then set as constants in the kinetic fitting routine in Origin7®.

A2.5 Development of Equations Using Laplace Transform Method

Determination of integrated rate equations for TM formation and reaction with Cu(II) using the Laplace Transform method [138].

A2.5.1 Thiomolybdate Formation

Kinetic scheme:

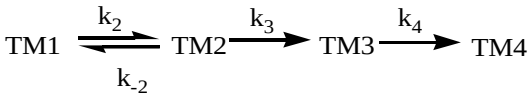

Let A = TM1, B=TM2, C=TM3, D=TM4

$$\frac{d[A]}{dt} = -k_2[A] + k_{-2}[B]$$

$$\frac{d[B]}{dt} = k_2[A] - (k_{-2} + k_3)[B]$$

$$\frac{d[C]}{dt} = k_3[B] - k_4[C]$$

$$\frac{d[D]}{dt} = k_4[C]$$

Let [A] = w, [B] = x, [C] = y, [D] = z

Rearrange:

$$w'(t) + k_2w(t) - k_{-2}x(t) = 0$$
$$-k_2w(t) + x'(t) + (k_{-2} + k_3)x(t) = 0$$
$$-k_3x(t) + y'(t) + k_4y(t) = 0$$

$-k_4y(t) + z'(t) = 0$

Take Laplace Transform:

$sw(s) - w(0) + k_2w(s) - k_{-2}x(s) = 0$

$-k_2w(s) + sx(s) - x(0) + (k_{-2}+k_3)x(s) = 0$

$-k_3x(s) + sy(s) - y(0) + (k_4)y(s) = 0$

$-k_4y(s) + sz(s) - z(0) = 0$

let w(0) = a, x(0) = b, y(0) = c, z(0) = d:

$sw(s) + k_2w(s) - k_{-2}x(s) = a$

$-k_2w(s) + sx(s) + (k_{-2}+k_3)x(s) = b$

$-k_3x(s) + sy(s) + (k_4)y(s) = c$

$-k_4y(s) + sz(s) = d$

Solve for w(x), x(s), y(s), z(s) using matrix method (Cramer's method or method of determinants):

$$\begin{bmatrix} a \\ b \\ c \\ d \end{bmatrix} = \begin{bmatrix} w(s) \\ x(s) \\ y(s) \\ z(s) \end{bmatrix} \begin{bmatrix} s+k_2 & -k_{-2} & 0 & 0 \\ -k_2 & s+k_{-2}+k_3 & 0 & 0 \\ 0 & -k_3 & s+k_4 & 0 \\ 0 & 0 & -k_4 & s \end{bmatrix}$$

$$D = \begin{bmatrix} s+k_2 & -k_{-2} & 0 & 0 \\ -k_2 & s+k_{-2}+k_3 & 0 & 0 \\ 0 & -k_3 & s+k_4 & 0 \\ 0 & 0 & -k_4 & s \end{bmatrix}$$

$= s^4 + s^3(k_2 + k_{-2} + k_3 + k_4) + s^2(k_2k_4 + k_{-2}k_4 + k_3k_4) + sk_2k_3k_4$

Let:

$f + g + h = k_2 + k_{-2} + k_3 + k_4$

$fg + fh + gh = k_2k_4 + k_{-2}k_4 + k_3k_4$

$fgh = k_2k_3k_4$

$D = s^4 + s^3(f + g + h) + s^2(fg + fh + gh) + s(fgh) = s(s + f)(s + g)(s + h)$

$$w(s) = \frac{1}{D}\begin{bmatrix} a & -k_{-2} & 0 & 0 \\ b & s+k_{-2}+k_3 & 0 & 0 \\ c & -k_3 & s+k_4 & 0 \\ d & 0 & -k_4 & s \end{bmatrix}$$

$= as^3 + s^2(a(k_{-2}k_3k_4) + bk_{-2}) + s(a(k_{-2}k_4 + k_3k_4) + bk_{-2}k_4)$

$= As^3 + Bs^2 + Cs + D$

Where:

$A = a, B = a(k_{-2}k_3k_4) + bk_{-2}, C = a(k_{-2}k_4 + k_3k_4) + bk_{-2}k_4, D = 0$

$$x(s) = \frac{1}{D}\begin{bmatrix} s+k_2 & a & 0 & 0 \\ -k_2 & b & 0 & 0 \\ 0 & c & s+k_4 & 0 \\ 0 & d & -k_4 & s \end{bmatrix}$$

$= bs^3 + s^2(ak_2 + b(k_2 + k_4)) + s(ak_2k_4 + bk_2k_4)$

$= As^3 + Bs^2 + Cs + D$

Where:

$A = b, B = ak_2 + b(k_2 + k_4), C = ak_2k_4 + bk_2k_4, D = 0$

$$y(s) = \frac{1}{D}\begin{bmatrix} s+k_2 & -k_{-2} & a & 0 \\ -k_2 & s+k_{-2}+k_3 & b & 0 \\ 0 & -k_3 & c & 0 \\ 0 & 0 & d & s \end{bmatrix}$$

$= cs^3 + s^2(bk_3 + c(k_2 + k_{-2} + k_3)) + s(ak_2k_3 + bk_2k_3 + ck_2k_3)$

$= As^3 + Bs^2 + Cs + D$

Where:

$A = c$, $B = bk_3 + c(k_2 + k_{-2} + k_3)$, $C = ak_2k_3 + bk_2k_3 + ck_2k_3$, $D = 0$

$$z(s) = \frac{1}{D}\begin{bmatrix} s+k_2 & -k_{-2} & 0 & a \\ -k_2 & s+k_{-2}+k_3 & 0 & b \\ 0 & -k_3 & s+k_4 & c \\ 0 & 0 & -k_4 & d \end{bmatrix}$$

$=ds^3 + s^2(ck_4 + d(k_2 + k_{-2} + k_3 + k_4)) + s(bk_3k_4 + c(k_{-2}k_4 + k_3k_4 + k_2k_4) + d(k_{-2}k_4 + k_3k_4 + k_2k_4 + k_2k_3)) + (a + b + c + d)(k_2k_3k_4)$

$= As^3 + Bs^2 + Cs + D$

Where:

$A = d$, $B = ck_4 + d(k_2 + k_{-2} + k_3 + k_4)$, $C = bk_3k_4 + c(k_{-2}k_4 + k_3k_4 + k_2k_4) + d(k_{-2}k_4 + k_3k_4 + k_2k_4 + k_2k_3)$, $D = (a + b + c + d)(k_2k_3k_4)$

Generic Laplace Equation:

$$w(s) = x(s) = y(s) = z(s) = \frac{As^3 + Bs^2 + Cs + D}{s(s + f)(s + g)(s + h)}$$

Inverse Laplace Transform from Conversion tables [139]:

$x(t) = w(t) = y(t) = z(t) =$

$$\frac{D}{fgh} + \frac{Af^3 - Bf^2 + Cf - D}{f(g - f)(h - f)}e^{-ft} + \frac{Ag^3 - Bg^2 + Cg - D}{g(f - g)(h - g)}e^{-gt} + \frac{Ah^3 - Bh^2 + Ch - D}{h(f - h)(g - h)}e^{-ht}$$

Substitute f, g and h for calculation of each component. Substitute appropriate values for A, B, C and D for each component.

A2.5.2 Reaction Between Copper(II) and TM4

Kinetic scheme:

$$TM4 + Cu^{2+} \underset{k_{-1}}{\overset{k_1}{\rightleftharpoons}} \text{Intermediate} \xrightarrow{k_2} \text{Product}$$

Using the methods described above:

$$[TM4] = -\frac{af^2 - (ak_{-1} + ak_2 + bk_{-2})f)e^{-ft}}{f(g - f)} - \frac{ag^2 - (ak_{-1} + ak_2 + bk_{-2})g)e^{-gt}}{g(f - g)}$$

$$[Int] = -\frac{bf^2 - (ak_1 + bk_1)f)e^{-ft}}{f(g - f)} - \frac{bg^2 - (ak_1 + bk_1)g)e^{-gt}}{g(f - g)}$$

$$[Prod] = \frac{(a + b + c)k_1k_{-1}}{fg} - \frac{\left(cf^2 - (bk_2 + c(k_1 + k_{-1} + k_2)\right)f + (a + b + c)(k_1 + k_2))e^{-ft}}{f(g - f)} - \frac{\left(cg^2 - (bk_2 + c(k_1 + k_{-1} + k_2)\right)g + (a + b + c)(k_1 + k_2))e^{-gt}}{g(f - g)}$$

Where:

$a = [TM4]_o$, $b = [Int]_o$, $c = [Prod]_o$

And:

$fg = k_1 + k_2$, $f + g = k_1 + k_{-1} + k_2$